



UNIVERSITY OF LIEGE - FACULTY OF APPLIED SCIENCES

ATFE0005-1

MASTER'S THESIS

SUPERVISED BY PR. GAËTAN KERSCEN

OUFTI-Next Nanosatellite: Feasibility Study and Mission Assessment

GRADUATION STUDIES CONDUCTED FOR OBTAINING THE MASTER'S DEGREE IN
AEROSPACE ENGINEERING BY DIMITRY SCHKLAR

Author:
Dimitry Schklar

Student Number:
S113125

Academic year 2016 - 2017

Acknowledgments

First of all, I would like to thank Xavier Werner who too took me under his wing during the whole semester. He shared his knowledge and experience with enthusiasm. His suggestions and expertise contributed greatly to this work and his patience, availability and happiness had a great impact on my personal fulfillment in this project.

I also wish to thank Prof. Gaëtan Kerschen who gave me the opportunity to take part in this ambitious project. His contributions were valuable and essential to this thesis.

Then, I would like to express my gratitude to Lamberto Dell'Elce for answering my numerous questions in a comprehensive and precise way. It contributed considerably to my personal experience.

The other members of the OUFTI-Next team are also warmly thanked: Prof. Serge Habraken and Prof. Jérôme Loicq for their availability and numerous excellent ideas emitted during the meetings. Enrico Ghidoli for his team spirit and deep involvement in the project.

Then, I would like to acknowledge Amandine Denis for her encouragement at a critical moment and AGI who provided us with a STK pro-licence for two more weeks.

Eventually, I deeply thank a dozen people around the world for sharing generously information on their respective CubeSat project without asking for anything in exchange. It is a beautiful example of humanity.

Sart Tilman, 3 June 2017

Abstract

Last Name	Schklar
First name	Dimitry
Section	Master's degree in Aerospace Engineering
Academic year	2016 - 2017
Promotor name	Pr. Gaëtan Kerschen
Thesis title	OUFTI-Next Nanosatellite: Feasibility Study and Mission Assessment

Abstract The University of Liege is convinced that CubeSats are particularly well suited for Earth observation from space. CubeSats are cheap nanosatellites which can be duplicated to create constellations. These multiple CubeSats are redundant and have a high rate of revisit compared to classical satellites. Therefore, the University of Liege is developing a project which objective is to detect hydric stress in agricultural fields. It would permit to manage more efficiently water resources through irrigation and evaluate yielding of crops. To this end, a technology demonstrator called OUFTI-Next must first be developed. The objective of this thesis is to assess the legitimacy and feasibility of the mission. The feasibility study of OUFTI-Next is carried out by performing different analyses. They cover several aspects such as lifetime, constellation, orbits, data and link budgets... At the end, certain points which must be carefully watched out are highlighted.

Keywords OUFTI-Next, CubeSat, Hydric Stress, Constellation, Feasibility Study, Orbit

Demonstrative images

This first figure displays how it is possible to obtain a daily coverage with only two orbits and eight satellites

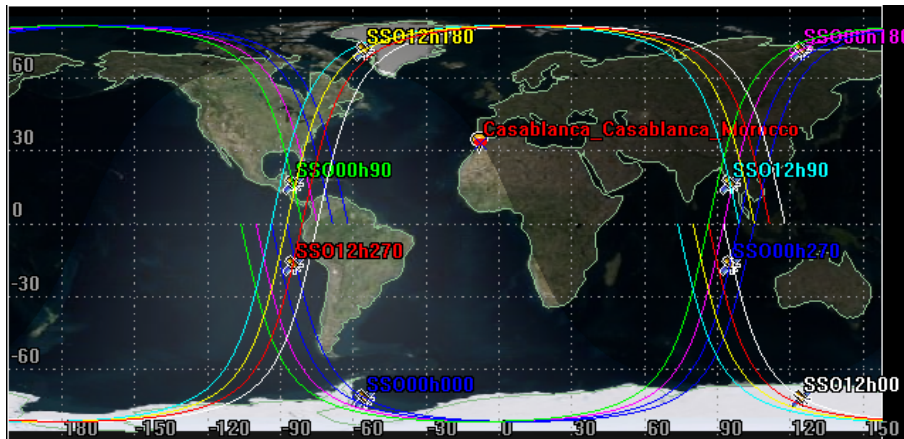


FIGURE 1: *Ground tracks of 800[km] SSO constellation*

The second figure presents a first CAD model of OUFTI-Next with its different subsystems.

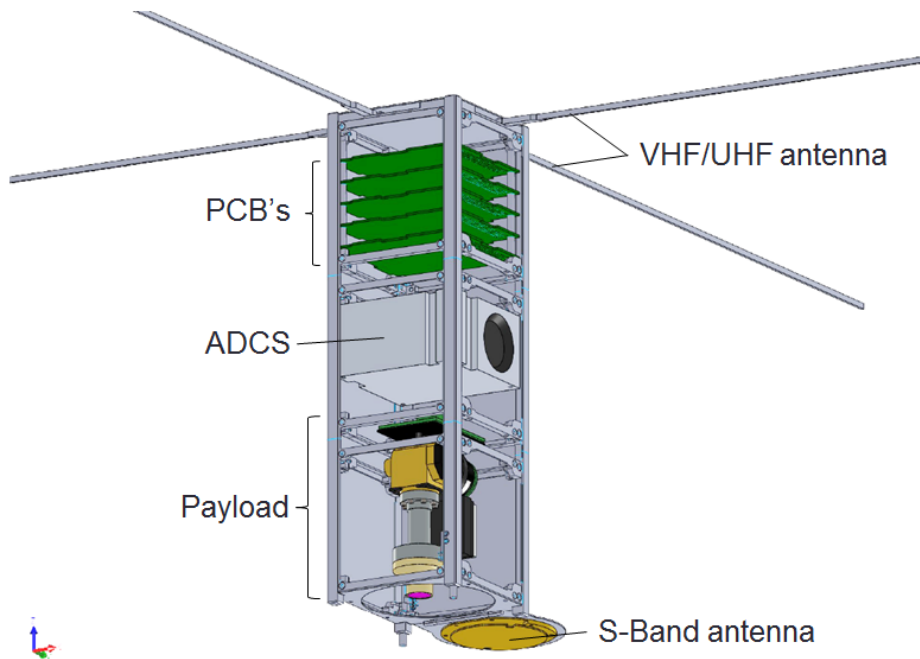


FIGURE 2: *OUFTI-Next CAD model*

Contents

1	Introduction	1
2	Analysis of the mission objectives and requirements	2
2.1	Mission objectives and requirements	2
2.2	Why is this mission legitimate?	3
2.2.1	The MWIR wavelength band	3
2.2.2	Why hydric stress detection is so important?	5
2.2.3	Is it an innovative mission?	5
2.3	Lifetime	5
2.4	Constellation	6
2.5	Conclusion	8
3	OUFTI-Next mission	9
3.1	Mission objectives and requirements	9
3.2	Payloads description	10
3.2.1	FLIR Neutrino MWIR detector	10
3.2.2	SCD Kinglet MWIR detector	11
3.2.3	TMA telescope	13
3.2.4	Classical camera	14
4	State of the art	15
4.1	Large MWIR missions	15
4.1.1	AVHRR: Advanced Very High Resolution Radiometer	15
4.1.2	VIIRS: Visible/Infrared Imager Radiometer Suite	16
4.1.3	MODIS: MODerate-resolution Imaging Spectroradiometer	17
4.1.4	MOPITT: Measurement Of Pollution In The Troposphere	18
4.1.5	Multi-spectral thermal infrared imager (HyspIRI)	18
4.2	Cubesats observing the Earth in the IR	19
4.2.1	Conclusion	28
5	Mission analysis	29
5.1	Orbits	29
5.1.1	Orbits characteristics	29
5.1.2	Space environment	31
5.2	Revisit time	32
5.2.1	ISS orbit	32
5.2.2	SSO 400[km]	33
5.2.3	SSO 800[km]	34
5.2.4	Conclusion	34
5.3	Lifetime	35
5.3.1	Parameters influencing the orbital decay	36

5.3.2	OUFTI-Next lifetime	38
5.3.3	Validation of the results	40
5.3.4	25 years rule	41
5.3.5	Conclusion	41
5.4	Summary	42
6	OUFTI-Next design	43
6.1	Attitude Determination Control Subsystem	43
6.1.1	Imaging techniques	43
6.1.2	ADCS market survey	44
6.2	Data & Link budgets	46
6.2.1	Data budgets	46
6.2.2	Link budgets	48
6.2.3	Conclusion	54
6.3	Power over a year	54
6.3.1	ISS orbit	55
6.3.2	Sun-synchronous orbits	57
6.3.3	Summary of the results	63
6.4	Power budget	64
6.4.1	ISS orbit	64
6.4.2	SSO 400[km]	66
6.4.3	SSO 800[km]	68
6.4.4	Conclusion	70
6.5	Mass budget and space occupation	71
6.5.1	Mass budget	71
6.5.2	Space occupation	72
6.5.3	Conclusion	72
6.6	Summary	73
7	Conclusion	75
	Appendices	77
A	SSO database	78
B	Large MWIR missions	81
	Bibliography	84

Acronyms

ADCS Attitude Determination and Control System

BCN BeaCoN

CCD Charge-Coupled Device

CAD Computer-Aided Design

COM COMunication subsystem

COTS Commercial Of-The-Shelf

CSA Canadian Space Agency

EPS Electrical Power Subsystem

FOV Field Of View

GHG Green House Gases

GSD Ground Sampling Distance

ISS International Space Station

IR InfraRed

LEO Low Earth Orbit

LTDN LongiTude of Descending Node

LWIR Long-Wave InfraRed

MEMS MicroElectroMechanical Systems

MWIR Mid-Wave InfraRed

NASA National Aeronautics and Space Administration

NEDT Noise-Equivalent Difference Temperature

NDVI Normalized Difference Vegetation Index

NIR Near InfraRed

NOAA National Oceanic and Atmospheric Administration

OBC On-Board Computer

OUFTI-Next Orbital Utility For Thermal Imaging Next

OUFTI 1 & 2 Orbital Utility For Telecommunication Innovation 1 & 2

PCB Printed Circuit Board

RAAN Right Ascension of Ascending Node

SRP Solar Radiation Pressure

SSO Sun-Synchronous Orbit

STK Satellite Tool Kit

SWIR Short-Wave InfraRed

TDI Time Delay Integration

THER THERmal subsystem

TMA Three Mirrors Anastigmat

UHF Ultra High Frequency

VHF Very High Frequency

VIS VISible

List of Figures

1	<i>Ground tracks of 800[km] SSO constellation</i>	iv
2	<i>OUFTI-Next CAD model</i>	iv
2.1	<i>Thermal image of different fields</i>	3
2.2	<i>Earth atmospheric transmission</i>	3
2.3	<i>Earth and Sun spectra in the MWIR</i>	4
2.4	<i>6U CubeSats lifetime for different SSO</i>	6
2.5	<i>Revisit time for a 800[km] SSO</i>	6
2.6	<i>3D view of 800[km] SSO constellation</i>	7
2.7	<i>Ground tracks of 800[km] SSO constellation</i>	8
3.1	<i>FLIR Neutrino MWIR detector</i>	10
3.2	<i>Dimensions of the FLIR Neutrino [inch]</i>	11
3.3	<i>Photograph of an airport hangar taken with the FLIR Neutrino</i>	11
3.4	<i>Kinglet MWIR detector in two configurations</i>	12
3.5	<i>Dimensions of the Kinglet [mm]</i>	12
3.6	<i>Path of the light in the TMA</i>	13
3.7	<i>3D section of the TMA showing the mechanical structure</i>	14
3.8	<i>TMA inside a 1U CubeSat</i>	14
4.1	<i>Surface temperature in function of NDVI</i>	16
4.2	<i>Vegetation health using VIIRS (left) and AVHRR (right)</i>	17
4.3	<i>Arkyd-6</i>	24
4.4	<i>QBITO</i>	24
4.5	<i>CIRAS</i>	26
4.6	<i>Arkyd-100</i>	27
5.1	<i>SSO 800[km] with LTDN 12h and 18h</i>	31
5.2	<i>Revisit time for ISS orbit</i>	33
5.3	<i>Revisit time for a 400[km] SSO</i>	33
5.4	<i>Revisit time for a 800[km] SSO</i>	34
5.5	<i>Ground tracks of ISS, 400[km] SSO and 800[km] SSO</i>	35
5.6	<i>Drag coefficient vs CubeSat form factor for observed decay</i>	37
5.7	<i>F10.7cm emissions</i>	38
5.8	<i>Lifetime prediction with three different atmospheric density models</i>	39
5.9	<i>Lifetime prediction in function of LTDN</i>	40
6.1	<i>Signal integration with TDI scanning</i>	44
6.2	<i>Imaging with attitude control</i>	44
6.3	<i>ADCS main characteristics</i>	45
6.4	<i>Payload and telemetry data downlink budget in VHF</i>	49
6.5	<i>Payload and telemetry data downlink budget in UHF</i>	49

6.6	<i>Payload data downlink budget in S-band</i>	51
6.7	<i>Payload data downlink budget in X-band</i>	51
6.8	<i>Uplink budget in VHF</i>	53
6.9	<i>Uplink budget in UHF</i>	53
6.10	<i>3U model with telescope placed on +y face</i>	55
6.11	<i>3U model with telescope placed on -z face</i>	55
6.12	<i>Power over a year for an ISS orbit with the first model</i>	56
6.13	<i>Power over a year for an ISS orbit with the second model</i>	56
6.14	<i>Power over a year for a SSO 800[km], best case without attitude control</i>	57
6.15	<i>Power over a year for a SSO 800[km], best case with attitude control</i>	58
6.16	<i>Power over a year for a SSO 800[km], worst case without attitude control</i>	58
6.17	<i>Power over a year for a SSO 800[km], worst case with attitude control</i>	59
6.18	<i>Mean altitude vs inclination for LEO satellites</i>	59
6.19	<i>Lighting vs LTDN for a 800[km] SSO</i>	60
6.20	<i>Number of satellites vs LTDN for a 800[km] SSO</i>	60
6.21	<i>Power generated over a year, mean case without attitude control</i>	61
6.22	<i>Power generated over a year, LTDN 22h30 without attitude control</i>	62
6.23	<i>Power generated over a year, mean case with attitude control</i>	62
6.24	<i>Power generated over a year, SSO 400[km], 10h30 LTDN without attitude control</i>	63
6.25	<i>Batteries cycles over a year, ISS orbit</i>	65
6.26	<i>Batteries cycles during the first day, ISS orbit</i>	66
6.27	<i>Batteries cycles over a year in 400[km] SSO, LTDN 10h30</i>	67
6.28	<i>Batteries cycles during the first day, 400[km] SSO</i>	68
6.29	<i>Batteries cycles over a year in 800[km] SSO, LTDN 12h00</i>	69
6.30	<i>Batteries cycles during the first two days, 800[km] SSO</i>	70
6.31	<i>OUFTI-Next CAD model</i>	74
6.32	<i>OUFTI-Next CAD model with body mounted solar panels</i>	74
B.1	<i>Past large MWIR missions</i>	81
B.2	<i>Operational large MWIR mission</i>	82
B.3	<i>Future large MWIR missions</i>	83

List of Tables

2.1	<i>Visible and infrared wavelength bands</i>	4
3.1	<i>Distance between the optics</i>	13
4.1	<i>VIIRS compared with predecessor AVHRR</i>	17
4.2	<i>Chemical components detection with related channel</i>	18
5.1	<i>ISS initial orbital elements</i>	30
5.2	<i>Main characteristics of circular orbits [min]</i>	31
5.3	<i>Main characteristics of SSO [min]</i>	31
5.4	<i>OUFIT-Next lifetime</i>	39
5.5	<i>Lifetime comparison with real missions [days]</i>	41
6.1	<i>Communication bands properties</i>	47
6.2	<i>Amount of payload data downlinked per pass</i>	47
6.3	<i>Amount of payload data downlinked per day</i>	47
6.4	<i>Downlink System Link Margins for different orbits and bands</i>	52
6.5	<i>Uplink System Link Margins in VHF and UHF for different orbits</i>	54
6.6	<i>Power generated for ISS orbit</i>	63
6.7	<i>Power generated for 800[km] SSO, 18h LTDN (Best case)</i>	63
6.8	<i>Power generated for a 800[km] SSO, 12h LTDN (Worst case)</i>	63
6.9	<i>Power generated for 10h30 LTDN SSO (Mean case)</i>	64
6.10	<i>High consumption power budget for ISS orbit</i>	64
6.11	<i>High consumption power budget for 400[km] SSO, LTDN 10h30</i>	67
6.12	<i>High consumption power budget for 800[km] SSO, LTDN 12h00</i>	68
6.13	<i>Mass budget</i>	71
A.1	<i>SSO database with corresponding LTDN/LTAN</i>	80

Chapter 1

Introduction

The OUFTI-Next project was thought as a continuation of OUFTI-1 satellite whose successful launch in April 2016 opened the path to more ambitious projects. It started on November 2016 during an ideation session which gathered professors from different faculties and industrial partners. The aim of this session was to collect general ideas in order to define a specific mission objective.

Many interesting proposals were submitted and the OUFTI-Next team was charged to value the most promising one. This team composed of Prof. Serge Habraken, Prof. Gaëtan Kerschen, Prof. Jérôme Loicq and Xavier Werner selected Prof. Bernard Tychon's idea to detect hydric stress in agricultural fields of arid regions. Prof. Tychon teaches at the University of Liège and is specialized in agrometeorology. The aim pursued with his proposal is to manage more efficiently water resources through irrigation and therefore elevate yieldings. Indeed, 70% of fresh water in the world is used to irrigate crops but the irrigation efficiency reaches only 40%.

Hydric stress detection is possible by taking mid-wave infrared images from space. These infrared data must be provided each day to users for an efficient management of crops and irrigation. A constellation of satellites which permits a daily revisit is thus mandatory. The cost of such a constellation should be as low as possible that is why CubeSats have been preferred notwithstanding the fact that they are also particularly well suited for this task.

Before launching a constellation of CubeSats in space, one must ensure that mid-wave infrared images can be taken and sent back to the ground station. It is at this stage that the 3U CubeSat OUFTI-Next is relevant. OUFTI-Next, standing for *Orbital Utility For Thermal Imaging*, is a technology demonstrator; the *Next* permits to distinguish this mission from OUFTI 1 & 2 missions. The aim is to take MWIR images of the Earth and detect hydric stress in agricultural fields. Performing MWIR measurements with such a small satellite would be a world premiere!

The objective of this thesis is to assess the legitimacy and feasibility of the project. First, the mission objectives and requirements are presented. The legitimacy of the mission is appraised by analyzing the mid-wave infrared band and the state of the art of infrared CubeSats. A constellation able to provide daily information is modelled and its lifetime assessed. Then, objectives and requirements of the technology demonstrator OUFTI-Next are detailed with a special attention dedicated to the payload description. Finally, an analysis is carried out to assess the feasibility of OUFTI-Next mission under certain working assumptions. This analysis covers various fields such as orbits, data & link budgets, power generation, revisit time, lifetime, mass budget and space occupation.

Chapter 2

Analysis of the mission objectives and requirements

The aim of this chapter is to present the mission objectives and requirements. It will also be demonstrated why this mission is legitimate and useful. Eventually, a constellation will be created to meet one of the requirement and the lifetime assessed.

2.1 Mission objectives and requirements

The primary goal of the mission is to provide valuable information to users on the hydric stress level of their fields. By knowing this hydric stress level, farmers can better evaluate if they must irrigate their fields or not. These information must be provided each day for an efficient management of crops and irrigation.

Hydric stress detection is possible thanks to MWIR measurements. A plant without enough water closes its stomas which are small apertures at the leaves surface. These stomas are used to exchange water vapour with the atmosphere which leads to the transpiration of the plants. Transpiration is essential to conserve an ideal temperature for growing. When stomas are closed, plants heat up and it is a sign of hydric stress. Finally, it is possible to evaluate this level of stress by measuring the difference of temperature between the plants and ground surface thanks to MWIR measurements. This difference in temperature is not negligible and can go up to 10°C. The picture below is a thermal image showing fields at different temperatures [71]. Some of them have been irrigated (in blue) and others not (in red). Hydric stress detection is not the only scientific objective of the mission. The instrument can also provide valuable information in other scientific domains such as oceanography, for example.

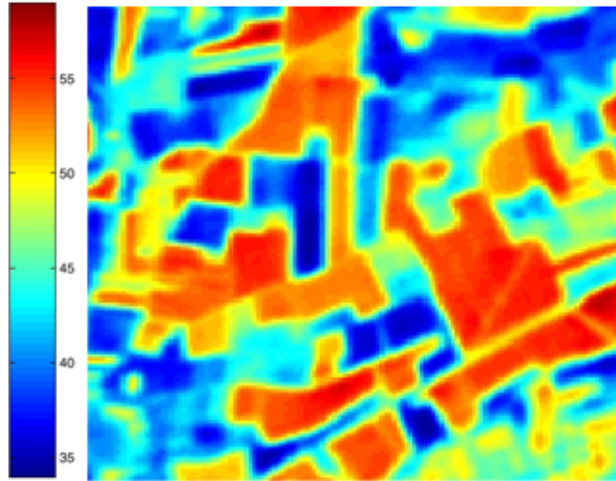


FIGURE 2.1: *Thermal image of different fields*

A daily revisit over the same region is not achievable by a single satellite. A constellation of CubeSats which can provide a daily coverage is thus required. Furthermore, a maximum GSD of 50[m] is necessary to detect one field from another. Eventually, it would be appreciable to pass over the same region each day at the same time. In this way, comparisons between daily measurements would be facilitated. One of the properties of SSO is precisely to cross the equator each time at the same local solar time.

2.2 Why is this mission legitimate?

2.2.1 The MWIR wavelength band

The MWIR band is the 3-5[μm] portion of the electromagnetic spectrum. Usually, small satellites observe the Earth in visible or near infrared wavelengths while big satellites can also observe in the thermal infrared. Thanks to the developments in infrared detectors and the miniaturization of cryocooler technology, MWIR instruments can now be packaged in CubeSats. In the past, MWIR measurements were widely used for military applications such as heat-seeking missiles for instance.

Unfortunately, it is not possible to observe the Earth surface with all wavelengths because the atmosphere is only transparent to certain bands (Fig 2.2). [67]

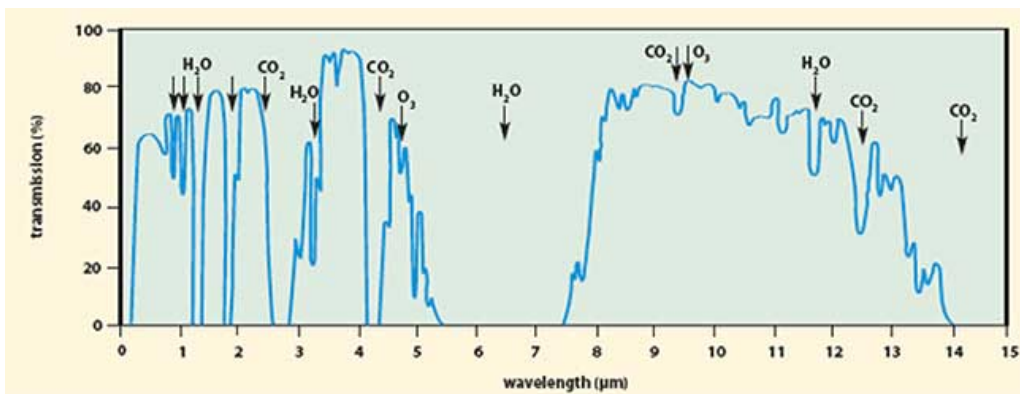


FIGURE 2.2: *Earth atmospheric transmission*

From this figure, one can deduce that it is useless to observe the Earth surface in a band between 5.5-7.5[μm] since the atmosphere is totally opaque to these wavelengths. For this reason, the infrared part of the electromagnetic spectrum is usually divided in bands which are transmitted by the atmosphere. From 0.4 to 15[μm] these wavelength bands are:

Band	Wavelength [μm]
Visible (VIS)	0.40-0.75
Near-infrared (NIR)	0.75-1.0
Short-wave infrared (SWIR)	1.0-2.5
Mid-wave infrared (MWIR)	3.0-5.0
Long-wave infrared (LWIR)	8.0-15.0

TABLE 2.1: Visible and infrared wavelength bands

Compared to the common LWIR band, MWIR measurements offer several advantages. The MWIR signal is composed of reflected light as well as thermal emissive signal as can be seen in Figure 2.3. This double composition offers the possibility for imaging at night when it is easy to detect the thermal emissive signal from the ground and during the day to obtain information from the reflected light. Furthermore, it is less subject to diffraction and less disturbed by radiation of its own instrument [55]. It means that the detector must be less cooled compared to a LWIR detector which is a serious advantage in the frame of this mission. Nowadays, there are even uncooled MWIR detectors with a moderate sensitivity.

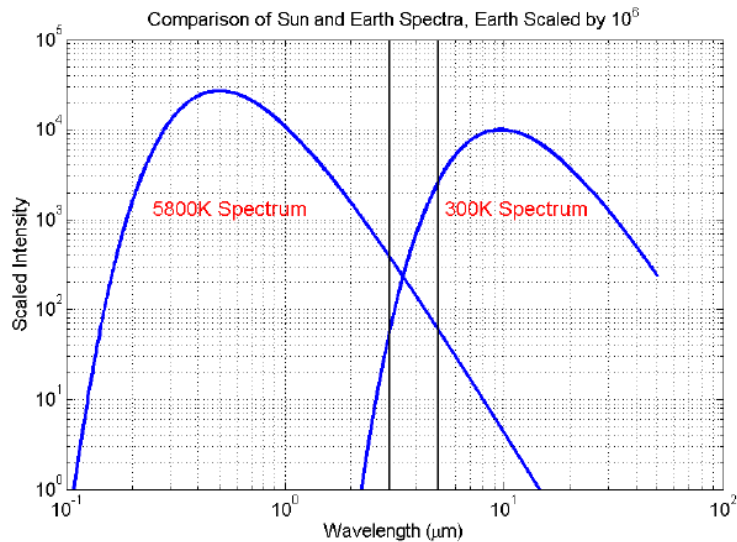


FIGURE 2.3: Earth and Sun spectra in the MWIR

The MWIR band is also useful for the detection of certain chemical components responsible for greenhouse effect. Figure 2.2 shows that molecules favouring greenhouse effect such as H_2O , CO_2 and O_3 can be detected. These molecules have different energy levels and absorb radiation at these specific wavelengths.

2.2.2 Why hydric stress detection is so important?

In the world, one quarter of farmlands are irrigated. These irrigated farmlands produce one third of the world food production and are also 3.5 times more efficient than non-irrigated crops. Hence, irrigation is essential in arid regions and necessary to obtain high yields. At the world scale, agriculture is the biggest freshwater consumer (70%) followed by industry (20%) and eventually domestic consumption (10%). Nevertheless, nowadays the irrigation mean efficiency is inferior to 40% which leads to a enormous waste of freshwater. [71]

The detection of hydric stress linked to a lack of water is thus of paramount importance for increasing the crops yields and decreasing the waste of freshwater. Hydric stress detection in arid regions can help local farmers to manage more efficiently their crops. A CubeSat is particularly well suited for this task. Indeed, a constellation of 8 satellites in SSO at 800[km] can provide a daily coverage and valuable information to farmers (see Section 2.4). The use of drones is far more expensive due to maintenance and cannot stand the comparison in terms of area covered.

2.2.3 Is it an innovative mission?

Observing the Earth in the MWIR region is not a new idea. More than 50 MWIR instruments have been developed or are currently in orbit and 24 are being developed or proposed (Appendix B for complete lists). Nevertheless, none of these instruments are specifically designed for hydric stress detection in farmlands.

Concerning CubeSats, only four of them are or will be equipped with a MWIR instrument (see Section 4.2). Among them, Planetary Resources (US-based company) plans to launch Arkyd-6 and Arkyd-100 which will provide data for irrigation and water use in agriculture. This interest of a US commercial company in hydric stress detection should reinforce our conviction in the legitimacy of this mission. [61]

2.3 Lifetime

In this section, the lifetime of a 6U CubeSat is assessed for SSO at different altitudes. A 6U CubeSat is assumed because one considers that the constellation is composed of 6U CubeSats. Figure 2.4 displays the lifetime of a 6U CubeSat for SSO at different altitudes ranging from 400 to 600[km]. Higher altitudes are not displayed for more clarity. A mean drag area = $0.055[m^2]$ and drag coefficient of 2.2 are assumed. The simulation begins in 2017.

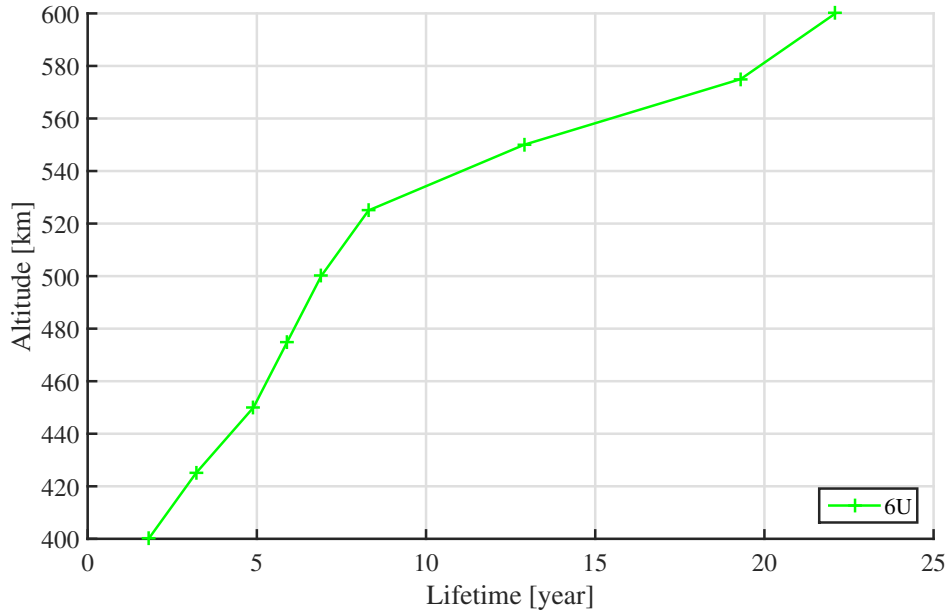


FIGURE 2.4: 6U CubeSats lifetime for different SSO

At 400[km], CubeSats decay after 1.9 years. Then, it increases to 5.9 years at 500[km] and 22.1 years for a 600[km] orbit. It exceeds 100 years at 800[km]. It is really important to notice that these lifetime predictions are highly dependent on the epoch, especially for low altitudes. Therefore, these predictions are only first approximations of the constellation lifetime.

2.4 Constellation

The goal is to create a cheap constellation of CubeSats able to provide a daily coverage. The cost increases with the number of satellites. It also increases with the number of different orbits required. Hence, a constellation with a minimum number of satellite and orbit is optimal. If the CubeSats are designed to operate for 2 years, all SSO above 400[km] can be considered.

The number of passes over a specific region increases with the altitude. 800[km] SSO should be used to decrease the number of satellite required while keeping a decent GSD. With a FOV set to 11.46° [54], there are 104 passes during a year over a specific place with a single CubeSat. These passes over a year are displayed in Figure 2.5. The specific region considered is Casablanca.

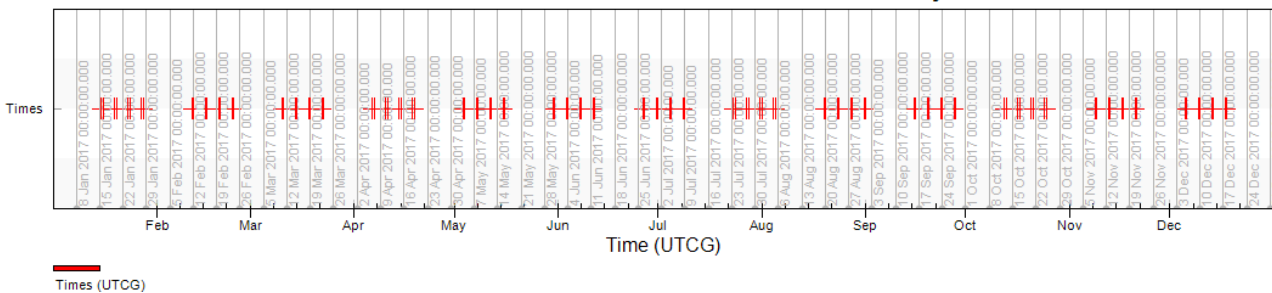


FIGURE 2.5: Revisit time for a 800[km] SSO

These passes are organized according to a specific pattern. Firstly, passes always go by groups of 8. These groups of 8 passes have an exact duration of 12.47 days. Between each

group of passes, there is a gap of 14.54 days. Then, inside the groups, passes go by pairs. These pairs of passes have a duration of 0.47 day. Between each pair of passes, there is a gap of 3.53 days without any pass. To summarize, a quick check must be performed:

$$(4 \text{ pairs} \times 0.47) + (3 \text{ gaps} \times 3.53) = 12.47 \text{ days} \quad (2.1)$$

12.47 is actually the total duration of a group of 8 passes.

In order to obtain a daily coverage, a constellation must be created by adding satellites. The first objective is to obtain passes every day inside a group by "filling" the gaps. These gaps of 3.53 days can be filled by placing 4 satellites evenly distributed on the same orbit. Their true anomalies are shifted by 90° .

Then, one must fill the gaps of 14.54 days between the groups. Four satellites evenly distributed can provide a daily coverage for 16 days (32 passes separated by gaps of approximately 0.5 days). So, 4 satellites evenly distributed placed on an adequate orbit can fill these gaps of 14.54 days. This adequate orbit must have its LTDN shifted by 12h compared to the first one.

To sum up, a daily coverage can be obtained with 2 orbits and 8 satellites. Such a constellation can be visualized on Figures 2.6 and 2.7. In this case, one orbit has a 0h LTDN and the other a 12h LTDN.

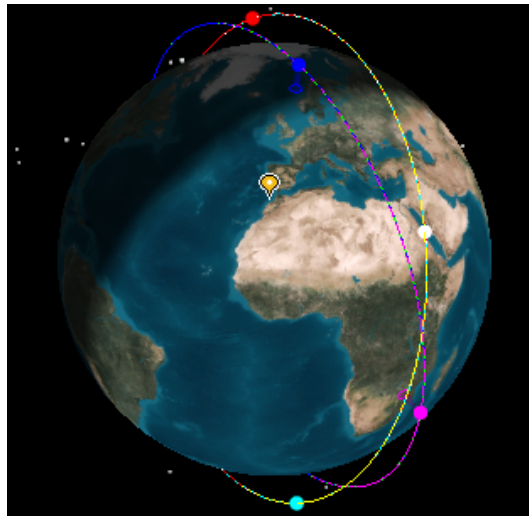


FIGURE 2.6: *3D view of 800[km] SSO constellation*

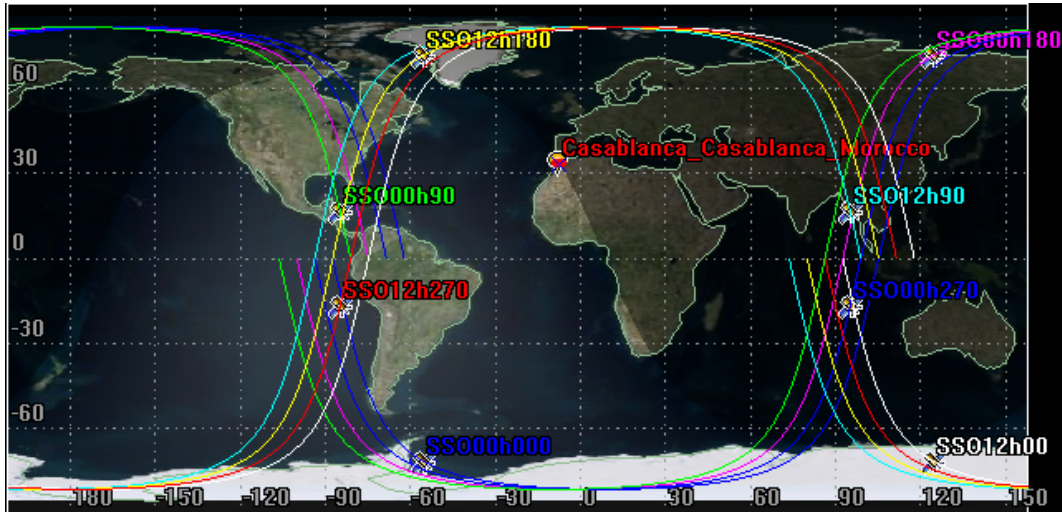


FIGURE 2.7: *Ground tracks of 800[km] SSO constellation*

2.5 Conclusion

This mission is legitimate for three principal reasons. Firstly, the MWIR region is a wavelength band particularly interesting for Earth surface imaging because the atmosphere is nearly transparent to these wavelengths and the MWIR signal is composed of both reflected light and thermal emissive radiation. Furthermore, compared to the LWIR, it is less subject to diffraction and less disturbed by radiation of its own instrument. This last point is crucial since only a moderate cooling of the detector is required.

Secondly, hydric stress detection is of prime importance for increasing food production yields and for decreasing the waste of freshwater. Since agriculture is responsible for 70% of the freshwater consumption in the world, a constellation of 8 CubeSats in SSO could provide daily information to farmers for agricultural decision-making process.

Thirdly, this mission is innovative in the sense that none of the large satellites are specialized in hydric stress detection. Concerning CubeSats, only the Arkyd mission is planning to use MWIR imaging for agriculture purposes which shows that the mission is relevant.

Eventually, a constellation of only 8 satellites in two different orbits is required. With such a constellation, daily information can be provided to users on the hydric stress level of their crops.

Chapter 3

OUFTI-Next mission

Before launching a constellation of satellites in orbit, it is essential to test if one is able to take MWIR images and downlink them to the ground station. It is in this frame that OUFTI-Next mission is crucial. Throughout the rest of the document, OUFTI-Next is assumed to be a 3U CubeSat. It is only a work hypothesis. Nevertheless, it would be a world premiere if MWIR measurements of the Earth could be performed thanks to a 3U CubeSat.

3.1 Mission objectives and requirements

OUFTI-Next is a technology demonstrator. The primary objective of the mission is to operate the main payload in orbit. This payload is composed of a small telescope provided by AMOS and a MWIR detector. The telescope is a compact TMA (Three Mirrors Anastigmat) which focuses the light on the MWIR detector. Thanks to this system, the CubeSat is able to take MWIR images of the Earth surface. Then, one must be sure to be able to downlink these images.

The second objective is to take real photographs of the Earth thanks to a small camera which is the secondary payload. This objective is not essential but a real image is usually more appealing for the general public than a black and white MWIR image. Furthermore, it could be used to confirm that the CubeSat is targeting the correct area. Even for scientists and engineers, it is easier to recognize a particular field with a classical image than a MWIR image.

Contrary to OUFTI 1 & 2 missions, this one is not particularly dedicated to education. Furthermore, the development and conception of the CubeSat must be realized in a shorter amount of time. Indeed, the earliest would be the best and targeting a launch in 2019 should be feasible. In order to spare time, only specific components which are not commercially available will be developed by the University. Nevertheless, one should keep in mind that it is still a University project so, education should not be neglected. This is why students will continue to work on this project via master thesis for instance.

These objectives lead to certain requirements which are a bit relaxed compared to the constellation mission. The first obvious requirement is to have a MWIR detector inside the CubeSat. Secondly, the GSD should be below 100[m]. Since this mission is only a technology demonstration, it is not that important to reach a fine resolution. Furthermore, OUFTI-Next will certainly be smaller than the CubeSats composing the constellation. Thus, it is more difficult to reach a high spatial accuracy.

3.2 Payloads description

The aim of this section is to present the different payloads and their specifications. The correct functioning of the payloads will depend on all other subsystems. These subsystems will be designed depending on the payloads specifications.

3.2.1 FLIR Neutrino MWIR detector

To this day, the most serious lead concerning the detector is a FLIR Neutrino MWIR detector (Fig 3.1). It is the smallest and lightest cooled camera from FLIR. It uses a 640×512 Insb $15[\mu\text{m}]$ array and the detector is cooled thanks to a sterling cryocooler (included in the FLIR Neutrino).

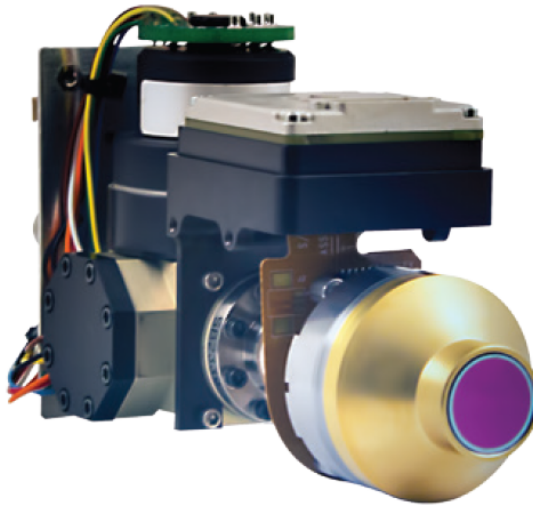


FIGURE 3.1: *FLIR Neutrino MWIR detector*

The principal specifications are listed below [1]:

- **Spectral band** : $3.4 - 5.1[\mu\text{m}]$
- **Size of the array** : 640×512 pixels
- **Pixels size** : $15[\mu\text{m}]$
- **Frame rate** : $25[\text{Hz}]$
- **Sensitivity (NEDT)** : $<25[\text{mK}]$
- **Time to image** : <6 min at room temperature, <10 min at 71°C
- **Digital data** : 8 or 14 bit
- **Size** : $12.70 \times 5.01 \times 7.37[\text{cm}]$ (Fig 3.2)
- **Mass** : $454[\text{g}]$
- **Power** : $8[\text{W}]$ cooldown, $5[\text{W}]$ steady state
- **Operating temperature range** : -40°C to 71°C
- **Non-operating temperature range** : -55°C to 80°C

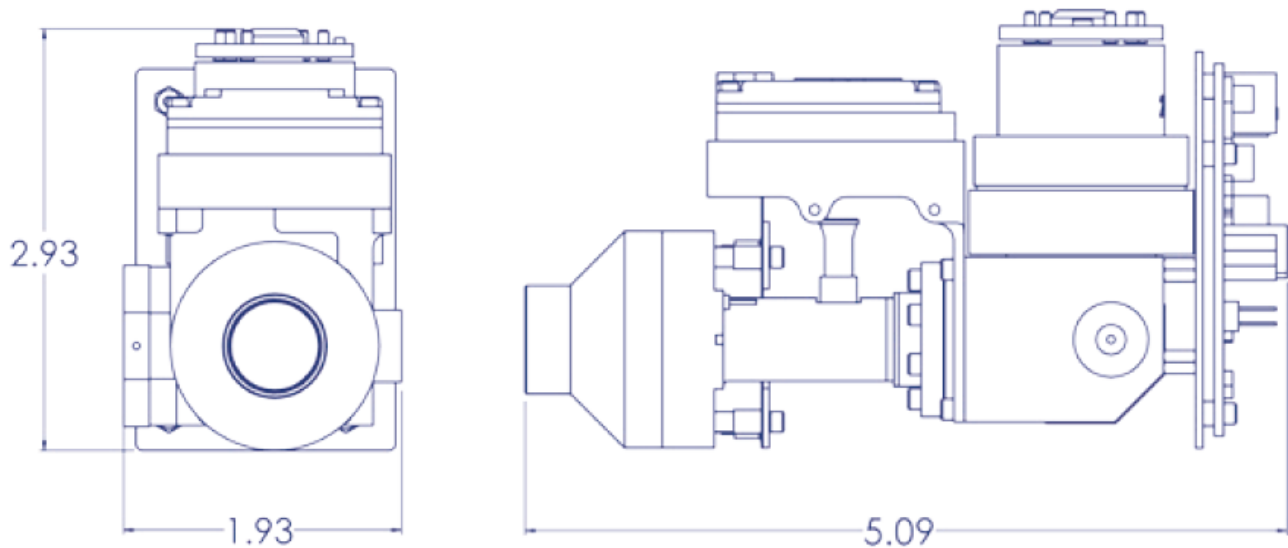


FIGURE 3.2: *Dimensions of the FLIR Neutrino [inch]*

The following photograph shows what kind of image is obtained thanks to this detector. It has been shot from an aircraft above an airport hangar. White zones of the image indicate the hotter parts. The darkest zones indicate colder elements.



FIGURE 3.3: *Photograph of an airport hangar taken with the FLIR Neutrino*

It is important to mention that it is maybe possible to buy this detector in other configurations. For instance, it may be possible to fold it in order to place the cryocooler next to the photosensitive part instead of behind. In this way, it would be more compact.

3.2.2 SCD Kinglet MWIR detector

Another lead concerning the MWIR detector is the Kinglet MWIR detector from SCD, Israel (Fig 3.4). It is a reduced SWaP (Size, Weight and Power) MWIR detector with increased reliability. It uses a 640 x 512 InAsSb 15[μm] array with a Ricor cooler.



FIGURE 3.4: *Kinglet MWIR detector in two configurations*

The main specifications are [2]:

- **Spectral band** : 3.6 - 4.2[μm]
- **Size of the array** : 640 x 512 pixels
- **Pixels size** : 15[μm]
- **Detector temperature** : 150[K]
- **Frame rate** : > 100[Hz]
- **Sensitivity (NEDT)** : <23[mK]
- **Time to image** : <5 min at 23°C
- **Size** : 5.95 x 3.8 x 8.0 [cm] (Fig 3.5)
- **Mass** : < 300[g]
- **Power** : 3.5[W] cooldown

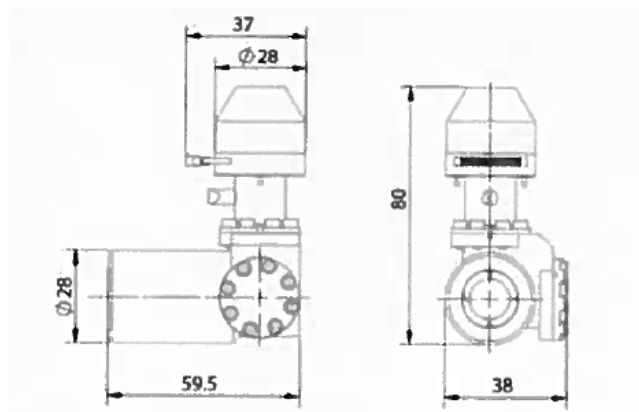


FIGURE 3.5: *Dimensions of the Kinglet [mm]*

3.2.3 TMA telescope

Of course, a detector is useless without a telescope in front of it to collect and focus the light. An analogy with a common camera can be done. If one takes a photograph without a lens in front of the camera, the result is not satisfying. In the present case, one solution is to use a three mirrors anastigmat (TMA) telescope. A compact TMA developed by AMOS inspired by the Proba V design is presented here. It is not the version that will be used in OUFTI-Next but it is still interesting to understand its functioning and have some figures (size, mass...) in mind for further calculations.

The list below presents the main characteristics of the TMA. A 600[km] altitude orbit is assumed.

- **Focal length** : 40[mm]
- **F#** : 6
- **Field of view** : 50° across track, 3° along track
- **GSD** : 90[m]
- **Swath** : 565[km]
- **Mass** : 150[g]
- **Size** : 60 x 50 x 30[mm]

The TMA is composed of 3 mirrors. M2 is a spherical convex mirror while M1 and M3 are aspherical concave mirrors. The focal plane is placed near M2. The path of the light coming from the Earth can be seen in Figure 3.6. In this figure, the Earth is located on the left of the TMA. Distances between mirrors can be found in Table 3.1.

	Distance [mm]
M1-M2	15.556
M2-M3	19.976
M3-Focal plane	39.784

TABLE 3.1: *Distance between the optics*

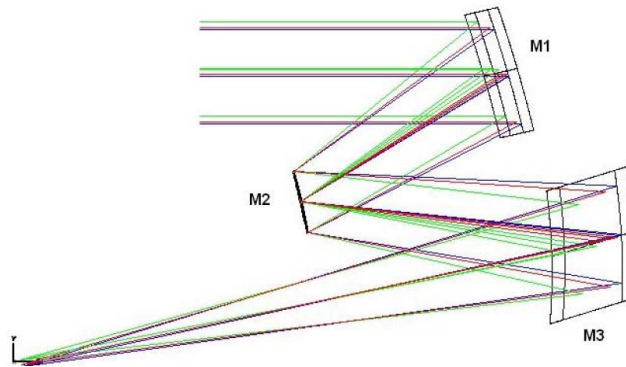


FIGURE 3.6: *Path of the light in the TMA*

Since the telescope structure and mirrors are made out of the same material, there is no problem with varying temperatures. The whole instrument will deform uniformly and the only effect is a slight variation of the GSD. The mechanical structure of the TMA and its volume occupation in a 1U CubeSat are shown in the following figures. This compact structure ensures an easy adjustment during the alignment phase of the telescope. [60]

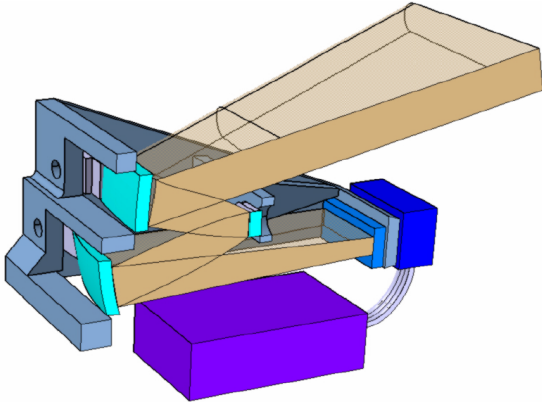


FIGURE 3.7: *3D section of the TMA showing the mechanical structure*

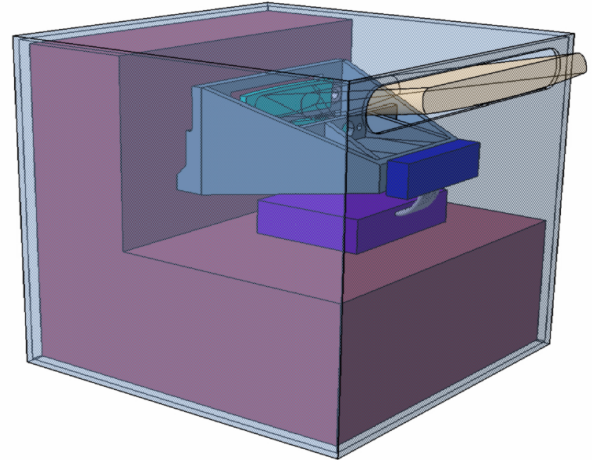


FIGURE 3.8: *TMA inside a 1U CubeSat*

TMA is an innovative concept. Such mirror assembly can be used as a telescope whatever the wavelength of interest from visible to thermal infrared. The utilization of lenses may be easier but different glasses are required for different wavelengths. Furthermore, such glasses can be very expensive for longer wavelengths.

3.2.4 Classical camera

A classical visible camera must be incorporated inside OUFTI-Next for two main purposes. First, for communication. A real image is often more appealing for the general public than a MWIR image. Second, it can be useful to recognize which part of the Earth OUFTI-Next is pointing to.

The camera model has not been chosen yet. Nevertheless, the TMA telescope can be used to focus the light on the visible detector. In this way, another aperture at the surface of the satellite is not required and one takes advantage of the TMA which can be used with a large spectrum of wavelengths.

Chapter 4

State of the art

Being aware of other similar existing missions is a crucial preliminary step towards the development of the project. Even if observing the Earth in the MWIR is already well-established for big satellites, it is far less common for CubeSats. This chapter is dedicated to the presentation of certain large MWIR missions. Then, a deeper analysis is led concerning CubeSat missions in the IR.

4.1 Large MWIR missions

In this section, five large MWIR missions are developed: one completed, three currently operating and a future one. These missions have been chosen for two purposes:

- To show improvements in the instruments quality for a particular application: detection of hydric stress in vegetation
- To present the large spectrum of applications with MWIR measurements from space

It is important to stress that these instruments developed for large missions are not uniquely MWIR sensors. Usually, it is a combination of both visible and infrared detectors. A list of these instruments is given in Appendix B. The instruments are sorted according to their mission status: completed, operational or future.

4.1.1 AVHRR: Advanced Very High Resolution Radiometer

AVHRR was a multi-purpose imaging VIS/IR radiometer. This instrument, developed by NOAA (National Oceanic and Atmospheric Administration), is no longer operational. It equipped NOAA-9 (1984 - 1997) to NOAA-14 (1994 - 2005) and had a resolution of 1.1[km] with a swath of 3000[km] approximately. AVHRR could observe in the VIS and IR in the following bands:

- VIS : 0.58 - 0.68 [μm]
- NIR : 0.725 - 1.1 [μm]
- MWIR : 3.55 - 3.93 [μm]
- TIR : 10.3 - 11.3 [μm], 11.5 - 12.5 [μm]

Thanks to these wavelength bands, the instrument was able to collect data of land and sea temperature, cloud, snow and ice cover, soil moisture, vegetation indices as well as data for volcanic eruptions monitoring. [3]

It could also provide data for large-scale forest fire danger. This is based on the hydric stress detection of the forest vegetation by acquiring MWIR data of the surface temperature. One indicator of fire danger is derived from ground surface temperature and NDVI (Normalized Difference Vegetation Index) values. NDVI is defined as follows [4]:

$$NDVI = \frac{NIR - VIS}{VIS + NIR} \in [-1.0, 1.0] \quad (4.1)$$

where VIS and NIR are respectively the spectral reflectance in the visible and near-infrared regions.

The plant leaves absorb the solar radiation in the visible wavelength band (except in the green) and use it as a source of energy for photosynthesis. Contrariwise, leaves re-emit solar radiation in the NIR. As a consequence, NDVI is a good indicator for vegetation density. When the vegetation is very dense, NDVI tends to 1.

Indeed, the relationship between ground temperature and the amount of vegetation measured thanks to NDVI is an indicator of water stress. Water stress can then be linked to fire danger. The following graph plots the surface temperature T versus $NDVI$ in a 20 x 20[km] sector.

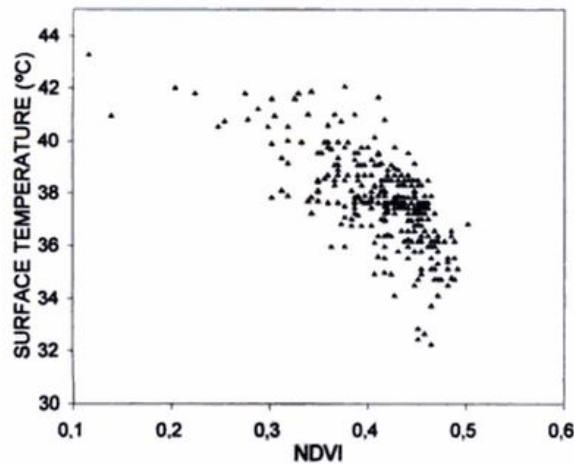


FIGURE 4.1: *Surface temperature in function of NDVI*

A linear negative slope is observed which means that the ground surface temperature decreases while the vegetation density increases. This is partly due to evapotranspiration. A greater slope implies a greater hydric stress and thus, a greater fire danger. [70]

4.1.2 VIIRS: Visible/Infrared Imager Radiometer Suite

VIIRS is a multi-purpose imaging VIS/IR radiometer developed by NOAA. It is currently operating on Suomi NPP (Suomi National Polar-orbiting Partnership) (2011 - 2020) with a resolution varying from 400[m] to 1.6[km] and a swath of 3000[km]. It operates on a quasi-circular SSO at an altitude of 834[km]. VIIRS is able to observe from VIS to TIR (0.4 - 12.5[μm]) with 22 channels. This large wavelength band is used for global observations of

land, ocean as well as for cloud/weather imagery, sea-surface temperature, ocean colour, land surface vegetation indices. [3]

VIIRS/Suomi NPP data can enhance drought monitoring and hydric stress detection and thus give warnings on potential crop losses. This can be achieved thanks to several significant improvements compared to AVHRR. The table below shows the similarities and improvements between AVHRR and VIIRS.

Similarity	Improvement
Multi-year servicing	Higher resolution
SSO	Narrow response function
Afternoon	Swath edge sharper
	More channels
	Higer data accuracy

TABLE 4.1: VIIRS compared with predecessor AVHRR

As a consequence, VIIRS can provide better data on vegetation stress compared to the old sensor. The following figure shows the improvement made on the spatial resolution relative to the vegetation health. [5]

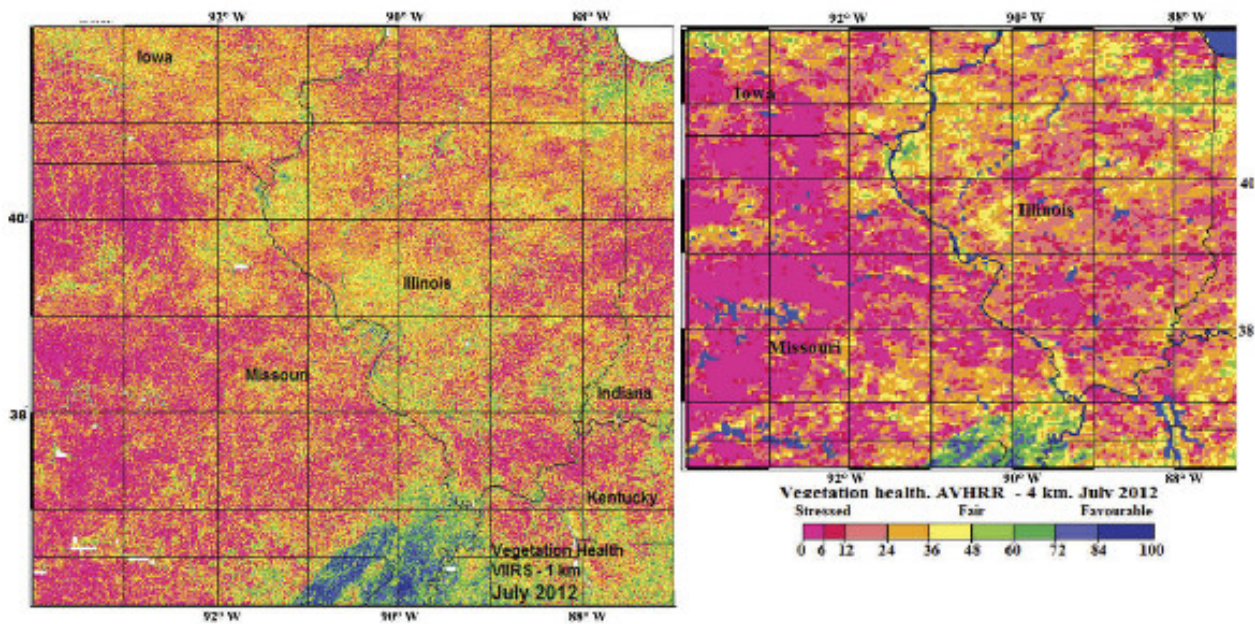


FIGURE 4.2: Vegetation health using VIIRS (left) and AVHRR (right)

One can observe that stress patterns are relatively the same when comparing both images but significant improvement has been made when looking along rivers where water is not lacking. Hence, one can better assess drought impacts on crop losses on small areas.

4.1.3 MODIS: MODerate-resolution Imaging Spectroradiometer

MODIS is a medium-resolution spectro-radiometer developed by NASA and currently equipping Aqua (2002 - 2017) and Terra (1999 - 2017) satellites. It has a resolution of 250 to 1000[m] with a maximum swath of 2330[km]. MODIS can observe from VIS to TIR (0.4 - 14.4 [µm]) with 36 distinct bands. It is able to collect data on biological and physical processes on the

Earth surface and in the lower atmosphere. It can also measure surface temperatures of land and ocean, land and cloud cover as well as chlorophyll fluorescence. [3]

MODIS is particularly well suited for measurements of sea-surface temperature. Indeed, it was the first space radiometer to have multiple MWIR bands. It is because the atmosphere is more transparent and less variable than in LWIR window that MWIR region is so well adapted for measurements of sea-surface temperatures. Furthermore, MWIR region offers more sensibility than LWIR for this range of temperatures. It is also important to highlight that MODIS was the first instrument to measure ocean temperatures only with MWIR window. Previously, sea-surface temperatures were measured with MWIR in conjunction with LWIR. [6]

4.1.4 MOPITT: Measurement Of Pollution In The Troposphere

MOPITT is a high-resolution spectrometer principally developed by CSA (Canadian Space Agency) in collaboration with NASA. It equips Terra (1999 - 2017) and collects data in the SWIR and MWIR regions (2.3, 2.4 and 4.7[μm]). These 3 channels are used to measure concentration of chemical components in the atmosphere. [3]

The table below shows which components can be detected thanks to which wavelength.

Spectral Region	Approx. λ [μm]	Primary Measurement
SWIR	2.09	column CO_2 , clouds
SWIR	2.25	column CH_4 , N_2O , clouds
SWIR	2.33	column CH_4 , CO , H_2O , clouds
MWIR	3.33	CH_4 , H_2O and C_2H_6 column
MWIR	3.56	$HCHO$, CH_4 , N_2O , and maybe some O_3 info
MWIR	4.65	CO , O_3 and H_2O
LWIR	9.5	$HCHO$, O_3 partial column

TABLE 4.2: Chemical components detection with related channel

From this table, one can infer that the MWIR channel of MOPITT is able to provide data on carbon monoxide columns and ozone. Thanks to these data, scientists can better understand the dynamic of certain pollutants in the troposphere emitted by cars, fires, ships or airplanes. [68] [72]

4.1.5 Multi-spectral thermal infrared imager (HyspIRI)

HyspIRI is an imaging multi-spectral radiometer (VIS/IR) being developed by NASA. It is expected to be operational in 2023. It is a unique and urgent global mission for Earth observation. This instrument will be able to provide continuous spectral measurements in the VIS to SWIR (0.38 - 2.51 [μm]). The infrared region will be covered by 8 channels (3 - 13 [μm]). The spatial resolution will be of minimum 60[m] with 600[km] swath. The dedicated HyspIRI satellite is designed for SSO where the overpass time is 10:30am \pm 30min. The TIR will have a 5-day revisit at the equator at an altitude of 626[km]. [3]

The overall instrument has a wide field of applications including measurements of surface temperature and emissivity, cloud heights, local surface temperature and cloud imaging with high spatial resolution. This spatial resolution is the major improvement compared to previous

sensors which permits local measurements. For instance, it will be very helpful in the case of wild fires. Indeed, wild fires and biomass burning have a major role in both regional and global climate changes. The 4[μm] (MWIR) channel will permit a reliable detection of fires at local scales with a much higher resolution than actual instruments.

The MWIR channel combined with other IR channels will also provide data of land surface temperatures which can be linked to evapotranspiration and eventually to vegetation hydric stress. The high spatial resolution of the IR channels can provide useful information on water consumption at human management scales. It can also be helpful in the evaluation of performance of irrigation systems for instance. [59]

4.2 Cubesats observing the Earth in the IR

In this section, CubeSats observing the Earth in the infrared are listed. The following table lists these satellites with their principal characteristics: name, organization, launch, status/lifetime, size, mass, payload, instrument, power, communication, ADCS, orbit and mission. More detailed information are also provided for each satellite with a particular attention dedicated to CubeSats equipped with a MWIR instrument. The causes of failure or success are also discussed.

4.2. Cubesats observing the Earth in the IR

Name	Organisation	Launch	Status/Lifetime	Size	Mass	Payload	Instrument	Power	Com	ADCS	Orbit	Mission
We Wish	Meisei Electric, Japan	21/07/2012	No more Operational Re-entry: 11/03/2013	1U	1.2	Primary	Small uncooled thermal infrared camera	0.7W for camera	D: 430MHz U: 145MHz	?	ISS	Environmental studies and promotion of utilization of data from cubesats
SRMSat	SNM University, India	12/10/2012	Active	~9U	10.9	Primary	NIR (0.7 - 1.7µm) Grating spectrometer	~10W	U: UHF(434.5MHz) at 2.4kbit/s I: VHF(145.8MHz) at 1kbit/s	Magnetometer, GPS + 3 magnetorquer coils	LEO, 867km, i=20°	Monitor green house gases (GHG)
COPPER	Saint Louis University, USA	20/11/2013	No signal Reentry: 04/02/2016	1U	1.3	Primary	LWIR (7.0 - 13.0µm) Tau camera from FLIR Uncooled microbolometer array	2W	D: 2.4 GHz at 9.6kbit/s U: 437.29 MHz	Permanent magnets, hysteresis rods	LEO, 500km, i=40.5°	Test the abilities of uncooled microbolometer array for infrared images
Lemur-1	Spire, USA	19/06/2014	Active	3U	4.0	Secondary	Low resolution IR imaging system	?	D: 2.4 GHz U: 402 MHz	Magnetorquers	SSO, 617 x 704km i= 98.0°	Demonstration of science payloads + prototype for constellation of Lemur-2
Antelsat	University of the Republic, Uruguay	19/06/2014	Inactive	2U	2.0	Primary	NIR camera	?	D: 2.403 GHz U: 145.86 MHz	Magnetometer, photodetectors + 3 magnetorquers	SSO, 606 x 621km i = 97.9°	Pure technological demonstrator + transmit colour and infrared images of the Earth
Lilacsat-2	Harbin Institute of Technology, China	09/09/2015	Active	8U	12.5	Secondary	LWIR camera	?	D: 437.2 MHz FM U: 144.35 MHz FM	Star tracker, sun sensor, GPS, gyroscope, magnetometer + magnetorquers, fly wheels	SSO, 520km, i=97°	Amateur radio communication technology demonstration
STACEM	Utah State University, USA	04/11/2015	Launch failure	3U	?	Primary	NIR + hyperspectral channels	?	/	?	LEO, 415 x 490km i = 94.7°	Collect imagery of the Earth scenes for environmental analysis and monitoring
Sathyabamasat (SINSAT)	Sathyabama University, India	22/06/2016	Active	2U	1.6	Primary	NIR (0.9 - 1.7µm) Argus 1000 IR grating spectrometer	4.2W	D: 145.98 MHz U: UHF	Gyroscope, sun sensor + magnetorquers Pointing accuracy < 8° Drift rate < 1°/s	SSO, 501 - 524km i=97.5°	Measure the densities of the GHG
Kausat - 5	Korea Aerospace University, South Korea	xx/xx/2017	1 year	3U	4.0	Primary	Infrared camera	<13W	D: 2.413 GHz at 9.6kbit/s	Magnetometer, sun sensor, gyro + Control moment gyro, magnetorquer	SSO, 450 x 720km i=97.73°	Demonstration of a light, small and cheap cubesat for environmental monitoring
Arkyd - 6	Planetary resources, USA	xx/xx/2017	?	6U	10.0	Primary	MWIR (3 - 5 µm) imaging system	35W	D: X-band at 6 Mbit/s U: S-band at 500 kbit/s	Magnetorquers and sun sensors for coarse pointing Dual star trackers and reaction wheels for fine tracking	SSO, 450 x 720km i=98.28°	Test of the instruments for Arkyd-100
												Sun sensors, Earth sensor,

4.2. Cubesats observing the Earth in the IR

QBTO	Polytechnic University of Madrid, Spain	30/03/2017	3 months	2U	1.8	Secondary	MWIR (3 - 5 μm) uncooled detector	2.1W	D : UHF 436.81 at 9.6 kbit/s U : VHF at 1.2 kbit/s	Sun sensors, Earth sensor, rate sensor, magnetometer, GPS + 3 magnetorquers, + 3 momentum	ISS	Q850 Test MWIR detector
Lilacsat-1	Harbin Institute of Technology, China	30/03/2017	3 months	2U	2.0	Secondary	Thermal infrared camera	?	D : 436.51 MHz and 437.985 MHz U : VHF	Sun sensors, Earth sensor, rate sensor, magnetometer, GPS + 3 magnetorquers, + 3 momentum	ISS	Q850 Amateurs can telecommand to take images and download data
Corvus BC	Astro Digital (Aquila Space), USA	xx/xx/2017	?	6U	10.0	Primary	NIR (0.77 - 0.9 μm) camera	?	D : Ka-band at 40 Mbit/s	Star tracker, gyroscope, GPS + 3 reaction wheels	SSO, 600km 11am ascending node	Disaster monitoring, precision agriculture, land classification, forest management, etc
Corvus HD	Astro Digital (Aquila Space), USA	xx/03/2017	?	16U	20.0	Primary	NIR (0.77 - 0.9 μm) camera	?	D : Ka-band at 480 Mbit/s	2 star trackers, gyroscope, GPS + 3 reaction wheels	SSO, 620km 11am ascending	Precision agriculture, urban planning and business intelligence
COPPER-2	Saint Louis University, USA	xx/05/2017 On hold	TBD	3U	4.0	Primary	LWIR (7.0 - 13.0 μm) Tau camera from FLIR Uncooled microbolometer array	TBD	TBD	Permanent magnets, hysteresis rods	TBD	Reflight of COPPER Test the abilities of uncooled microbolometer array
Parikshit	Manipal Institute of Technology, India	xx/xx/2017	1 year	2U	2.0	Primary	LWIR (7.5 - 13.5 μm) Uncooled microbolometer array camera from FLIR (Quark-640-FLIR)	1.18Wh	D : UHF 437.8 MHz	Sun sensors, 3 magnetometers, gyroscope, GPS + magnetorquers	SSU (SSU - 03UK11) i = 98.7° 10:30am ascending node (local time)	Study ocean surface temperature, observe cloud cover, observe temperature variations between rural and urban area
CalNOP	Carthage College, USA	xx/04/2018	TBD	3U	2.23	Primary	NIR (0.7 - 1.1 μm) OCI-M Hyperspectral Camera (Bayspec, Inc.)	10.7W max	D : S-band	2 horizon sensors, 1 magnetometer + 3 momentum wheels, 3 electromagnetic torque	TBD	Multi-spectral imaging of global forest to understand large-scale biomass production
CIRAS	NASA, USA	xx/xx/2018	TBD	6U	8.5	Primary	MWIR (4.8 - 5.1 μm) Cooled grating spectrometer	37.5W	TBD	TBD	SSO, 600km i=98.7°	Enable hyperspectral IR atmospheric sounding on a cubesat for T ¹ and water vapor measurements
TRISAT	University of Maribor, Slovenia	xx/xx/2018	min 2 years	3U	4.56	Primary	SWIR (0.95 - 1.67 μm) multispectral imager	max 27W	D : S-band at 4 Mbit/s U : S-band at 1 Mbit/s	Star tracker + reaction wheels Pointing accuracy < 0.1°	SSO, 700 km	Perform in-orbit demonstration of the platform + acquisition of data for research
CIRIS	Bell Aerospace, USA	xx/xx/2018	3 months	6U	>6.0	Primary	LWIR (7.5 - 13 μm) Uncooled infrared radiometer	?	?	?	LEO	Technology demonstration of new uncooled
Arkyd - 100	Planetary resources, USA	xx/xx/2018	TBD	12U	20.0	Primary	MWIR (3 - 5 μm) imaging system	90W	D : X-band at 40 Mbit/s U : S-band at 2 Mbit/s	Magnetorquers and sun sensors for coarse pointing Dual star trackers and reaction wheels for fine tracking	SSO, 550km	Demonstration for Arkyd-200 + precision agriculture, crop insurance, pollution monitoring, etc
Golden Eagle 1	Marquette University, USA	Cancelled	Cancelled	1U	1.0	Primary	Thermal infrared camera	?	D : UHF	?	Polar, 802 x 443 km	Learning experience + take VIS and IR photographs of the Earth

We-Wish (World Environmental Watching & Investigation from Space Height)

The principal mission of We-Wish was to take infrared images of the Earth surface and downlink them with amateur radio frequency. It had no real scientific objective. The mission was a success and images could be uploaded. The uncooled thermal infrared camera was a cube of 4[cm] with a low resolution of 320 x 256 pixels and a wide field of view (90°). [7] [8]

SRMsat (Sri Ramaswamy Memorial satellite)

SRMsat is a CubeSat developed by students under the guidance of the Indian Space Research Organization. The main objective was to give experience to these students and to the university faculty in general. The scientific goal was to monitor CO_2 and water vapour levels in the atmosphere to determine how much carbon dioxide each individual city gives out. The spectrometer did not work but the satellite is still active and gives primary information. Indeed, a final-minute problem in the OBC occurred. They had to replace it with a new one (different model) but it led to an issue when patching the spectrometer program. Eventually, the payload turned off after one frame of data while in orbit. [9] [10]

COPPER (Close Orbiting Propellant Plume and Elemental Recognition)

COPPER primary mission was to test the abilities of an uncooled microbolometer infrared array for LWIR images (Tau camera from FLIR). This camera has a field of view of 103 x 138[km]. The secondary mission was to take images of the Earth's oceans and atmosphere with no real scientific goal. The mission was a failure since they did not receive any signal. The cause is still unsure. According to Michael Swartwout, assistant professor at St. Louis University: "Our best guess is that it was an unfortunate combination of factors, such as the antennas failing to deploy on time, leading to the solar panels being blocked and the battery draining beyond the point of recovery." [63] [11] [12].

Lemur-1

It has been built by Spire, USA, whose primary mission is a technology demonstration of payloads. It is also a prototype for a future constellation of Lemur-2. In addition, it carries an electro-optical imaging system plus a low resolution IR imaging system as secondary payload. No uploads could be received from the experiments but it successfully sent data from temperature sensors and the magnetometer. [13] [58] [14]

Antelsat

Antelsat was the first Uruguayan satellite. The primary mission was a pure technology demonstration of all subsystems. The spacecraft was also designed to transmit colour and infrared images of the Earth as well as provide services to radio amateurs. The mission was a success for a while. They could upload and process 60 images from both colour and IR cameras. Nevertheless, transmissions ceased unexpectedly April 25, 2015. Some people speculate that Antelstat may have been interfered by some annoying amateur radio. [15] [16] [17] [18] [19]

LilacSat-2

Developed by the Harbin Institute of Technology, China, LilacSat-2 is a low-cost CubeSat for education and amateur radio communication. It is a technology demonstrator which has embarked a LWIR thermal camera as secondary payload. This satellite is still active and operates as expected. [20] [21]

STACEM

STACEM tried to demonstrate that its small multi-spectral payload was able to acquire Earth images in the visible and NIR wavelengths. The final objective was to monitor GHG. The satellite was never operational because its launcher, Super Strypi, broke off shortly after liftoff. It was the first launch of Super Strypi. [22]

Sathyabamasat

Sathyabamasat is a 2U CubeSat developed by Indian students under the technical guidance and support from Indian Space Research Organization. Its mission is to monitor GHG over specific regions and downlink data over Chennai. No information could be found whether the mission was a success or not. Currently, the satellite is still active emitting a weak signal. [23] [24] [25]

Kausat-5

Kausat-5 is a 3U CubeSat developed at the Korea Aviation University in South Korea. The main objectives are to observe the Earth using an IR camera for environmental monitoring and to measure the amount of radiation around LEO. Hence, Kausat-5 has two payloads on board: an infrared imaging system and a Geiger-Müller tube. [26] [27] [56]

Arkyd-6

Arkyd-6 is a 6U CubeSat developed by Planetary Resources. Planetary Resources ultimate objective is to prospect and extract materials from asteroids. Arkyd-6 is just a step towards this objective. The satellite will test systems for the Arkyd-100 CubeSats. The primary payload is a MWIR imaging system sizing 1.5U which is able to precisely measure temperature differences. The MWIR instrument is built around an indium antimonide (InSb) detector. It is cooled thanks to a sterling cryocooler to 77K. The principal MWIR instrument characteristics are:

- **Spectral Range** : 3.4 – 5.1 [μm]
- **Array Size** : 640 x 512 pixels
- **Focal Length** : 200[mm]
- **Ground Footprint** : 19 x 15 [km]
- **GSD** : min 26[m]

Because of its “modest” resolution, it will not be used commercially. Instead, it is more a technology demonstrator to check the instrument in space environment and validate the data processing chain. [62]



FIGURE 4.3: *Arkyd-6*

QBITO (QB50)

QBITO is a 2U CubeSat developed by students of the Polytechnic University of Madrid which is part of the QB50 educational project. The principal objective of this mission is to operate its primary payload (Ion Neutral Mass Spectrometer) in orbit. One of its secondary payloads is a MWIR detector. This uncooled MWIR detector based on a new vapour phase deposited PbSe technology is an experiment to test its behaviour in space condition. This detector has been developed by a Spanish company called NIT (New Infrared Technologies). [28]

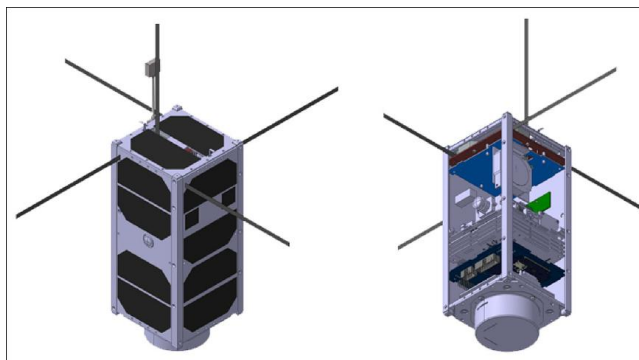


FIGURE 4.4: *QBITO*

Lilacsat-1 (QB50)

Lilacsat-1 has several purposes: education, technology demonstration, upper atmosphere science and amateur radio communication. The satellite is equipped with a thermal infrared camera. Any licensed radio amateur can telecommand the camera to take photos and upload them. There is no scientific objective with this IR camera. [29] [30]

Corvus BC

Corvus BC is a 6U Earth observation CubeSat developed by Astro Digital. It is able to observe in 3 spectral bands: green, red and NIR (0.77 – 0.9 μm) with a swath width of 220[km] and a GSD of 22[m]. Each single frame is 70 Mpx. In the future, a constellation of 10 satellites will be launched. Thanks to this constellation, Astro Digital will be able to provide medium-resolution images of all arable lands around the world each day. There are various applications such as precision agriculture, disaster monitoring, forest management... [64] [31] [32]

Corvus HD

Considered as Corvus BC big brother, it is able to observe in 5 spectral bands: blue, green, red, red edge and NIR with a swath width of 25[km] and a GSD of 2.5[m]. A constellation of 20 Corvus HD will be deployed in a near future. Applications include precision agriculture, urban planning and business intelligence. [33] [64]

COPPER-2

COPPER-2 is a reflight of the 1U COPPER. Nevertheless, COPPER-2 is a 3U CubeSat presenting noticeable differences inside. It integrates a new power system, new processors and an additional camera. Its size has been increased to 3U to accommodate the extra items, wiring/cabling and greater solar cell area. [63] [11] [12]

Parikshit

Parikshit is a 2U Indian CubeSat with two mission objectives: observe the Earth in LWIR region and test a device to deorbit the CubeSat. Parikshit will take images of India thanks to an uncooled microbolometer thermal camera supplied by FLIR. There are various applications: study the ocean surface temperature variations, study the temperature variations for different types of clouds or observe temperature variations between the urban and rural areas caused by GHG. [65] [34] [35]

CaNOP (Canopy Near-IR Observing Project)

CaNOP is a 3U CubeSat developed by Carthage College, Wisconsin. The scientific mission is to image forests and collect reflectance data to understand the large-scale biomass consumption thanks to a NIR (0.7 – 1.1 μm) camera. The sensor is a 1000 x 2000 pixels grid. The 2000 pixels side is divided into 8 spectral bands of 250 pixels per band. The technological goal is to prove that one can obtain data of similar quality with nowadays CubeSats than with older MODIS and LandSat instruments. [36]

CIRAS (Cubesat InfraRed Atmospheric Sounder)

The objective of CIRAS is to develop an infrared atmospheric sounder in a CubeSat. It should be able to obtain comparable quality measurements as AIRS and CrIS instruments. Hence, CIRAS will measure Earth radiation in the MWIR (4.78 – 5.03 [μm]) with a cooled grating spectrometer achieving a spatial resolution of 13.5[km] with a scan range of 165[km]. The telescope focuses the energy onto the entrance slit of the MWIR spectrometer. Then, the spectrometer disperses the energy and produces a 2D image with one spatial direction (504 pixels) and the other spectral (625 channels). The spectrometer and the detector are respectively cooled to 190K and 120K. The optics is cooled using a Ricor cryocooler. [37]

Remark : building of the spacecraft has not yet begun.

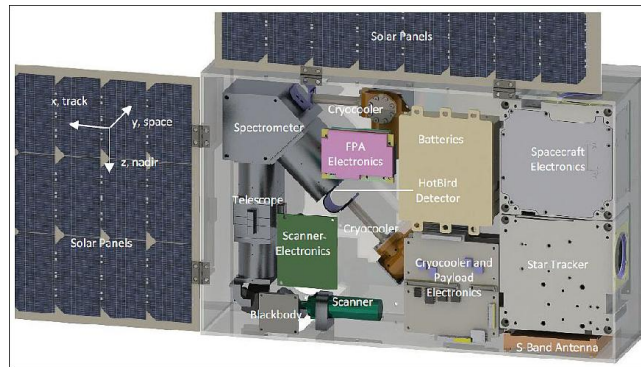


FIGURE 4.5: *CIRAS*

TRISAT

The principal objective of this Slovenian CubeSat is educational. But TRISAT mission also contains a technological aspect: to perform in-orbit demonstration of the EPS, COM and OBC subsystems. The primary payload is a SWIR (0.95 – 1.67 [μm]) multispectral imager with a swath width of 67[km] and a GSD of 105[m]. [38]

CIRiS (Compact Infrared Radiometer in Space)

CIRiS is a thermal infrared radiometric imaging instrument being developed by Ball Aerospace, USA. Its primary mission is a technology demonstration to adapt an existing instrument to be compatible with a CubeSat platform and validate this instrument performance in LEO. It is a demonstrator for future Landsats for instance. The data collected may be used for diverse applications including water resource, drought management as well as land use and vegetation monitoring. [39] [40] [41]

Arkyd-100

Arkyd-100 is the next generation of CubeSat coming right after Arkyd-6. Developed by Planetary Resources, it is a 12U CubeSat. Arkyd-100 main objective is to deliver valuable data for precision agriculture. Hence, a constellation of 10 satellites (CERES) is needed as well as a better resolution compared to Arkyd-6. The constellation will be able to provide data of a specific location twice in a day. In order to achieve a better GSD, larger optic diameter is required which can only fit in a 12U CubeSat. The MWIR payload main characteristics are:

- **Spectral Range** : 3.4 – 5.1 [μm]
- **Array Size** : 640 x 512 pixels
- **Focal Length** : 720[mm]
- **Optical Diameter** : 8"
- **Ground Footprint** : 19 x 15 [km]
- **GSD** : 15[m]

The larger form-factor is also used to allow greater solar cell area, which can provide more power used to increase the computational capabilities. This increase of size also enables a higher bandwidth communication. Aside from that, the MWIR instrument is the same as in Arkyd-6. Additionally, Arkyd-100 will also be equipped with a small propulsion technology demonstration and a VIS-NIR (0.4 – 0.9 [μm]) hyperspectral imager with 40 channels. The CERES constellation targets other markets than agriculture. For example, it could provide data for the oil and gas industry, pollution monitoring, forest fire early detection, forest management, toxic algae bloom detection... [62]



FIGURE 4.6: *Arkyd-100*

Golden Eagle 1

It was a 1U CubeSat developed by Marquette University, USA. The primary objective was educational. GE 1 had two small payloads: one thermal infrared and one visible camera. The project seems to be cancelled maybe due to the deadline imposed. [42] [43] [44]

4.2.1 Conclusion

22 past, current and future CubeSats observing the Earth in the infrared have been reported. Only 4 of them have a MWIR detector as payload. Nearly half of these 22 CubeSats are technology demonstrators. Their goal is to test their payload in space environment. The other half has scientific or commercial objectives. Some examples of applications are: GHG or disasters monitoring, ocean surface temperature study, precision agriculture...

Only 8 of these CubeSats have been launched to this day. Among them, 4 missions failed (SRMsat, COPPER, Lemur-1 and STACEM). WE-WISH, Antelsat and Lilacsat-2 were able to downlink infrared images but none of them had real scientific objectives. They were technology demonstrators. No information could be found on Sathyabamasat.

Concerning the future missions, 8 of them are planning to use the infrared images collected for scientific or commercial purposes. They are Kausat-5, Corvus BC, Corvus HD, Parikshit, CaNOP, CIRAS, CIRis and Arkyd-100. The smallest one is Parkshit and sizes 2U. All of them have active ADCS actuators such as reaction wheels and magnetorquers. A fine pointing accuracy is required to take images of precise zones of the Earth. This fine pointing is not achievable with passive ADCS actuators. These active ADCS actuators need various amounts of power to operate.

The more data they have to downlink, the higher frequency communication band is used. For instance, Parikshit will only take images over certain regions of India. They do not need a very high frequency communication band. The UHF band at 437.8[MHz] is sufficient. On the other hand, Arkyd-100 will take images all around the world with a great resolution. In order to downlink this large amount of data, an X-band (8 -12 [GHz]) must be used. One must pay attention that downlinking data with a high frequency communication band needs a lot of power. That is why Parikshit could not use an X-band for example.

The ideal orbit for Earth observation with CubeSats is a low circular Sun-synchronous orbit. Indeed, one needs a LEO to maintain acceptable spatial resolution. It should be circular to have the same image scale anywhere on Earth. Finally, a Sun-synchronous orbit is desirable since images taken on multiple overpasses are more comparable. In this way, no correction for illumination angle variations is required. Each 22 satellites are in LEO but only 7 of them are in the ideal low quasi-circular Sun-synchronous orbit. The others are in LEO with various inclinations or in elliptical SSO. For most of them, the orbit was not chosen freely but imposed by their launcher. Furthermore, some of these CubeSats do not have an infrared instrument as primary payload and may need another kind of orbit for their main mission. That is why all satellites are not on low circular SSO.

To conclude, no CubeSat has already achieved to collect infrared images of the Earth and use them for scientific or commercial purposes. In the future, only 8 of them are planning to do so. Among these 8 satellites, only 3 will take MWIR images. They are Arkyd-6, CIRAS and Arkyd-100. Indeed, the Arkyd mission is very close to OUFIT-Next mission: collect MWIR images of the Earth for agriculture purposes (hydric stress detection of crops). Eventually, one should stress that there are strong relations between the size, power consumption, ADCS and communication bands used.

Chapter 5

Mission analysis

In general, the orbit is chosen so that the satellite can perform its mission optimally. This choice is also driven by the design requirements. It is thus a crucial decision that will impact the whole mission. Nevertheless, in the case of OUFTI-Next, the orbit cannot be chosen freely as CubeSats are usually secondary payloads in launchers. Thus, the orbit is imposed by the main payload in the launcher. There is one exception to this rule: the ISS orbit. CubeSats are sent to the ISS and they are launched in space thanks to the orbital deployer.

For this reason, the following discussion is based on several plausible orbits. These orbits are the ISS orbit and several SSO ranging from 400 to 800[km]. First, these orbit properties are detailed then, an analysis of the revisit time and lifetime is performed. This mission analysis will be useful for designing OUFTI-Next platform.

5.1 Orbits

In the frame of this mission, a LEO is desirable not only for design requirements but also to keep the GSD below 100[m]. LEO are orbits around the Earth ranging between 160 and 2000[km]. Different kinds of LEO are possible: ISS, circular, elliptical, SSO... Some of them are convenient and others not. A circular orbit would be appropriate to facilitate the comparison between image scales anywhere on Earth. A highly elliptical orbit is thus inappropriate. A weakly inclined orbit does not offer the possibility to pass over high-latitude regions and can be dismissed. Eventually, a SSO orbit would be optimal for the following reason: a satellite in SSO passes over the equator each time at the same solar time. It means that images taken on multiple overpasses over a region are more comparable since the illumination is nearly constant. To sum up, inclined circular LEO, SSO and ISS orbit will be studied with a particular attention dedicated to the two latter ones for practical reasons. Indeed, the cheapest launch is from the ISS and is very common for CubeSats.

5.1.1 Orbits characteristics

The goal of this part is to present the main characteristics of the selected orbits which are key-drivers for the platform design. The visibility has been computed for a ground station based in Sart Tilman which is able to communicate with OUFTI-Next when it is 10° above the horizon. Mean visibility duration is essential for the data and link budgets to evaluate how much data can be downlinked per day. These data and link budgets have then a major influence on the power budget. Indeed, the power consumption increases with the communication duration. The worst case for the power budget is consequently when there are communications during all the maximum visibility duration.

The eclipse time is another important parameter. When the satellite is hidden by the shadow of the Earth, solar panels do not produce power anymore. Batteries are then used to deliver power to the CubeSat subsystems during all the eclipse duration. The design of the batteries are therefore in relation with eclipses. The worst case being when the eclipse duration is the longest.

The orbits studied are an ISS orbit with its initial orbital elements displayed in Table 5.1, 4 circular orbits between 400 and 800[km] with a 70° inclination and 4 SSO between 400 - 800[km] with 12h and 18h LTDN.

	ISS
Semi-major axis	$a = 6731.32[km]$
Inclination	$i = 51.65^\circ$
Eccentricity	$e = 0.0017$
RAAN	$\Omega = 224.56^\circ$
Argument of periapsis	$\omega = 51.65^\circ$
True anomaly	$\nu = 224.56^\circ$

TABLE 5.1: *ISS initial orbital elements*

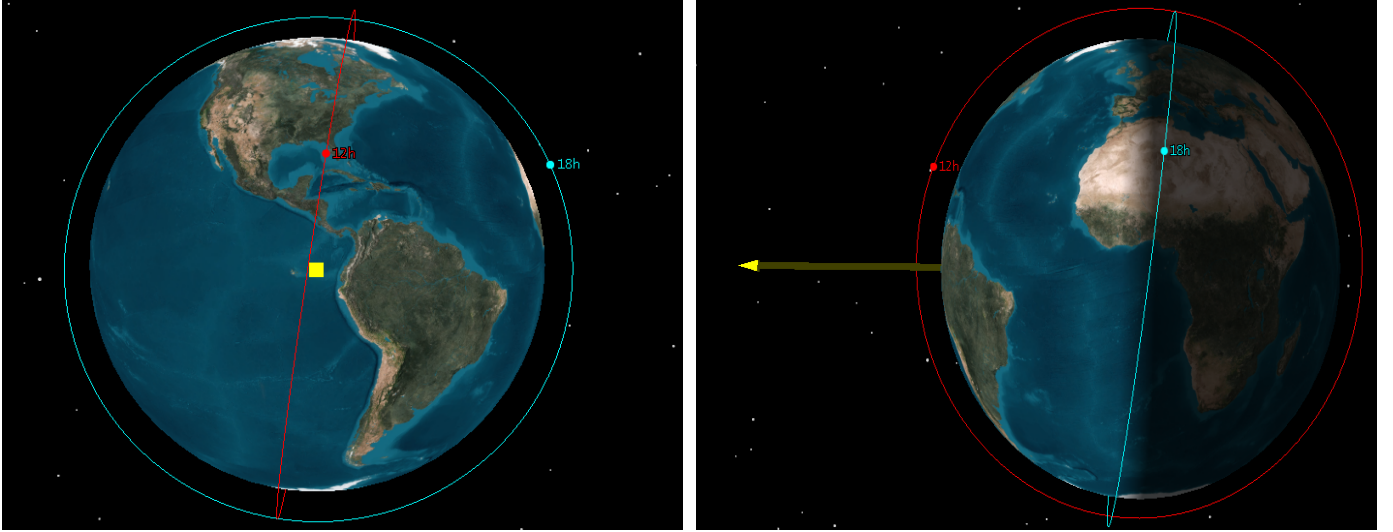
A Sun-synchronous orbit combines altitude and inclination in such way that the satellite crosses a given point of the Earth at the same local solar time. It also means that the plane of a SSO always makes a constant angle with respect to the Sun direction. This is achieved by having the orbital plane precess by 0.9856° ($\simeq 360^\circ/365.25$) each day eastward in order to take into account the Earth rotation around the Sun [45]. This precession is due to the oblateness of the Earth and is known as the J2 effect. Mathematically, this precession is quantified by:

$$\dot{\Omega}_{J_2} = -\frac{3}{2} \frac{\sqrt{\mu} J_2 R^2}{(1 - e^2) e^2 a^{\frac{7}{2}}} \cos(i) \quad [rad/s] \quad (5.1)$$

Where Ω , a , e and i are orbital elements, R is the radius of the Earth, μ is the Earth gravitational constant and $J_2 = 0.001082$ is the constant taking into account the Earth oblateness.

Thanks to this formula, the inclination can be computed to obtain a precession of 0.9856° per day. For altitudes between 400 and 800[km], i must be approximately equal to 98° . A SSO is thus a near polar orbit.

The longitude of descending node (LTDN) is the time at which the satellite crosses the equator when descending. A LTDN of 12h and 18h are special cases of SSO. For noon/midnight orbit (LTDN 12h), the spacecraft crosses the equator at noon when descending and at midnight when ascending. For dawn/dusk orbit (LTDN 18h), the orbital plane of the satellite is always nearly perpendicular to the Sun direction which implies that it always sees the Sun. It is true for nearly 9 months in a year. For approximately 3 months, there are short eclipses. Figure 5.1 displays views of these special orbits at an altitude of 800[km]. The yellow axis is the Sun direction. The orbit in red is the noon/midnight (LTDN 12h) orbit while the blue one represents the dawn/dusk (LTDN 18h) orbit.

FIGURE 5.1: *SSO 800[km] with LTDN 12h and 18h*

Tables 5.2 and 5.3 present the important characteristics of the orbits detailed above. These values have been computed for the whole year 2017. Nevertheless, one should not observe large differences from one year to another so these results can be considered as valid for the future.

Circular	ISS	70° 400	70° 600	70° 800
Period	91.6	92.6	96.7	100.9
Max visibility	6.2	6.5	8.8	11.0
Mean visibility	5.3	5.1	6.8	8.0
Max eclipse	36.1	35.8	35.2	34.9

TABLE 5.2: *Main characteristics of circular orbits [min]*

SSO	400 12h	600 12h	800 12h	400 18h	600 18h	800 18h
Period	92.6	96.7	100.9	92.6	96.7	100.9
Max visibility	6.3	8.6	10.6	6.3	8.6	10.6
Mean visibility	5.0	6.7	8.3	5.0	6.7	8.3
Max eclipse	35.7	35.1	34.8	19.6	16.0	12.7

TABLE 5.3: *Main characteristics of SSO [min]*

Obviously, the period and the visibility duration increase with the altitude. One interesting thing is that the visibility duration does not change with the LTDN. Furthermore, visibility duration is nearly the same for SSO and circular orbits at the same altitude. Also, the eclipse time for dawn/dusk SSO is very small. As discussed earlier, this is linked to the position of the orbital plane compared to the Sun. Furthermore, there are eclipses only for 3 months in a year.

5.1.2 Space environment

A satellite in LEO is subjected to numerous hazards that are not encountered on Earth. This is due to its environment which is drastically different. Understanding this hostile environment is a key point to minimize its effects. OUFTI-Next should perform laboratory tests to design the platform correctly against these hazards.

First of all, the residual atmosphere at these altitudes contains **oxygen atoms** which impact at high speed the CubeSat due to its own velocity (7.67[km/s] for the ISS). Oxygen atoms are highly reactive and cause damages through chemical reactions to the spacecraft. Satellites are also surrounded by charged particles composing the **plasma**. These particles charge electrically the spacecraft. It eventually leads to electric discharges which can cause electronic issues for instance. **Outgassing** is another key element to stand at attention. It is the release of a gas, which was previously absorbed in some material, due to the vacuum conditions. Outgassing products can condense onto optical elements or solar cells and thus, decrease their efficiency. For this reason, some materials are prohibited for space applications such as composite materials. [46]

Space **radiation** consists essentially of ionizing radiation in the form of high-energy charged particles. There are three natural sources of space radiation: trapped radiation, galactic cosmic radiation and solar particle events. Due to the relatively low altitude of the selected orbits, OUFTI-Next should not be influenced by trapped protons and electrons from the inner Van Allen Belt except near the South Atlantic Anomaly or when the solar activity is intense.

Contrariwise, it could be subject to galactic cosmic radiation carrying ionized atoms ranging from a proton to a uranium nucleus. The collision of these particles with the spacecraft is unlikely because their flux level is very low. However, they can produce intense ionization as they pass through the spacecraft. These cosmic rays are stopped by the magnetic field but they have free access over polar regions.

Furthermore, the spacecraft can be subject to solar particle events. They are electrons, protons, alpha particles and heavier particles ejected by the Sun. Coronal mass ejections which are huge bubbles of plasma are particularly dangerous for satellites. [47]

There are also more and more concerns about **space debris**. Space debris include both natural (meteoroids) and artificial objects. While meteoroids are in orbit around the Sun, artificial debris orbit the Earth. Even if they are usually small, the danger comes from their high relative velocity. Nevertheless, more than 20,000 pieces of debris have been reported larger than a baseball. In LEO, the risk of a collision with artificial debris is higher than with meteoroids. Unfortunately, it is not possible for CubeSats to protect themselves against these debris once in orbit. [48]

5.2 Revisit time

The goal of this section is to predict OUFTI-Next revisit time over a particular location of the Earth for different orbits. The orbits studied are: an ISS orbit, a 400[km] SSO and an 800[km] SSO. The particular location is the city of Casablanca. It was chosen arbitrarily in Morocco. All simulations were performed using STK and the satellite field of view (FOV) is set to 11.46° [54]. This information is essential to know how often OUFTI-Next can take images over a particular place.

5.2.1 ISS orbit

During one year, OUFTI-Next has 71 times Casablanca in its FOV. It means that there is a pass every 5.14 days on average. Nevertheless, this average does not mean anything since general patterns can be deduced. Figure 5.2 shows the passes (vertical red bars) over time.

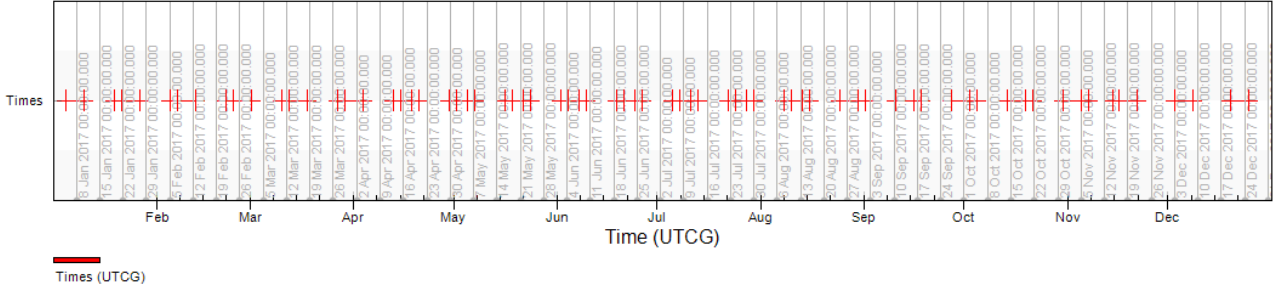


FIGURE 5.2: *Revisit time for ISS orbit*

Between January 10 and December 2, passes always go by 3 or 4. These groups of passes have an exact duration of 7.54 days. Between these groups of passes, there are always 9.17 days without any pass.

Between December 2 and January 10, passes always go by 2 and have an exact duration of 5.57 days. Between these groups of passes, there are always 11.14 days without any pass.

General statistics on passes are the following:

- Min duration: 6.0[s]
- Max duration: 21.3[s]
- Mean duration: 16.5[s]
- Total duration: 1168.4[s] = 19.5[min]

5.2.2 SSO 400[km]

OUFTI-Next has 57 times Casablanca in its FOV when placed on a 400[km] SSO. So there is one pass every 6.4 days on average. Once again, this value is meaningless and general patterns can be deduced. The passes over time are displayed in Figure 5.3.

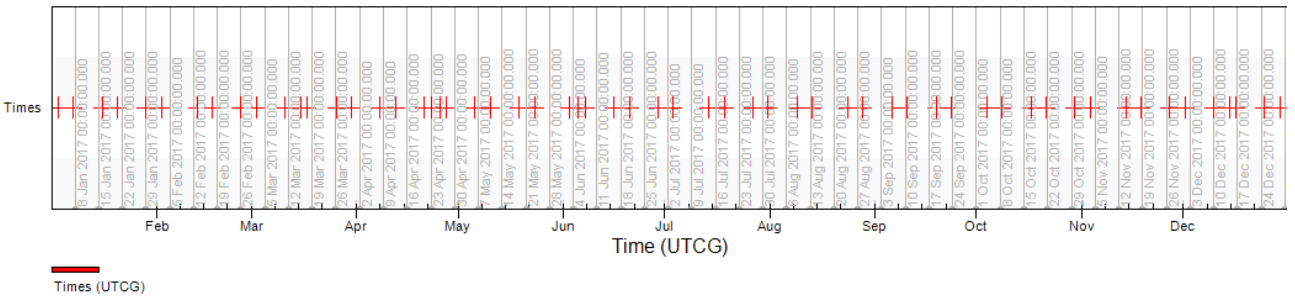


FIGURE 5.3: *Revisit time for a 400[km] SSO*

Generally, passes go by pairs but they can be gathered by 3 or even by 4. These groups of passes have a duration of 4.53 days, but in 3 cases only the duration is exactly 6.52 days. Between these groups of passes, there are 8.48 or 10.47 days without any pass.

Statistics on these passes are:

- Min duration: 1.3[s]
- Max duration: 22.7[s]
- Mean duration: 17.4[s]
- Total duration: 1028.5[s] = 17.1[min]

5.2.3 SSO 800[km]

Revisit time for a 800[km] SSO has already been computed to create a constellation (see Section 2.4). Therefore, a short summary of the results obtained is presented here.

There are 104 passes over Casablanca in a year if OUFTI-Next is on an 800[km] SSO. So, there is a pass every 3.51 days on average. A general pattern could also be deduced based on Figure 2.5. Passes always go by groups of 8 and inside these groups, passes go by pairs.

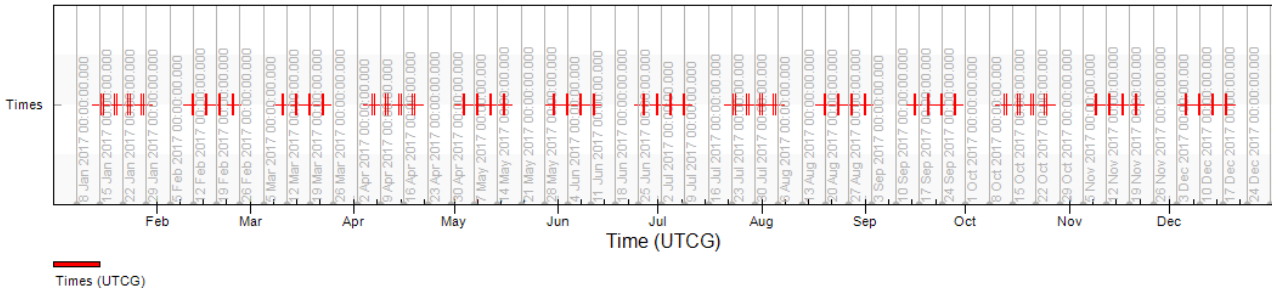


FIGURE 5.4: *Revisit time for a 800[km] SSO*

Finally, statistics on these passes are as follows:

- Min duration: 15.7[s]
- Max duration: 48.8[s]
- Mean duration: 38.5[s]
- Total duration: 4003.6[s] = 66.7[min]

5.2.4 Conclusion

This analysis is crucial to determine how many times in a year OUFTI-Next is able to take images of a particular location on Earth. It also permits to determine for how long this place can be observed. A satellite orbiting a 800[km] SSO is the most convenient as it can observe a specific place for the longest time. Then, comes the ISS orbit closely followed by the 400[km] SSO.

This analysis was performed for the city of Casablanca (33.56°N 7.59°W). Nevertheless, in the case of the SSO, similar results would be obtained for any location on Earth situated between 60°S and 60°N in latitude. This is due to the relative constant slope of the SSO ground tracks between these latitudes. Concerning the ISS orbit, the same kind of results would be obtained for latitudes ranging between 30°S and 30°N . Ground tracks of these 3 orbits can be visualized on Figure 5.5.

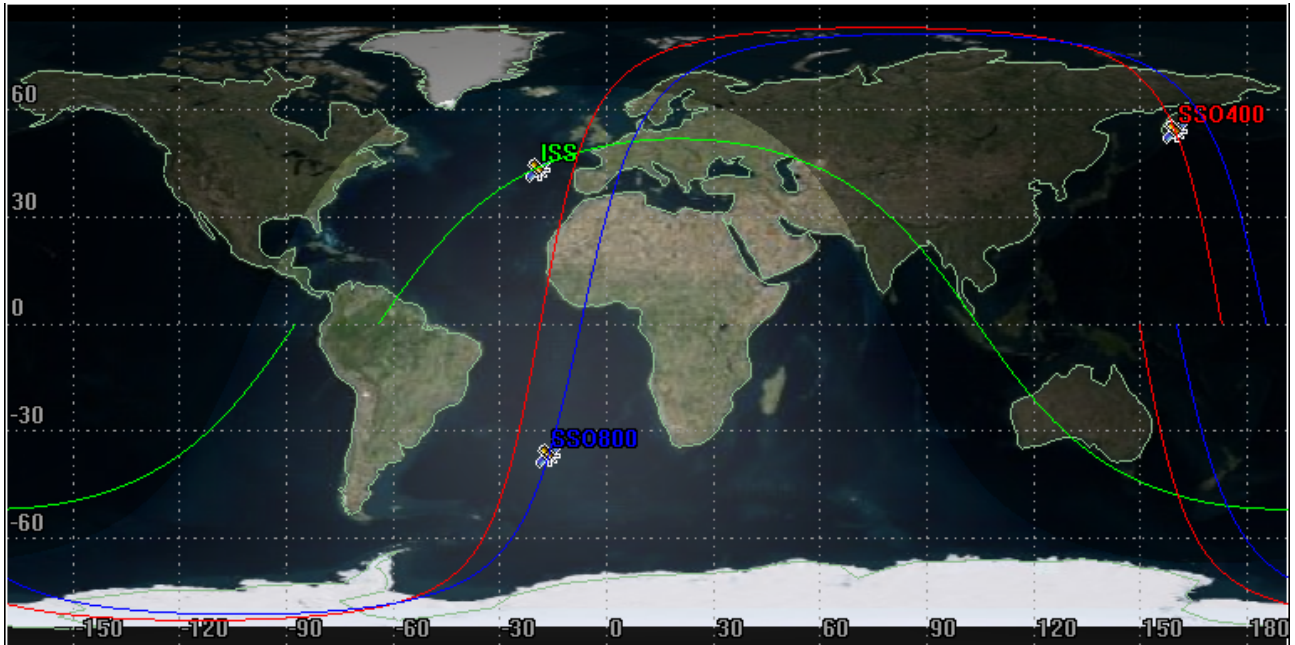


FIGURE 5.5: *Ground tracks of ISS, 400[km] SSO and 800[km] SSO*

5.3 Lifetime

The orbital decay of a satellite in LEO is principally due to the drag caused by the residual atmosphere. The effect of the drag is to contract the semi-major axis due to mechanical energy dissipation. For an elliptical orbit, the apogee height decreases far more rapidly than the perigee height which remains relatively constant [57]. SRP and other perturbations also cause a satellite to decay.

Evaluating the lifetime of a satellite is an essential step for its design. For example, if a satellite lifetime prediction is 9 months, it is then useless to design systems able to operate for 20 years. Simulations of OUFTI-Next lifetime have been performed with the STK tool *lifetime* for different orbits and CubeSat orientations. The different parameters influencing the orbital decay are studied. Then, a comparison between two real missions and simulations is performed to assess the accuracy of present results. Eventually, a short description of the 25 years rule is presented.

5.3.1 Parameters influencing the orbital decay

Several parameters have impacts on a satellite lifetime. It is important to understand how these parameters influence the orbital decay to evaluate them as accurately as possible and eventually obtain a trustworthy prediction. For CubeSats, the main parameters are:

- Orbit
- Atmospheric model
- Drag coefficient C_D
- Drag area
- Solar flux
- Mass

Indeed, SRP has a minor influence on Cubesats orbital decay because of their small area exposed to the Sun. It rather plays a major role on satellites with large deployable solar panels.

All listed parameters influence the drag on a CubeSat. Drag creates an acceleration in the opposite direction of the spacecraft velocity. This acceleration is given by the following formula:

$$\ddot{\mathbf{r}}_D = -\frac{1}{2}C_D \frac{A}{m} \rho v_r^2 \frac{\mathbf{v}_r}{v_r} \quad (5.2)$$

where C_D is the drag coefficient, A the drag area, ρ is the atmospheric density which is linked to the altitude, atmospheric model and solar flux, m is the mass of the satellite. \mathbf{v}_r is the velocity with respect to the atmosphere and is computed thanks to:

$$\mathbf{v}_r = \mathbf{v} - \omega_{\oplus} \times \mathbf{r} \quad (5.3)$$

where \mathbf{v} is the inertial velocity and ω_{\oplus} is Earth's angular velocity.

Orbit

Various orbits are studied: an ISS orbit and several SSO at different altitudes. For these orbits, the main parameters influencing the orbital decay are the altitude, inclination and LTDN.

Atmospheric density models

Ten atmospheric density models are available in STK. They all differ by their level of complexity, number of parameters, kind of model implemented (analytical, empirical...), etc. For the following simulations, 3 atmospheric density models are used:

- **Jacchia 1971**: "Computes atmospheric density based on the composition of the atmosphere, which depends on the satellite's altitude as well as a divisional and seasonal variation" [49]. It is the standard model for long-term predictions.
- **NRLMSIS 2000**: "Empirical density model developed by the US Naval Research Laboratory based on satellite data. Finds the total density by accounting for the contribution of N, N₂, O, O₂, He, Ar and H. Includes anomalous oxygen" [49]. It is the most evolved model which should give the best predictions.

- **1976 Standard:** "A table look-up model based on the satellite's altitude. This model is oversimplified and not trustworthy" [49]. It is used here to emphasize the impact of the atmospheric model on the lifetime prediction.

Drag coefficient C_D

The drag coefficient is a dimensionless parameter. It is difficult to estimate for satellites because it depends on numerous parameters. For this reason, the best practice is to use empirical results. Figure 5.6 displays drag coefficients for 1U and 3U CubeSats. It is based on 45 observed decays.

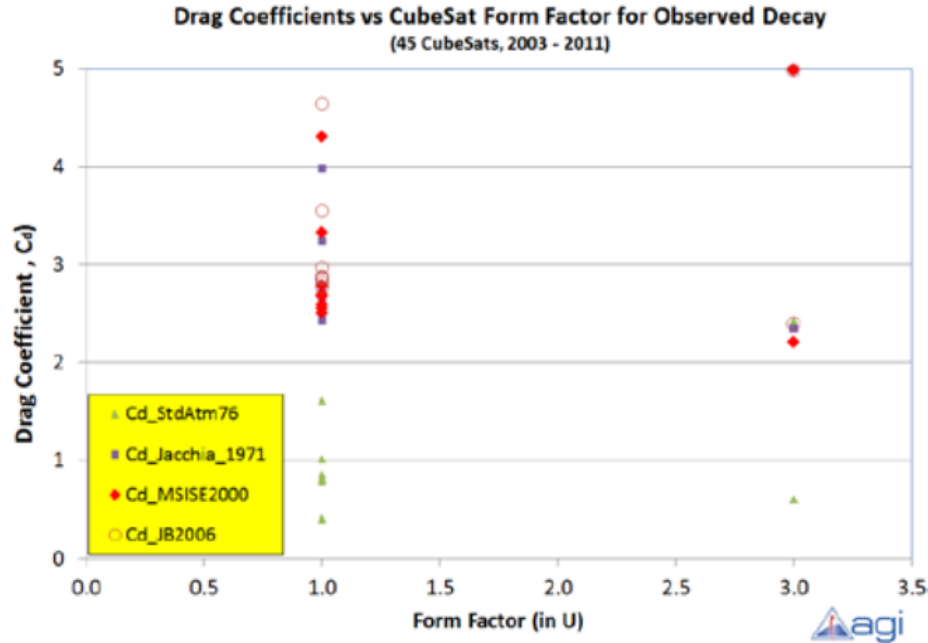


FIGURE 5.6: *Drag coefficient vs CubeSat form factor for observed decay*

Based on this plot and OUFTI-1 drag coefficient analysis, $C_D = 2.6$ is used for simulations with 1U CubeSats. Still based on this plot and on a general recommendation, $C_D = 2.2$ is used for 3U CubeSats. [53]

Drag area

Drag area is another name for the cross section area. It varies depending on the satellite attitude. For OUFTI-Next, two different configurations have been proposed: one where the short face points to the NADIR direction and one where the long face points to this direction. Hence, the drag area for the first case (telescope on $-z$ face) is equal to $0.03[m^2]$. For the case where the telescope is on $+y$ face, it is equal to $0.01[m^2]$.

When the attitude of the satellite is unknown, one should compute a mean drag area. A composite flat-plate model can be used. It has been demonstrated that for a plane sheet of area S , its mean drag area is $S/2$ when all possible viewing angles have been averaged. For cubic or rectangular parallelepiped satellites, this mean cross section area is [53]:

$$A_{mean} = \frac{1}{2}(S_1 + S_2 + S_3) \quad (5.4)$$

So, it is equal to $0.015[m^2]$ for a 1U and $0.035[m^2]$ for a 3U CubeSats with unknown attitude.

Solar flux

The solar flux influences the atmosphere density and increases with the solar activity. When the solar flux is high, it increases the density of the atmosphere upper layers and inversely. More precisely, it is the solar flux at 10.7cm that is used to compute the atmospheric density because it is an excellent indicator of solar activity. Sun's activity has an 11-year period. The current solar cycle began in 2008 and should end in 2019. The F10.7cm clearly shows this 11-year period (Fig. 5.7).

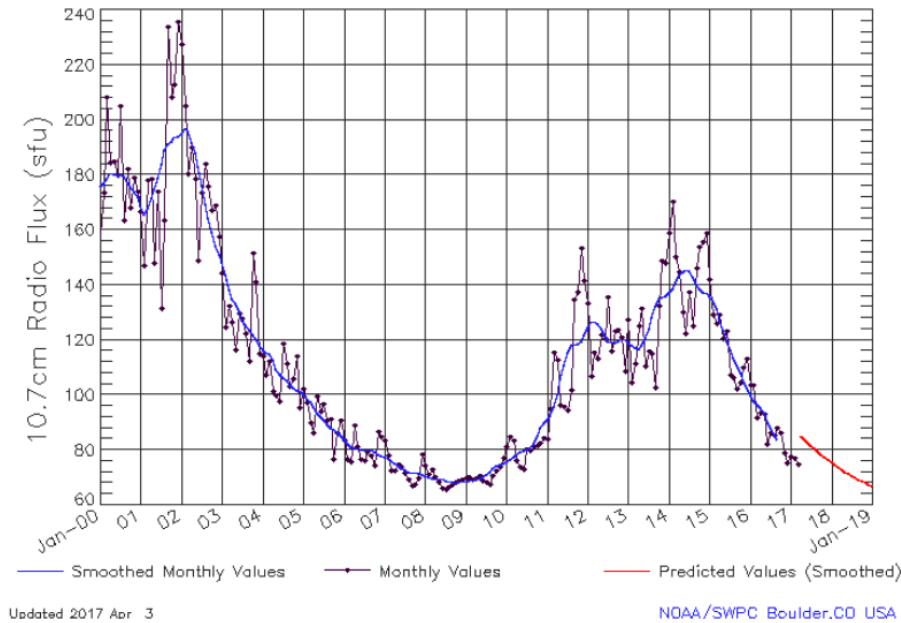


FIGURE 5.7: *F10.7cm emissions*

Thanks to this graph, it can also be assessed that a satellite launched in 2014 has a shorter lifetime than if it was launched in 2016 for instance. Indeed, orbital decay for LEO satellites is highly dependent on this parameter.

Mass

Finally, the mass of the satellite is another key parameter. The momentum of the satellite increases with its mass and the negative acceleration induced by the drag is decreased. In other words, orbital decay decreases when mass increases. For OUFTI-Next, the mass is set to 4.0[kg] which is the maximum mass allowed for a 3U CubeSat.

5.3.2 OUFTI-Next lifetime

Table 5.4 presents the lifetime prediction of OUFTI-Next for an ISS orbit (401 x 409[km]), a 400[km] and 800[km] SSO, 12h LTDN. Three attitude controls are simulated:

- Mean: unknown attitude control
- -z: short face pointing to the NADIR direction
- +y: long face pointing to the NADIR direction

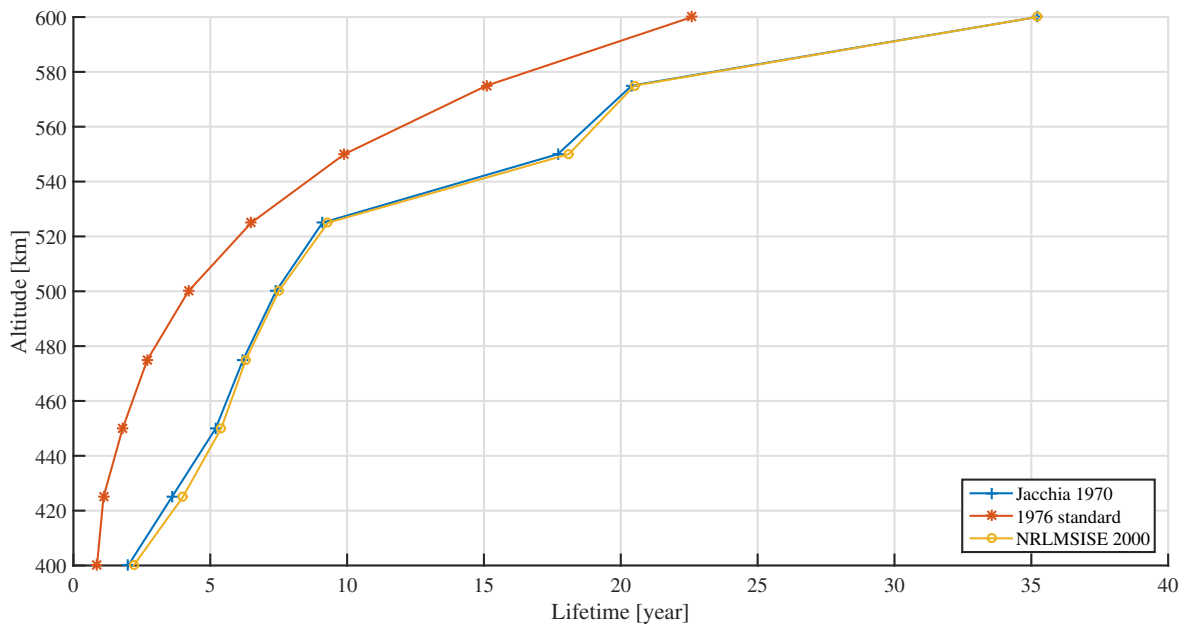
As discussed earlier, C_D is set to 2.2 and the mass to 4.0[kg]. The simulations begin January 1, 2017.

Orbit	Orientation	Drag area [m ²]	NRLMSISE 2000 [year]	1976 Standard [year]
ISS	mean	0.035	1.8	0.7
ISS	-z	0.03	2.0	0.8
ISS	+y	0.01	5.0	2.2
SSO 400	mean	0.035	1.9	0.62
SSO 400	-z	0.03	2.2	0.72
SSO 400	+y	0.01	5.4	2.2
SSO 800	mean/-z/+y	0.035/0.03/0.01	>100	>100

TABLE 5.4: *OUFTI-Next lifetime*

Depending on the orientation, the lifetime prediction of OUFTI-Next is between 1.8 and 5 years for the ISS orbit with *NRLMSISE 2000* model. For the 400[km] SSO, it varies between 1.9 and 5.4 years. Eventually, it exceeds 100 years for a 800[km] SSO.

When comparing results for both atmospheric density models, differences are clearly huge. *1976 Standard* model is systematically too pessimistic and this model should be avoided as demonstrated here after. Figure 5.8 compares the lifetime predictions for 3 different atmospheric models including the widely used *Jacchia 1970*, the most evolved *NRLMSISE 2000* and the oversimplified *1976 Standard*. The orbits are SSO, 12h LTDN with different altitudes. The CubeSat is OUFTI-Next with the short face pointing to the NADIR direction.

FIGURE 5.8: *Lifetime prediction with three different atmospheric density models*

Jacchia 1970 and *NRLMSISE 2000* give similar results with differences that do not exceed a fraction of year. On the other hand, *1976 Standard*, always underestimates the lifetime by several years. It is now clear that some atmospheric density models such as *1976 Standard* must not be used.

Until now, only 12h LTDN SSO have been studied. Indeed, orbital decay also depends on LTDN. Figure 5.9 displays the evolution of a 3U CubeSat lifetime (same configuration as above) in function of the LTDN with 400[km] SSO. This time, the atmospheric density model used is *Jacchia 1971* which is the evolution of *Jacchia 1970*

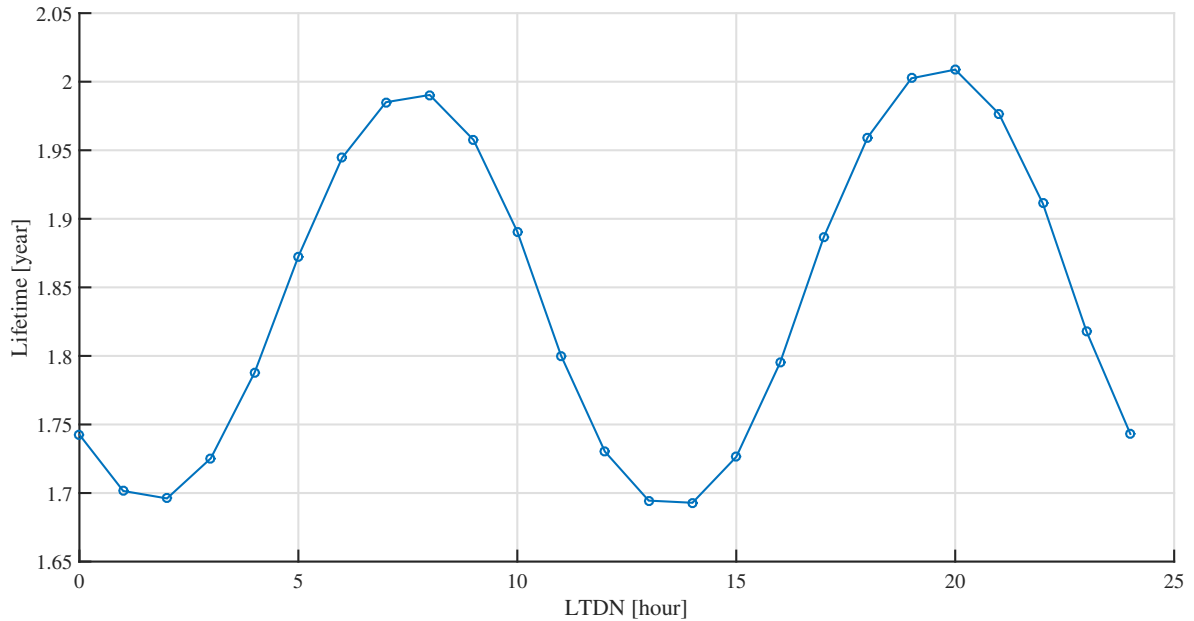


FIGURE 5.9: *Lifetime prediction in function of LTDN*

Lifetime is maximum around 8h and 20h LTDN. It is minimum at 2h and 14h LTDN. Indeed, there is day-to-night variation in the atmosphere density. The upper atmosphere which is sunlit has a greater density than the part of the atmosphere which is in the night. The solar flux produces an atmosphere bulge of greater density. This *diurnal bulge* points in the sky at approximately 30° east of the Sun. Hence, the density of the upper atmosphere is greater around 14h local solar time. [57] [50]

It is exactly what is observed in Figure 5.9. When a satellite is in a 14h or 2h LTDN SSO, it crosses the diurnal bulge at every revolution so that, its lifetime is reduced. On the contrary, when the satellite orbits are far away from the bulge ($LTDN \approx 8h$ or $20h$), it has a longer lifetime.

5.3.3 Validation of the results

Even if models are really sophisticated, lifetime prediction still provides approximate results. This is why one should compare the results of simulations to real cases. Two real missions were chosen: Fitsat-1 and TechHedSat. Both 1U CubeSats were launched from the ISS on 4 October 2012. Tables 5.5 compares the observed lifetime with the lifetime prediction for Fitsat-1 and TechHedSat. Unfortunately, the attitude control is unknown. For this reason, 3 different simulations were performed for each satellite with different attitude controls. These 3 configurations correspond to the least ($0.01[m^2]$), mean ($0.015[m^2]$) and largest drag area ($0.017[m^2]$). The density model used is *NRLMSISE 2000* and $C_D = 2.6$. Lifetime values are given in days.

Satellite	Mass [kg]	Real lifetime	0.01[m ²]	0.015[m ²]	0.015[m ²]
FitSat	1.33	273	311	199	178
TechHedSat	1.2	213	275	181	161

TABLE 5.5: *Lifetime comparison with real missions [days]*

For both satellites, the real lifetime is between the more optimistic and pessimistic predictions. It means that the simulations give realistic results but it is not possible to assess its accuracy. Nevertheless, one should remember that evaluating the orbital decay of satellites with a great precision is really difficult. Hence, it is already not bad at all to have an approximate idea of OUFTI-Next lifetime.

5.3.4 25 years rule

Space debris is a theme which is more and more evoked in the small satellite and CubeSat community. There are guidelines, recommendations, etc. to mitigate the amount of debris in LEO but so far, only few missions respect them. Perhaps because these recommendations are not legally binding on the international level...

The best-known rule is usually called the *25 years rule*. It states that a satellite cannot occupy a LEO for more than 25 years after operating. But when looking back to Figure 5.8, one can remark that if OUFTI-Next is placed on a SSO higher than 600[km], it will not decay before 25 years, violating consequently the 25 years rule.

If such orbits are considered, technical solutions to decrease the orbital lifetime of OUFTI-Next may perhaps be considered. Since most CubeSats and small satellites do not have thrusters to change their orbit, other solutions must be implemented. One of them being to deployed sails after the completion of the mission. Sails would increase the drag area and accelerate the orbital decay. Other solutions such as tethers may be considered. [53]

5.3.5 Conclusion

Orbital decay of CubeSats in LEO is principally due to drag. Several parameters have an influence on drag. Most of them are really complicated to evaluate and others, such as the solar flux must even be predicted. For these reasons, the predicted orbital lifetime of OUFTI-Next is only an approximation.

If OUFTI-Next was launched in 2017, it would decay between 1.8 and 5.4 years on an ISS orbit or 400[km] SSO depending on its attitude control. Its orbital lifetime should increase if it is launched in 2019 because the solar activity will be minimum. These approximate results are plausible since they match with data from real missions. Eventually, if a SSO above 600[km] is considered, solutions should be found to comply with the 25 years rule.

5.4 Summary

To sum up this mission analysis, there are two kinds of orbits which are appropriate and plausible: an ISS orbit and SSO ranging from 400[km] to 800[km]. The ISS orbit is the easiest to reach because OUFTI-Next can then be launched from the ISS. Besides, 44% of LEO satellites are in SSO. Therefore, SSO are also accessible.

Concerning the visibility, an ISS orbit offers more or less the same visibility time as a SSO at the same altitude (≈ 5 [min]). Then, the higher is the altitude, the longer is the visibility duration (8.3[min] on average for an 800[km] SSO). Nevertheless, the GSD increases with the altitude. There is thus a compromise to find between visibility time and GSD even if the spatial resolution is not that important for a technology demonstrator.

The revisit time over Casablanca has been computed with a FOV of 11.46° . For an ISS orbit, 400[km] and 800[km] SSO, there are respectively 71, 57 and 104 passes over a year. Similar results for SSO should be found for every location on Earth between 60°S and 60°N .

If OUFTI-Next was launched in 2017, it would have a lifetime between 1.8 and 5.0 years in ISS orbit depending on its orientation. In a 400[km] SSO, 12h LTDN, its lifetime would vary between 1.9 and 5.4 years. Above 600[km], it would exceed 25 years. If launched in 2019, these values should be revised upwards due to the low solar activity.

Chapter 6

OUFTI-Next design

Based on the mission analysis, it is possible to create a preliminary design of OUFTI-Next and assess if the mission is feasible under the working assumptions. First, a COTS ADCS compatible with the 3U CubeSat form-factor with specific characteristics driven by the detector must be found. To this end, a market survey is proposed. Then, data & link budgets are performed. Afterwards, the power generated by the CubeSat for different orbits and orientations is computed. These results are used to perform power budgets. Eventually, the mass and space occupation are evaluated. At the end of this chapter, one can deduce if OUFTI-Next mission is feasible under the working hypothesis.

6.1 Attitude Determination Control Subsystem

An appropriate ADCS must be chosen to perform the mission correctly. A precise attitude control is indeed required for imaging. To this end, two different techniques can be implemented. The first technique is called *Time Integration Delay (TDI)* scanning and the second is *target pointing strategy*.

Attitude control is also required for pointing to the NADIR direction and orientate the satellite properly towards the Sun if more power is needed (Section 6.3). OUFTI-Next should also be able to orientate itself towards the ground station when it is in its visibility zone (10° above the horizon). Indeed, an S-band antenna is chosen to downlink payload data (Section 6.2.2) but it does not radiate in all directions. This is why OUFTI-Next must orientate the S-band antenna towards Liege when it passes in its visibility zone in order to maximize the communication time.

The attitude control required for imaging must be far more precise than the ones concerning power generation and communication. Therefore, an ADCS respecting the requirements for imaging will also be suitable for other attitude controls.

6.1.1 Imaging techniques

With *Time Integration Delay (TDI)* scanning, OUFTI-Next always points to the NADIR direction while taking images. The goal is to increase the integration time by imaging the same object multiple times. The object is seen by a row of CCD pixels and shifts to the next row because of the satellite movement relative to the Earth. At the end, the object is seen by all the detector rows multiple times and the integration time is increased. Figure 6.1 illustrates this technique. [51]

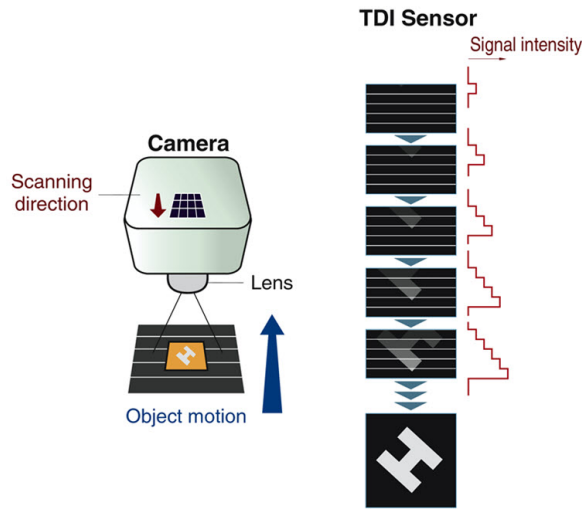


FIGURE 6.1: *Signal integration with TDI scanning*

The second technique called *target pointing strategy* is more intuitive. It that can also be implemented to increase the integration time. Instead of keeping the CubeSat in the NADIR direction, an attitude control is performed to point to a specific location for a certain amount of time. The satellite must rotate itself to keep pointing to the same location while moving. Figure 6.2 illustrates how OUFTI-Next must rotate to keep the exact same location in its FOV.

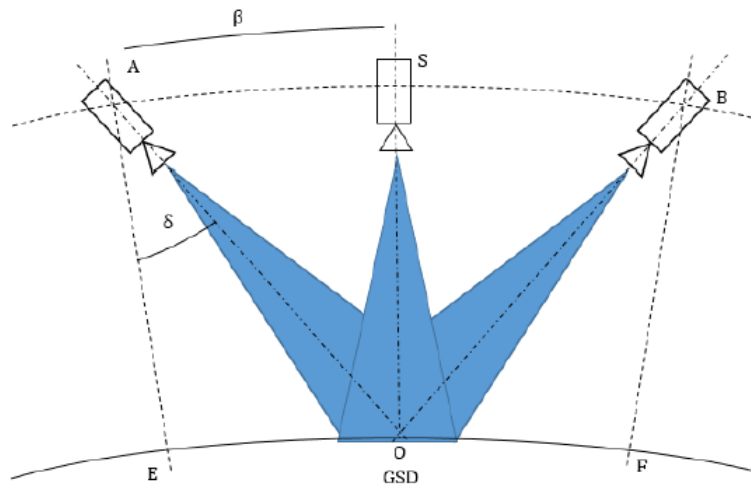


FIGURE 6.2: *Imaging with attitude control*

6.1.2 ADCS market survey

ADCS is indispensable for every attitude described above. A 3-axis attitude control with a pointing control accuracy below 1° is required. Table 6.3 presents a market survey of ADCS systems for 3U CubeSats with these constraints.

Name	Company	Sensors	Actuators	Power [W]	Size	Mass [g]	Operating Temperature	Pointing knowledge	Pointing control	Price
CubeADCS 3-Axis with Star Tracker	CubeSpace	Sun, Nadir, Magnetometers, Rate and Coarse Sun sensors, Star Tracker	Magnetorquers, 3 Small or medium or Large wheels	< 0.5	< 0.86U	< 600	-10°C to +60°C	0.01°	0.03°	41.700\$
MAI-400 ADACS	MAI	1 mems gyroscope, 1 magnetometer, 1 star tracker	3 Electromagnets, 3 reaction wheels	1.13 nominal 3.2 peak	0.5U	694	-40°C to +80°C	0.013°	0.1°	66.920\$
XACT	BlueCanyon Tech	IMU, Star Tracker, Sun Sensor, Magnetometer	3 Reaction Wheels, Torque Rods	< 3.0	0.5U	910	-30°C to +50°C	0.003° for 2 axes 0.007 for the 3rd axis	?	125.000\$
2U/3U Fine ADCS solution - 3 axis control (modified)	GOMspace	Magnetometers, Fine and Coarse Sun Sensors, Star Tracker	Reaction Wheels in tetrahedron Magnetorquers	2.05 (w/o GPS) 3.05 (with GSP)	0.75U	642	-20°C to +40°C	?	Between 0.1233° and 0.1320° (simulations)	130.000€
iADCS-100	Berlin Space Technologies Clyde Space	Star Tracker, 2-axes MEMS gyro, Magnetometer, Accelerometer	3 Reactions wheels, 3 Magnetorquers	0.5 nominal 1.8 peak	~0.3U	345	-10°C to +30°C	<1°	?	75.000€

FIGURE 6.3: ADCS main characteristics

Six ADCS systems have been listed. All of them have a star tracker to provide the minimum pointing accuracy. Sometimes, there are also other sensors such as magnetometers, Sun sensors, or MEMS gyroscopes. Every ADCS is equipped with 3 reaction wheels and magnetorquers. Magnetorquers can be used when reaction wheels are saturated for instance. Remark: ClydeSpace is still working on a an ADCS solution for OUFTI-Next but only few information are available as of now.

The pointing control accuracy depends on the mass inertia of OUFTI-Next which is still unknown. Values presented in the table are estimates for a 3U CubeSat with body mounted solar panels and telescope placed on a small face. The ADCS presenting the best pointing control accuracy is the *CubeADCS 3-Axis* from CubeSpace. It is equal to 0.03° . This value seems a bit optimistic since it is more than 3 times better than other ADCS. Furthermore, it is the cheapest one. On the other hand, it is also the biggest system in the list which would maybe explain why it is so efficient. In any case, a pointing control accuracy of 0.1° is achievable.

Another important characteristic which is not presented in the table is the pointing stability. Whatever the technique used for imaging, the satellite must be as stable as possible to perform correctly the integration of the signal. It has been computed that OUFTI-Next should not move more than $0.5[\text{arcmin}]$ per minute to image properly. The pointing accuracy of *CubeADCS 3-Axis* is below $0.5[\text{arcmin}]$ for $60[\text{s}]$. It is even better for *MAI-400 ADACS*. Its pointing stability is below $20[\text{arcsec}]$ for $500[\text{s}]$.

Finally, performances of the different ADCS should orientate its choice. Nevertheless, as the detector and TMA seem to take a lot of space inside the CubeSat ($\pm 1.5\text{U}$), the main characteristic that will guide the choice could be its size. There are 3 ADCS which do not exceed 0.5U : *XACT*, *MAI-400 ADACS* and *iADCS-100*.

6.2 Data & Link budgets

In this section, one will assess the number of images that can be downlinked per day. This number of images depends on two main parameters: the orbit and the frequency band used for communication. The orbit influences the communication time between the satellite and the ground station. The longer the satellite is visible by the ground station, the larger amount of data can be downlinked. The communication band plays also a major role in the data budget. The highest frequency is used, the more data can be sent per second. Then, the orbit and communication band influence the link budget.

6.2.1 Data budgets

Data budgets are performed for 3 orbits: an ISS, a $400[\text{km}]$ and a $800[\text{km}]$ SSO. There are 4 common communication bands used by radio amateurs willing to communicate with CubeSats: the VHF, UHF, S-band and X-band. Properties of these bands as well as companies who can provide such systems for CubeSats can be found in Table 6.1.

	Frequency [GHz]	Data rate [kbit/s]	Company	Price
VHF	0.03-0.3	1.2	ISIS	8500€
UHF	0.3-3	9.6	ISIS	8500€
S-band	2-4	100.0	ISIS	8500€
X-band	8-12	50,000	ClydeSpace	25,000\$

TABLE 6.1: *Communication bands properties*

Data rates listed in this table are common data rates at which the different communication systems are able to downlink. These values are used to perform the data budget. The higher frequency band is used, the higher data rate is achievable but the more power is needed. Eventually, link budgets are performed to assess which frequency bands can be used based on these common data rates.

Knowing the mean visibility duration for each orbit from Tables 5.2 and 5.3, it is possible to compute how much data can be downlinked per pass over Liege. It is assumed that half of the visibility is dedicated to downlinking payload data. Knowing that the FLIR detector has 640 pixels per row and that highest resolution MWIR images are coded in 14 bits per pixel, 8960 bits per row are required. If OUFTI-Next takes images using TDI scanning with a GSD of 100[m], one can compute the image "length" that can be downlinked per pass in average (Table 6.2).

	VHF [km/pass]	UHF [km/pass]	S-band [km/pass]	X-band [km/pass]
ISS	2.1	17.3	177.5	88,728
SSO 400[km]	2.0	16.2	165.7	82,868
SSO 800[km]	3.3	26.8	277.9	139,500

TABLE 6.2: *Amount of payload data downlinked per pass*

Knowing that the mean pass number for each orbit is:

- **ISS**: 4.67 [passes/day]
- **SSO 400[km]**: 3.49 [passes/day]
- **SSO 800[km]**: 5.18 [passes/day]

It is now easy to compute how much data can be downlinked per day (Table 6.3), month or year on average.

	VHF [km/day]	UHF [km/day]	S-band [km/day]	X-band [km/day]
ISS	9.8	80.8	828.9	414,355
SSO 400[km]	7.0	56.5	578.3	289,209
SSO 800[km]	17.1	138.8	1439.5	722,610

TABLE 6.3: *Amount of payload data downlinked per day*

These data budgets have been performed for high-quality images coded in 14[bits]. Images obtained by the Neutrino detector can also be coded in 8[bits]. If this coding is used, longer images can be downlinked per day. Compression should also be considered to increase the amount of data transmitted.

6.2.2 Link budgets

Three different main link budgets are required in the case of OUFTI-Next mission. One for the downlink of payload data, one for the downlink of telemetry data and one for the uplink. The most critical link budgets concern the downlink of data because the transmit power is limited. After analyzing the different downlink budgets for payload data, it will be possible to decide which communication band is the more appropriate and how much payload data can be downlinked each day.

Payload and telemetry data downlink budgets

There are 4 usual communication bands that can be used to downlink payload data. Hence, 4 link budgets must be performed to assess which one is the more appropriate. An ISS orbit is assumed for the following link budgets.

VHF VHF can be used to downlink payload data from OUFTI-Next. One has to respect the characteristics of the VHF transmitter provided by ISIS such as the transmission power, the frequency, the modulation... Dipole antenna system from ISIS (4500 - 5200 €) is considered. OUFTI-1 ground station characteristics are also used since this ground station is perfectly suited for this communication band. Usually, a data rate = 1.2 [kbit/s] is used in VHF. Figure 6.4 presents a summary of this link budget. The link budget is closed if the *System Link Margin* is greater than 0 with the *Eb/No Method*. Nevertheless, a target value should be approximately 6[dB] minimum. In the present case, the *System Link Margin* = 22.9[dB]. So, VHF can be used to downlink payload and telemetry data.

UHF A classical data rate equals to 9.6 [kbit/s] is ordinarily used with the UHF communication band. Characteristics of the UHF transmitter and dipole antenna system provided by ISIS are assumed. OUFTI-1 ground station is also suited for this communication band. Figure 6.5 shows the UHF downlink budget summary. The *System Link Margin* = 4.4[dB] which is below the minimum target value. Therefore, UHF cannot be used to downlink payload and telemetry data except if the data rate is reduced. For instance, if the data rate is reduced to 4.8[kbit/s], the *System Link Margin* = 7.5[dB] which is above the recommended margin. Eventually, this link budget should be refined and carefully watched out.

OUFTI-3		NOTE:
Downlink Telemetry Budget:		
Parameter:	Value:	Units:
Spacecraft:		
Spacecraft Transmitter Power Output:	0,5	watts
In dBW:	-3,0	dBW
In dBm:	27,0	dBm
Spacecraft Total Transmission Line Losses:	0,4	dB
Spacecraft Antenna Gain:	0,0	dBi
Spacecraft EIRP:	-3,4	dBW
Downlink Path:		
Spacecraft Antenna Pointing Loss:	0,0	dB
S/C-to-Ground Antenna Polarization Loss:	0,1	dB
Path Loss:	140,9	dB
Atmospheric Loss:	2,1	dB
Ionospheric Loss:	0,7	dB
Rain Loss:	0,0	dB
Isotropic Signal Level at Ground Station:	-147,2	dBW
Ground Station (Eb/No Method):		
----- Eb/No Method -----		
Ground Station Antenna Pointing Loss:	1,2	dB
Ground Station Antenna Gain:	10,5	dBi
Ground Station Total Transmission Line Losses:	2,5	dB
Ground Station Effective Noise Temperature:	246	K
Ground Station Figure of Merit (G/T):	-15,9	dB/K
G.S. Signal-to-Noise Power Density (S/No):	64,3	dBHz
System Desired Data Rate:	1200	bps
In dBHz:	30,8	dBHz
Telemetry System Eb/No for the Downlink:	33,5	dB
Demodulation Method Selected:	BPSK	
Forward Error Correction Coding Used:	None	
System Allowed or Specified Bit-Error-Rate:	1,0E-05	
Demodulator Implementation Loss:	1	dB
Telemetry System Required Eb/No:	9,6	dB
Eb/No Threshold:	10,6	dB
System Link Margin:	22,9	dB
Ground Station Alternative Signal Analysis Method (SNR Computation):		
----- SNR Method -----		
Ground Station Antenna Pointing Loss:	1,2	dB
Ground Station Antenna Gain:	10,5	dBi
Ground Station Total Transmission Line Losses:	2,5	dB
Ground Station Effective Noise Temperature:	246	K
Ground Station Figure of Merit (G/T):	-15,9	dB/K
Signal Power at Ground Station LNA Input:	-140,4	dBW
Ground Station Receiver Bandwidth (B):	10 000	Hz
G.S. Receiver Noise Power (Pn = kTB)	-164,7	dBW
Signal-to-Noise Power Ratio at G.S. Rcvr:	24,3	dB
Analog or Digital System Required S/N:	16,7	dB
System Link Margin	7,6	dB

FIGURE 6.4: Payload and telemetry data downlink budget in VHF

OUFTI-3		NOTE:
Downlink Telemetry Budget:		
Parameter:	Value:	Units:
Spacecraft:		
Spacecraft Transmitter Power Output:	0,5	watts
In dBW:	-3,0	dBW
In dBm:	27,0	dBm
Spacecraft Total Transmission Line Losses:	0,4	dB
Spacecraft Antenna Gain:	0,0	dBi
Spacecraft EIRP:	-3,4	dBW
Downlink Path:		
Spacecraft Antenna Pointing Loss:	0,0	dB
S/C-to-Ground Antenna Polarization Loss:	0,1	dB
Path Loss:	150,3	dB
Atmospheric Loss:	2,1	dB
Ionospheric Loss:	0,7	dB
Rain Loss:	0,0	dB
Isotropic Signal Level at Ground Station:	-156,6	dBW
Ground Station (Eb/No Method):		
----- Eb/No Method -----		
Ground Station Antenna Pointing Loss:	1,2	dB
Ground Station Antenna Gain:	10,5	dBi
Ground Station Total Transmission Line Losses:	2,5	dB
Ground Station Effective Noise Temperature:	246	K
Ground Station Figure of Merit (G/T):	-15,9	dB/K
G.S. Signal-to-Noise Power Density (S/No):	54,9	dBHz
System Desired Data Rate:	9600	bps
In dBHz:	39,8	dBHz
Telemetry System Eb/No for the Downlink:	15,0	dB
Demodulation Method Selected:	BPSK	
Forward Error Correction Coding Used:	None	
System Allowed or Specified Bit-Error-Rate:	1,0E-05	
Demodulator Implementation Loss:	1	dB
Telemetry System Required Eb/No:	9,6	dB
Eb/No Threshold:	10,6	dB
System Link Margin:	4,4	dB
Ground Station Alternative Signal Analysis Method (SNR Computation):		
----- SNR Method -----		
Ground Station Antenna Pointing Loss:	1,2	dB
Ground Station Antenna Gain:	10,5	dBi
Ground Station Total Transmission Line Losses:	2,5	dB
Ground Station Effective Noise Temperature:	246	K
Ground Station Figure of Merit (G/T):	-15,9	dB/K
Signal Power at Ground Station LNA Input:	-149,8	dBW
Ground Station Receiver Bandwidth (B):	10 000	Hz
G.S. Receiver Noise Power (Pn = kTB)	-164,7	dBW
Signal-to-Noise Power Ratio at G.S. Rcvr:	14,9	dB
Analog or Digital System Required S/N:	16,7	dB
System Link Margin	-1,8	dB

FIGURE 6.5: Payload and telemetry data downlink budget in UHF

S-band S-band is not suited for the transmission of telemetry data. The amount of telemetry data is too small compared to the data rate achievable with this communication band. The S-band transmitter from ISIS and a patch antenna are able to transmit data up to 100[kbit/s]. OUFTI-1 ground station is not appropriate for this communication band. A full ground station kit for S-band is available at ISIS for 46,500€. With characteristics of S-band transmitter, patch antenna and ground station, an S-band downlink budget can be performed (Fig 6.6). The *System Link Margin* = 13.6[dB] and the link budget is closed. Therefore, S-band can be used to downlink payload data.

X-band X-band is the highest frequency band presented. A data rate up to 50[Mbit/s] can be achieved. Nevertheless, it is very rarely used in CubeSats due to its high power consumption and atmospheric loss. A high gain X-band patch antenna is here assumed [52]. Its mass is around 300[g] and it sizes 10.16 x 12.7 x 0.64[cm]. The transmitted power can go up to 10[W] and its power consumption is even higher. The ground station is composed of a 3.7[m] diameter parabolic antenna which weighs 1600[kg] [69]. With a data rate of 50[Mbit/s], the link budget is not closed because the *System Link Margin* = -6.2[dB] (Fig 6.7). It can only be used if the data rate is reduced. If it is equal to 1[Mbit/s], the *System Link Margin* is greater than 6[dB]. Nevertheless, the utilization of an X-band is not recommended because it cannot operate to its full potential. Also, the power consumption, mass and size of such a patch antenna are very high for a 3U CubeSat. The cost, size and mass of the ground station parabolic antenna are also unfavourable factors.

OUFTI-3		NOTE:
Downlink Telemetry Budget:		
Parameter:	Value:	Units:
Spacecraft:		
Spacecraft Transmitter Power Output:	0,7	watts
In dBW:	-1,9	dBW
In dBm:	28,1	dBm
Spacecraft Total Transmission Line Losses:	0,4	dB
Spacecraft Antenna Gain:	8,0	dBi
Spacecraft EIRP:	5,7	dBW
Downlink Path:		
Spacecraft Antenna Pointing Loss:	0,0	dB
S/C-to-Ground Antenna Polarization Loss:	0,1	dB
Path Loss:	164,5	dB
Atmospheric Loss:	2,1	dB
Ionospheric Loss:	0,7	dB
Rain Loss:	0,0	dB
Isotropic Signal Level at Ground Station:	-161,6	dBW
Ground Station (Eb/No Method):		
----- Eb/No Method -----		
Ground Station Antenna Pointing Loss:	5,0	dB
Ground Station Antenna Gain:	35,4	dBi
Ground Station Total Transmission Line Losses:	0,5	dB
Ground Station Effective Noise Temperature:	185	K
Ground Station Figure of Merit (G/T):	12,2	dB/K
G.S. Signal-to-Noise Power Density (S/No):	74,2	dBHz
System Desired Data Rate:	100000	bps
In dBHz:	50,0	dBHz
Telemetry System Eb/No for the Downlink:	24,2	dB
Demodulation Method Selected:	BPSK	
Forward Error Correction Coding Used:	None	
System Allowed or Specified Bit-Error-Rate:	1,0E-05	
Demodulator Implementation Loss:	1	dB
Telemetry System Required Eb/No:	9,6	dB
Eb/No Threshold:	10,6	dB
System Link Margin:	13,6	dB
Ground Station Alternative Signal Analysis Method (SNR Computation):		
----- SNR Method -----		
Ground Station Antenna Pointing Loss:	5,0	dB
Ground Station Antenna Gain:	35,4	dBi
Ground Station Total Transmission Line Losses:	0,5	dB
Ground Station Effective Noise Temperature:	185	K
Ground Station Figure of Merit (G/T):	12,2	dB/K
Signal Power at Ground Station LNA Input:	-131,7	dBW
Ground Station Receiver Bandwidth (B):	10 000	Hz
G.S. Receiver Noise Power (Pn = kTB):	-165,9	dBW
Signal-to-Noise Power Ratio at G.S. Rcvr:	34,2	dB
Analog or Digital System Required S/N:	16,7	dB
System Link Margin	17,5	dB

FIGURE 6.6: Payload data downlink budget in S-band

OUFTI-3		NOTE:
Downlink Telemetry Budget:		
Parameter:	Value:	Units:
Spacecraft:		
Spacecraft Transmitter Power Output:	10,0	watts
In dBW:	10,0	dBW
In dBm:	40,0	dBm
Spacecraft Total Transmission Line Losses:	0,4	dB
Spacecraft Antenna Gain:	16,0	dBi
Spacecraft EIRP:	25,6	dBW
Downlink Path:		
Spacecraft Antenna Pointing Loss:	0,0	dB
S/C-to-Ground Antenna Polarization Loss:	0,1	dB
Path Loss:	175,7	dB
Atmospheric Loss:	2,1	dB
Ionospheric Loss:	0,7	dB
Rain Loss:	0,0	dB
Isotropic Signal Level at Ground Station:	-153,0	dBW
Ground Station (Eb/No Method):		
----- Eb/No Method -----		
Ground Station Antenna Pointing Loss:	17,9	dB
Ground Station Antenna Gain:	46,7	dBi
Ground Station Total Transmission Line Losses:	0,5	dB
Ground Station Effective Noise Temperature:	181	K
Ground Station Figure of Merit (G/T):	23,6	dB/K
G.S. Signal-to-Noise Power Density (S/No):	81,3	dBHz
System Desired Data Rate:	50000000	bps
In dBHz:	77,0	dBHz
Telemetry System Eb/No for the Downlink:	4,4	dB
Demodulation Method Selected:	BPSK	
Forward Error Correction Coding Used:	None	
System Allowed or Specified Bit-Error-Rate:	1,0E-05	
Demodulator Implementation Loss:	1	dB
Telemetry System Required Eb/No:	9,6	dB
Eb/No Threshold:	10,6	dB
System Link Margin:	-6,2	dB
Ground Station Alternative Signal Analysis Method (SNR Computation):		
----- SNR Method -----		
Ground Station Antenna Pointing Loss:	17,9	dB
Ground Station Antenna Gain:	46,7	dBi
Ground Station Total Transmission Line Losses:	0,5	dB
Ground Station Effective Noise Temperature:	181	K
Ground Station Figure of Merit (G/T):	23,6	dB/K
Signal Power at Ground Station LNA Input:	-124,7	dBW
Ground Station Receiver Bandwidth (B):	10 000	Hz
G.S. Receiver Noise Power (Pn = kTB):	-166,0	dBW
Signal-to-Noise Power Ratio at G.S. Rcvr:	41,3	dB
Analog or Digital System Required S/N:	16,7	dB
System Link Margin	24,6	dB

FIGURE 6.7: Payload data downlink budget in X-band

Downlink System Link Margins for the ISS orbit, 400[km] and 800[km] SSO are presented in Table 6.4. On one hand, VHF and S-band can be used whatever the orbit. On the other hand, UHF and X-band can never be used with the assumed data rates.

	VHF [dB]	UHF [dB]	S-band [dB]	X-band [dB]
ISS	22.9	4.4	13.6	-6.2
SSO 400[km]	23.0	4.5	12.8	-6.2
SSO 800[km]	19.2	0.7	9.0	-9.9

TABLE 6.4: *Downlink System Link Margins for different orbits and bands*

Uplink budgets

While downlink budgets are essential to know if it is possible to get data from the satellite, it is also important to communicate with OUFTI-Next from the ground station. With this purpose in mind, uplink budgets must be performed to assess under which conditions uplink communications are possible. Usually, uplink communications are in VHF or UHF because the amount of data to transmit is small. Furthermore, it is rarely a problem to close an uplink budget as the available power at a ground station is greater than in a satellite.

Figures 6.8 and 6.9 present respectively the uplink data budgets in VHF and UHF. VHF and UHF receivers from ISIS and OUFTI-1 ground station characteristics have been considered. As expected, both uplink budgets are closed and above the recommended margin. For VHF and UHF respectively, *System Link Margin* is equal to 30.2 and 20.8[dB]. Since the data rate used is the same (1.2[kbit/s]), the difference comes from the atmospheric loss. The higher is the frequency, the greater is the atmospheric loss. Finally, both VHF and UHF communication bands can be used to uplink data from the ground station to OUFTI-Next.

OUFTI-3			NOTE:
Uplink Command Budget:			
Parameter:	Value:	Units:	
Ground Station:			
Ground Station Transmitter Power Output:	100,0	watts	
In dBW:	20,0	dBW	
In dBm:	50,0	dBm	
Ground Stn. Total Transmission Line Losses:	2,6	dB	
Antenna Gain:	10,5	dBi	
Ground Station EIRP:	27,9	dBW	
Uplink Path:			
Ground Station Antenna Pointing Loss:	0,1	dB	
Gnd-to-S/C Antenna Polarization Losses:	3,0	dB	
Path Loss:	140,9	dB	
Atmospheric Losses:	2,1	dB	
Ionospheric Losses:	0,7	dB	
Rain Losses:	0,0	dB	
Isotropic Signal Level at Spacecraft:	-118,9	dBW	
Spacecraft (Eb/No Method):			
----- Eb/No Method -----			
Spacecraft Antenna Pointing Loss:	0,0	dB	
Spacecraft Antenna Gain:	0,0	dBi	
Spacecraft Total Transmission Line Losses:	0,9	dB	
Spacecraft Effective Noise Temperature:	232	K	
Spacecraft Figure of Merrit (G/T):	-24,5	dB/K	
S/C Signal-to-Noise Power Density (S/No):	85,2	dBHz	
System Desired Data Rate:	1200	bps	
In dBHz:	30,8	dBHz	
Command System Eb/No:	54,4	dB	
Demodulation Method Selected:	AFSK/FM		
Forward Error Correction Coding Used:	None		
System Allowed or Specified Bit-Error-Rate:	1,0E-05		
Demodulator Implementation Loss:	1,0	dB	
Telemetry System Required Eb/No:	23,2	dB	
Eb/No Threshold:	24,2	dB	
System Link Margin:	30,2	dB	
Spacecraft Alternative Signal Analysis Method (SNR Computation):			
----- SNR Method -----			
Spacecraft Antenna Pointing Loss:	0,0	dB	
Spacecraft Antenna Gain:	0,0	dBi	
Spacecraft Total Transmission Line Losses:	0,9	dB	
Spacecraft Effective Noise Temperature:	232	K	
Spacecraft Figure of Merrit (G/T):	-24,5	dB/K	
Signal Power at Spacecraft LNA Input:	-119,7	dBW	
Spacecraft Receiver Bandwidth:	9 600	Hz	
Spacecraft Receiver Noise Power (Pn = kTB):	-165,1	dBW	
Signal-to-Noise Power Ratio at G.S. Rcvr:	45,4	dB	
Analog or Digital System Required S/N:	19,0	dB	
System Link Margin	26,4	dB	

FIGURE 6.8: Uplink budget in VHF

OUFTI-3			NOTE:
Uplink Command Budget:			
Parameter:	Value:	Units:	
Ground Station:			
Ground Station Transmitter Power Output:	100,0	watts	
In dBW:	20,0	dBW	
In dBm:	50,0	dBm	
Ground Stn. Total Transmission Line Losses:	2,6	dB	
Antenna Gain:	10,5	dBi	
Ground Station EIRP:	27,9	dBW	
Uplink Path:			
Ground Station Antenna Pointing Loss:	0,1	dB	
Gnd-to-S/C Antenna Polarization Losses:	3,0	dB	
Path Loss:	150,3	dB	
Atmospheric Losses:	2,1	dB	
Ionospheric Losses:	0,7	dB	
Rain Losses:	0,0	dB	
Isotropic Signal Level at Spacecraft:	-128,3	dBW	
Spacecraft (Eb/No Method):			
----- Eb/No Method -----			
Spacecraft Antenna Pointing Loss:	0,0	dB	
Spacecraft Antenna Gain:	0,0	dBi	
Spacecraft Total Transmission Line Losses:	0,9	dB	
Spacecraft Effective Noise Temperature:	232	K	
Spacecraft Figure of Merrit (G/T):	-24,5	dB/K	
S/C Signal-to-Noise Power Density (S/No):	75,8	dBHz	
System Desired Data Rate:	1200	bps	
In dBHz:	30,8	dBHz	
Command System Eb/No:	45,0	dB	
Demodulation Method Selected:	AFSK/FM		
Forward Error Correction Coding Used:	None		
System Allowed or Specified Bit-Error-Rate:	1,0E-05		
Demodulator Implementation Loss:	1,0	dB	
Telemetry System Required Eb/No:	23,2	dB	
Eb/No Threshold:	24,2	dB	
System Link Margin:	20,8	dB	
Spacecraft Alternative Signal Analysis Method (SNR Computation):			
----- SNR Method -----			
Spacecraft Antenna Pointing Loss:	0,0	dB	
Spacecraft Antenna Gain:	0,0	dBi	
Spacecraft Total Transmission Line Losses:	0,9	dB	
Spacecraft Effective Noise Temperature:	232	K	
Spacecraft Figure of Merrit (G/T):	-24,5	dB/K	
Signal Power at Spacecraft LNA Input:	-129,2	dBW	
Spacecraft Receiver Bandwidth:	9 600	Hz	
Spacecraft Receiver Noise Power (Pn = kTB):	-165,1	dBW	
Signal-to-Noise Power Ratio at G.S. Rcvr:	35,9	dB	
Analog or Digital System Required S/N:	19,0	dB	
System Link Margin	16,9	dB	

FIGURE 6.9: Uplink budget in UHF

Uplink *System Link Margins* for the ISS orbit, 400[km] and 800[km] SSO are presented in Table 6.5. Both VHF and UHF bands can be used to uplink whatever the orbit.

	VHF [dB]	UHF [dB]
ISS	30.2	20.8
SSO 400[km]	30.3	20.8
SSO 800[km]	26.5	17.1

TABLE 6.5: *Uplink System Link Margins in VHF and UHF for different orbits*

6.2.3 Conclusion

From the link budgets and available COTS communication systems, there are two possibilities to downlink payload data. Whether the VHF band is used or the S-band. If one looks back at Table 6.3 relative to the data budget, it is clear that the S-band is more advantageous since it permits to downlink approximately 83 times more data than in VHF. If the amount of data downlinked per day is not sufficient, other ground stations in the world can be exploited. The amount of data downlinked would then be multiplied by the number of available ground stations.

Regarding the downlinking of telemetry data, only the VHF band can be used according to the link budget. Hence, if a full duplex transceiver is used, the uplink should be in UHF. Nevertheless, it is also possible to downlink in UHF and uplink in VHF if the UHF data rate is decreased.

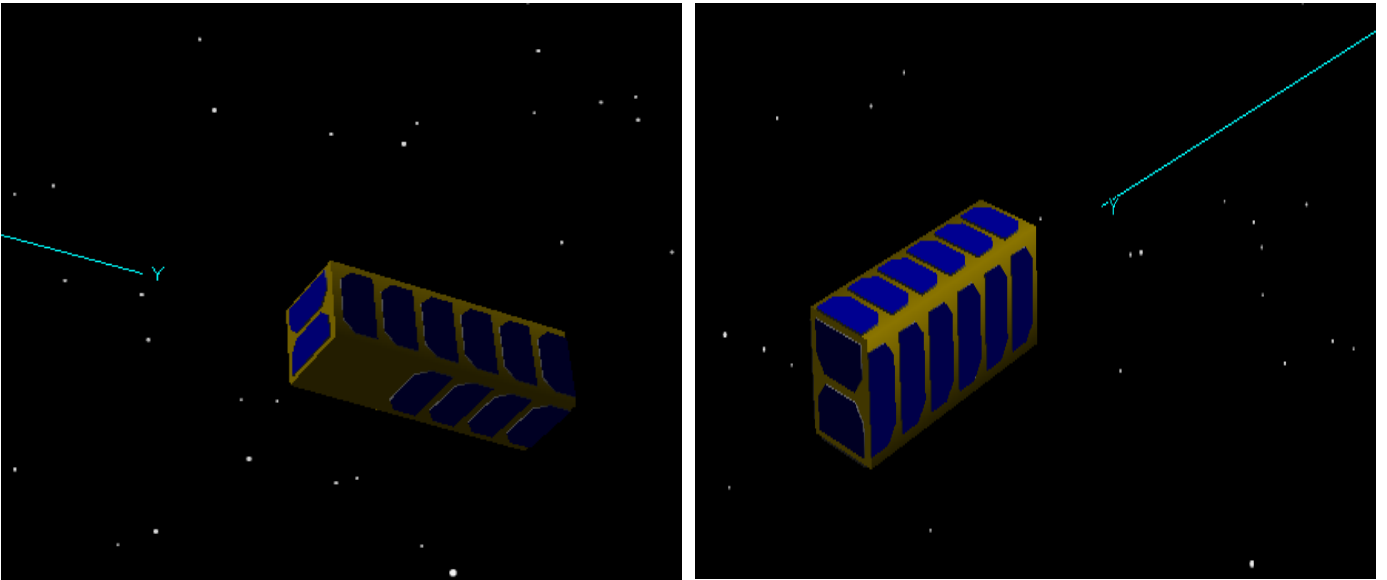
6.3 Power over a year

Power generated by solar panels depends on several parameters:

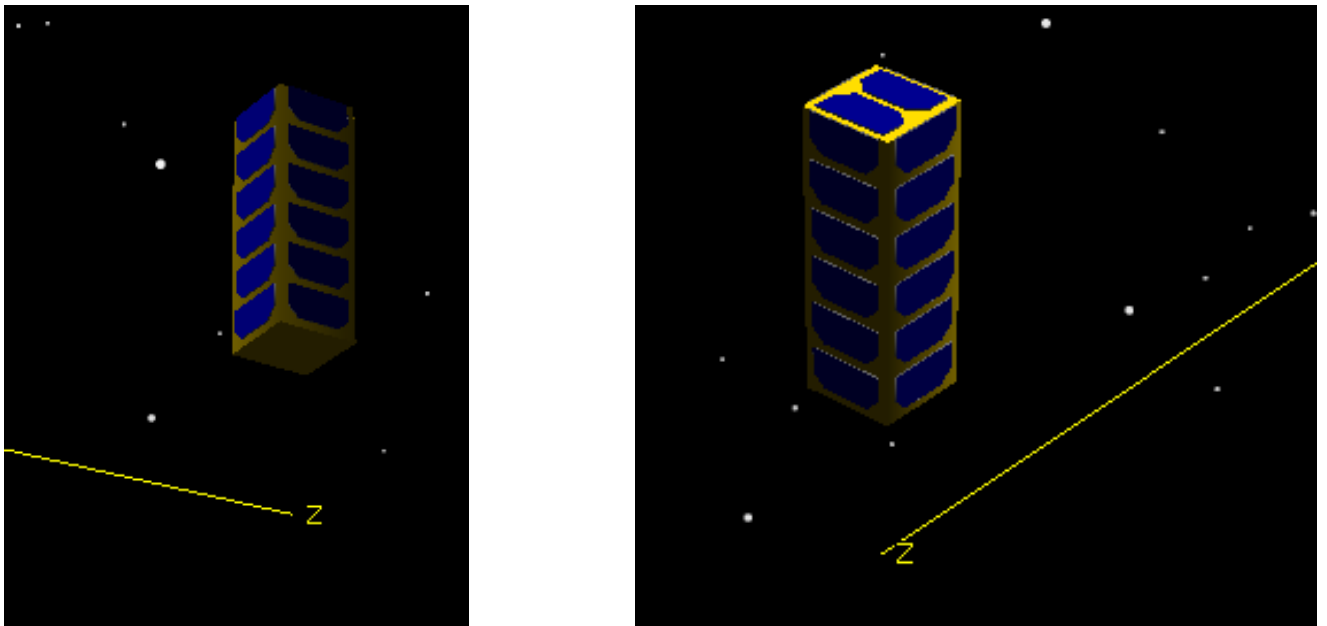
- Solar cells efficiency
- Solar panels orientation
- Orbit
- Period of the year

The aim of this section is to present the simulations results for various orbits and satellite orientations. All simulations were performed for a one-year period with solar cells efficiency of 30%. Solar cells from ISIS present similar efficiency. The SSO and ISS orbit are studied in detail. These results are essential to perform accurate power budgets.

Simulations were carried out using the *Solar panel tool* in STK. Two different models without star tracker were created to perform these simulations. The first model is a 3U CubeSat with the telescope placed on a long face (+y face). It contains 26 solar cells spread over all faces except on one part of a long face. Figure 6.10 displays two different views of this model.

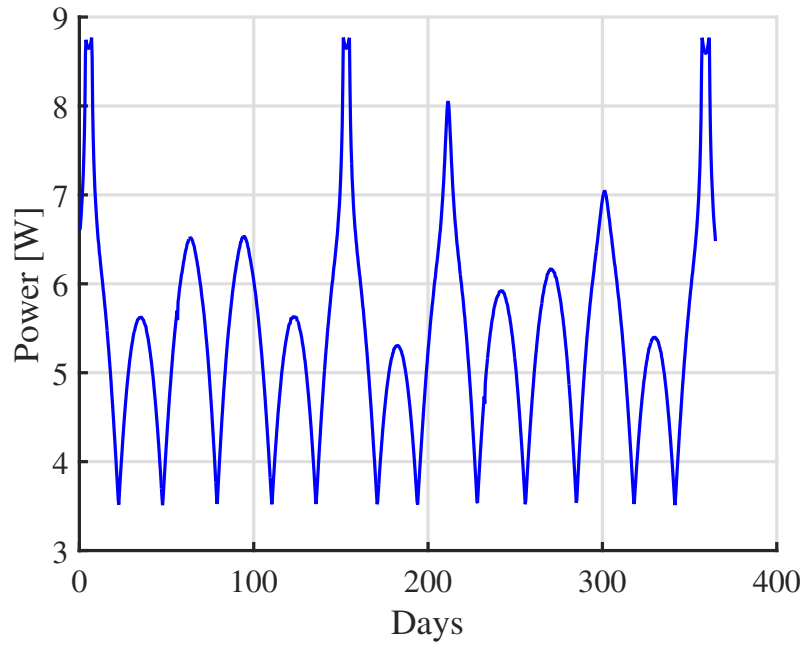
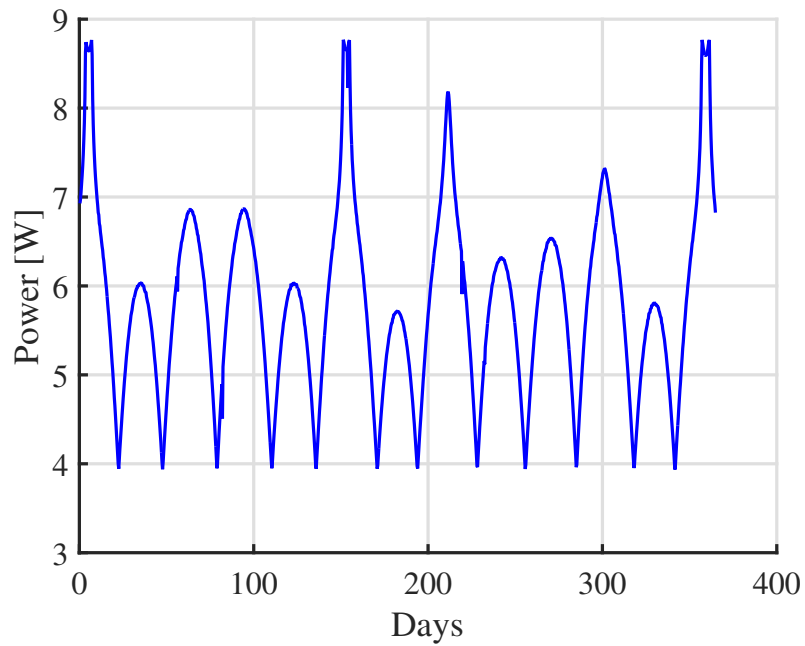
FIGURE 6.10: *3U model with telescope placed on +y face*

On the second model, the telescope is located on a short face ($-z$ face). It contains 26 solar cells spread over all faces except on a short face. Figure 6.11 shows two different views of this model. Indeed, all simulations for SSO were performed with this model because it is the easiest way to set the TMA and MWIR detector inside the CubeSat (section 6.5.2).

FIGURE 6.11: *3U model with telescope placed on -z face*

6.3.1 ISS orbit

For this orbit, two simulations with both models are presented. The telescope always points to the NADIR direction. Figure 6.12 and 6.13 display the power generated over a year for both models.

FIGURE 6.12: *Power over a year for an ISS orbit with the first model*FIGURE 6.13: *Power over a year for an ISS orbit with the second model*

The results are indeed very similar. Both graphs show 3 global maxima at 8.8[W]. They also present 12 minima but they are shifted. The minimum power generated is lower for the first model 3.6[W] than for the second model 4.0[W]. Nevertheless, the general shape of the curves is akin.

6.3.2 Sun-synchronous orbits

In this part, different SSO are studied. SSO can have different altitudes and longitude of descending nodes (LTDN). A thorough analysis of 800[km] SSO is led. The goal is to define a best, mean and worst case. Eventually, results of a simulation for a 400[km] SSO are presented.

SSO 800[km] : Best cases

The best case orbit is the one able to generate the maximum power over a year. Obviously, the more the satellite is in the light, the more it can produce power. By looking back at Table 5.3, one can see that the orbit with the least eclipse duration is dawn/dusk (LTDN 18h) orbit.

Two different cases can be analyzed. The first case is when the CubeSat always points to the NADIR direction without controlling its attitude to increase the power generation. Figure 6.14 displays the power generated over a year for this first best case which will be called *best case without attitude control*. Indeed, one should pay attention to the fact that there is still an attitude control which orientates the satellite to the NADIR direction.

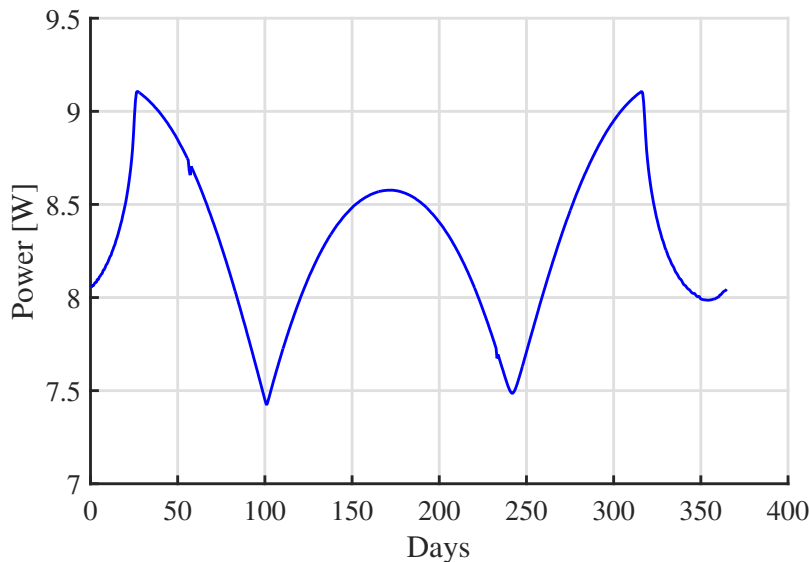


FIGURE 6.14: Power over a year for a SSO 800[km], best case without attitude control

This curve presents two global maxima at 9.1[W] and one global minimum at 7.4[W]. It is nearly symmetrical and there are two local minima at 60 and 230 days. These local minima are due to the passage of the Moon in front of the satellite. As the Moon eclipse time is relatively short, it has only a light effect on the total power generated over a year.

The second case is when the CubeSat always points to the NADIR direction with an attitude control to rotate itself along the z-axis. In this way, the satellite can always show the largest solar panel surface to the Sun and produce more power. Figure 6.15 shows the power generated over a year for this *best case with attitude control*. When the satellite is oriented in such way, it cannot take images of the Earth.

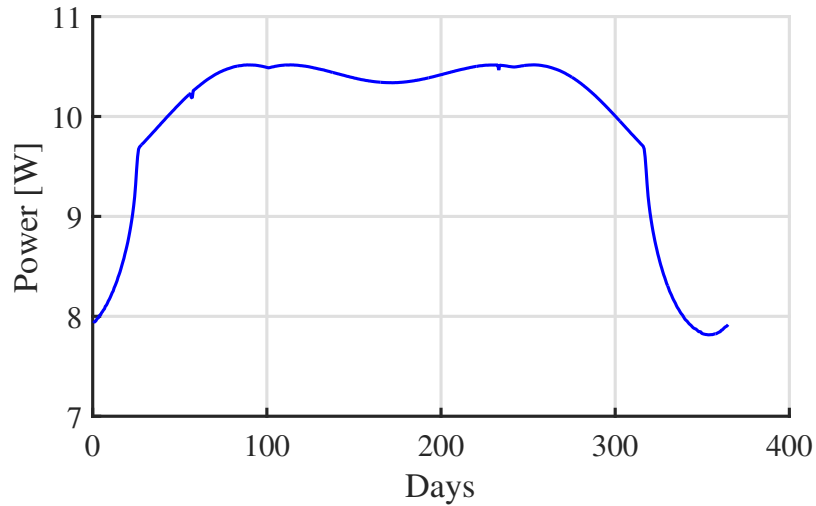


FIGURE 6.15: *Power over a year for a SSO 800[km], best case with attitude control*

Thanks to this attitude control, the minimum and maximum power generated are respectively increased to 7.8[W] and 10.5[W]. Once again, eclipses due to the passage of the Moon are clearly visible.

SSO 800[km] : Worst cases

The worst case orbit is the one offering the least lighting time to the satellite. A noon/midnight SSO (LTDN 12h) has this characteristic. It can be confirmed by Table 5.3. Once again, two cases can be studied: one with and one without attitude control. The attitude control is the same as the one described before and has the same objective: to increase the solar panel surface which is turned to the Sun. Figure 6.16 presents the power generated over a year without attitude control (except NADIR pointing). Figure 6.17 displays the power generated with attitude control.

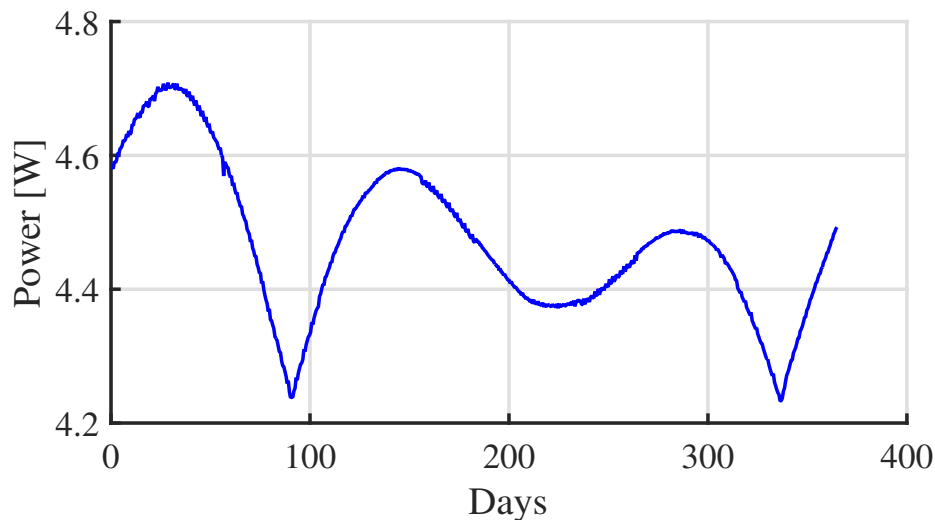


FIGURE 6.16: *Power over a year for a SSO 800[km], worst case without attitude control*

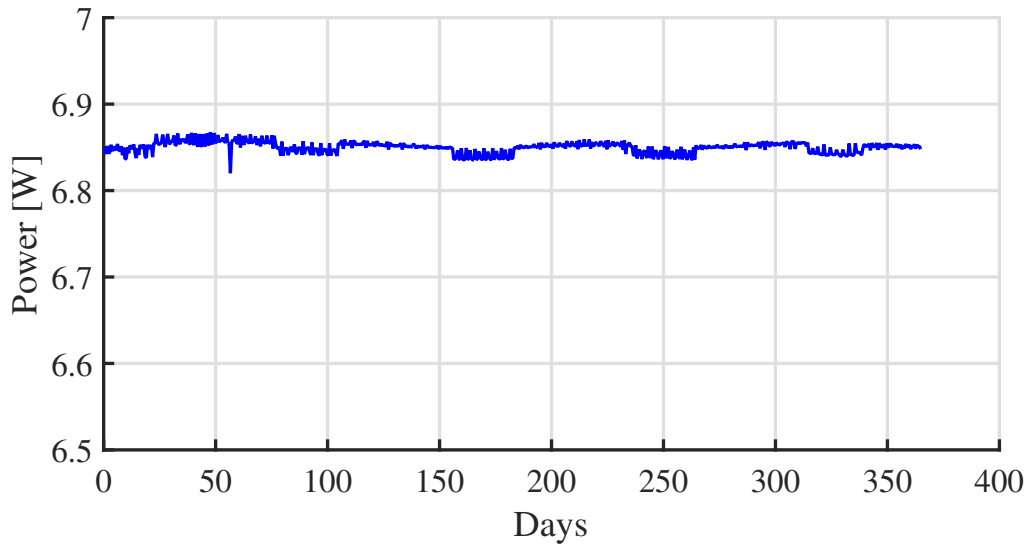


FIGURE 6.17: *Power over a year for a SSO 800[km], worst case with attitude control*

Without attitude control, the power generated varies between 4.24[W] and 4.7[W]. With attitude control, it is nearly constant and equals to 6.85[W]. In this case, the attitude control offers more than 2[W] of power compared to the case without attitude control.

SSO 800[km] : Mean case

Now that best and worst cases have been identified, the aim is to define a mean case for the power generated. Although a mean case does not really exist, it can nevertheless be defined based on statistics rather than physical parameters. First of all, one should check if a 800[km] SSO is common. Figure 6.18 presents the mean altitude in function of the inclination of LEO satellites. SSO satellites are highlighted in red.

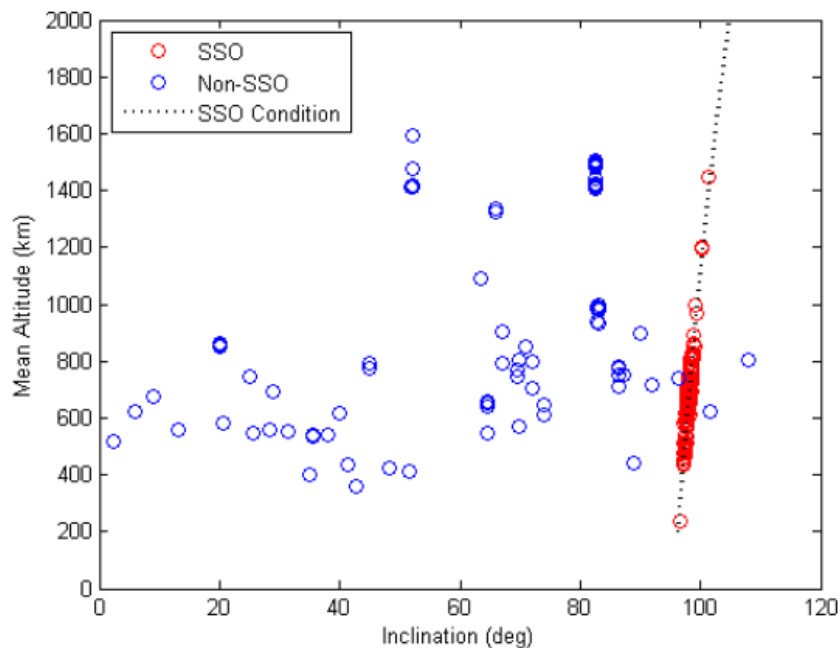


FIGURE 6.18: *Mean altitude vs inclination for LEO satellites*

44% of LEO satellites are in SSO [66]. Furthermore, the large majority of SSO satellites are between 400 and 800[km]. It means that a 800[km] SSO can be chosen as a mean case.

Now, one has to define what is the mean LTDN of a 800[km] SSO. To do so, a non-exhaustive database of more than 80 SSO satellites with their corresponding LTDN has been created (Appendix A). Figure 6.20 shows the number of satellites at each LTDN. This figure must be analyzed in relation with Figure 6.19 which displays the percentage of lighting per period for different LTDN in winter.

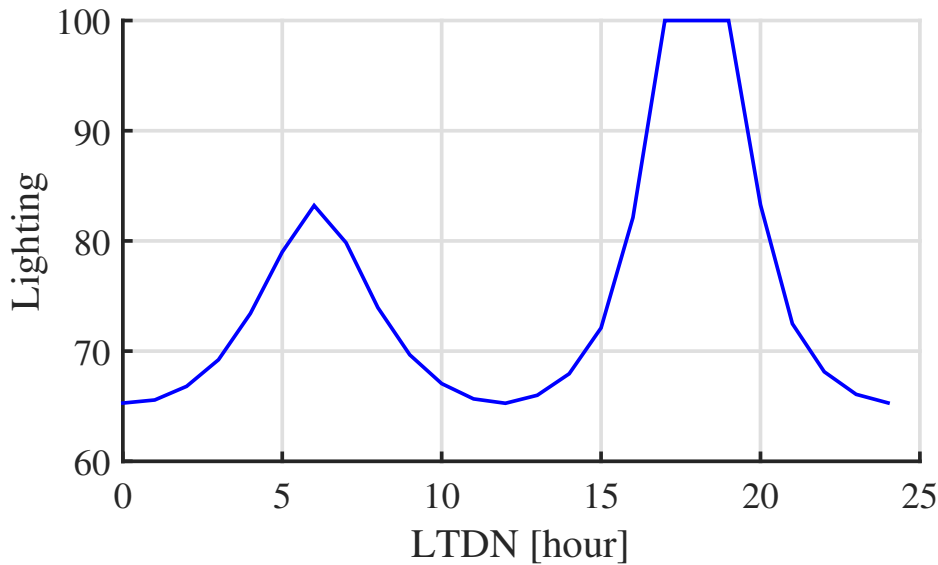


FIGURE 6.19: *Lighting vs LTDN for a 800[km] SSO*

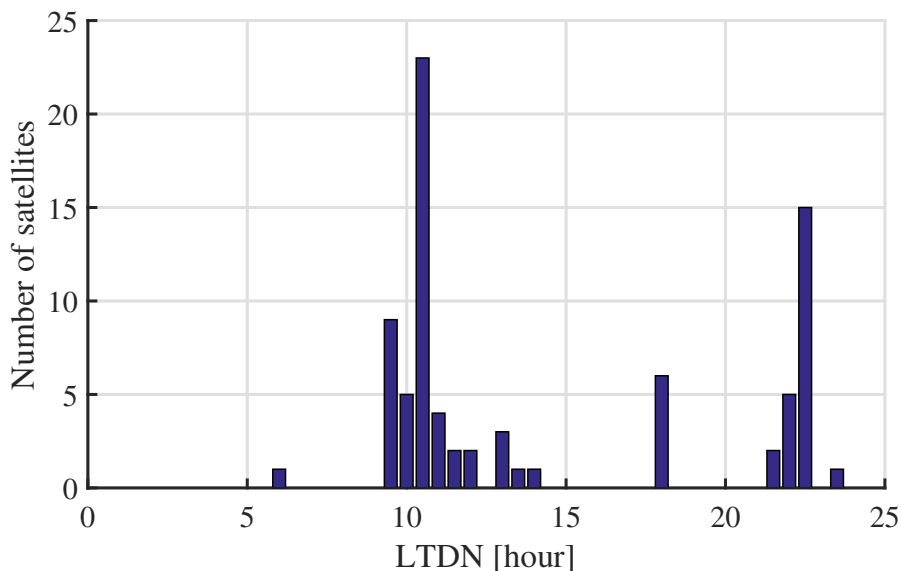


FIGURE 6.20: *Number of satellites vs LTDN for a 800[km] SSO*

A priori, one could believe that the majority of Sun-synchronous satellites are in orbits which offer the maximum lighting (LTDN between 17h and 19h) to maximize the power generation but it is not the case. Most satellites are in a 10h30 LTDN orbit where the lighting percentage

is nearly minimum. Hence, the **mean case** is a **800[km] SSO, 10h30 LTDN**. Nevertheless, it could be interesting to understand why there is such a distribution of satellites.

First, the curve in Figure 6.19 is not symmetrical. Indeed, even dawn/dusk orbits (LTDN 6h and 18h) experience short eclipses which happen for 3 months. For a 6h LTDN, this 3-month period with eclipses happens in winter. For a LTDN of 18h, it happens in summer. For this reason, a satellite in a 6h LTDN orbit is only 83% of the time in the light during winter.

When analyzing deeper the database, one realizes that the majority of satellites in dawn/dusk orbits have a radar payload. This is the case for HJ-1C, Radarsat-2 and SMAP for example. A radar needs a large amount of power to operate. A dawn/dusk orbit is thus optimal since it offers nearly continuous lighting throughout the year. Other satellites use this kind of orbit but it is for very specific applications. For instance, SMOS is in a 755[km] SSO with a 6h LTDN because 6:00 AM is the best time to perform their observations near the equator.

In fact, this constant illumination can lead to thermal issues. Furthermore, Earth observation satellites prefer noon/midnight orbits because the Earth is more illuminated while descending. Dawn/dusk orbits usually do not offer enough light for visible observations since they are always at the edge of the Earth's umbra. Of course, this is not a problem for radar satellites because a radar does not need light to operate.

Eventually, two different cases can be analyzed for the power generation over a year. Once again, one case is OUFTI-Next pointing to the NADIR direction without attitude control to rotate itself to the Sun. The other case being when the satellite is able to orientate optimally its solar panels towards the Sun while pointing to the NADIR direction.

For the first case, Figure 6.21 displays the power generated for one year for the mean case orbit (LTDN 10h30). It is also interesting to look at the counterpart of a 10h30 LTDN which is a 22h30 LTDN and see what are the differences. The power generated over a year for a 800[km] SSO, 22h30 LTDN is shown on Figure 6.22.

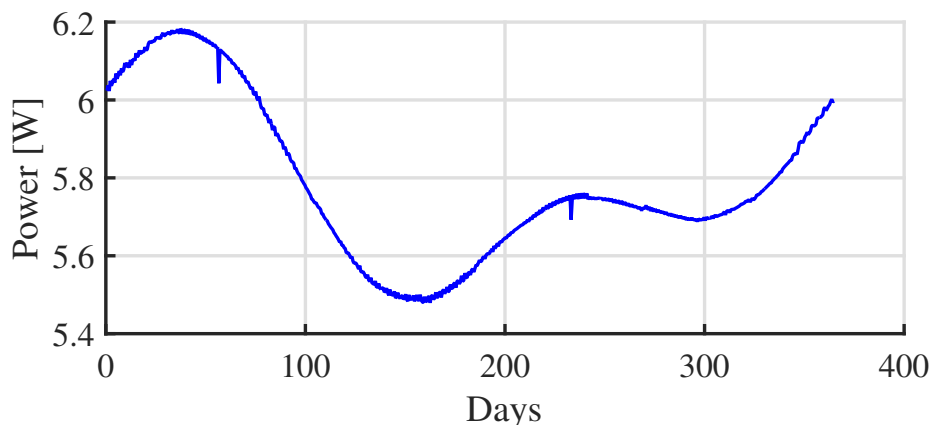


FIGURE 6.21: *Power generated over a year, mean case without attitude control*

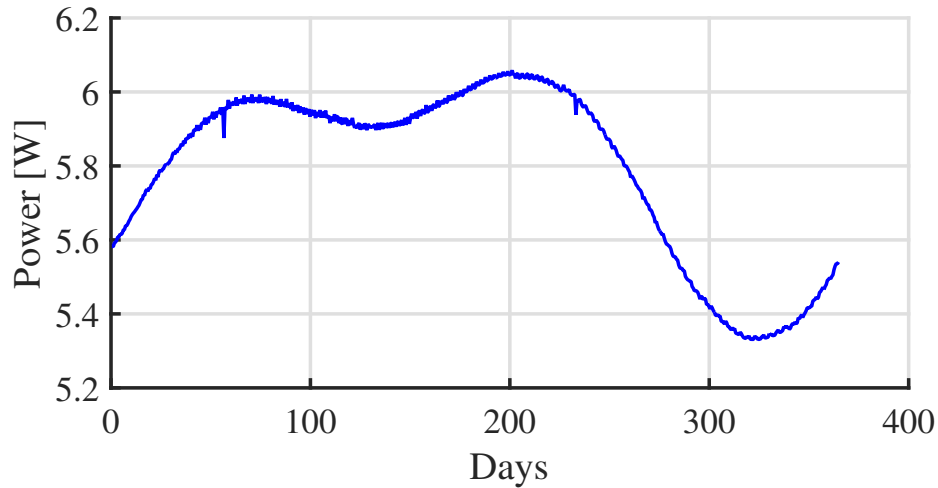


FIGURE 6.22: *Power generated over a year, LTDN 22h30 without attitude control*

Both graphs are approximately similar except that one is rotated of 180° compared to the other. The mean case (LTDN 10h30) can produce a bit more power ($\approx 0.15[\text{W}]$). The eclipses due to the Moon happen at the same time. Still concerning the mean case, the minimum and maximum power generated are respectively $5.5[\text{W}]$ and $6.2[\text{W}]$.

If more power is needed, an attitude control to orientate the satellite optimally towards the Sun is required. Figure 6.23 displays the power generated over a year for such a configuration.

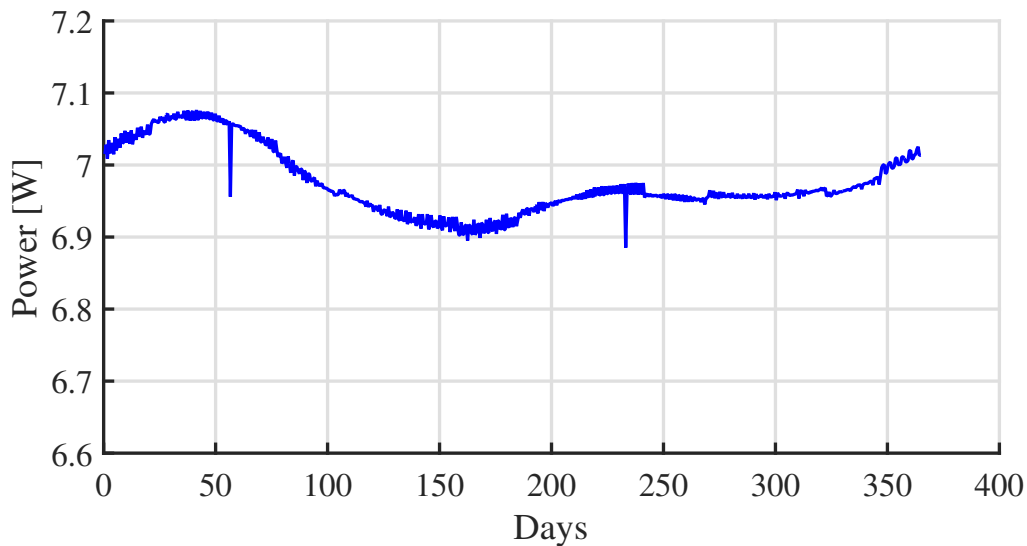


FIGURE 6.23: *Power generated over a year, mean case with attitude control*

The power generated is between 6.9 and $7.1[\text{W}]$ except during a Moon's eclipse when it is just below $6.9[\text{W}]$.

SSO 400[km]

Now that a detailed analysis has been led on 800[km] SSO, it could be interesting to predict a general trend for lower orbits. With this aim in mind, Figure 6.24 presents the power generated over a year for a 400[km] SSO, 10h30 LTDN without attitude control. This figure should be compared to Figure 6.21 which shows the power generated for the same configuration but at an 800[km] altitude.

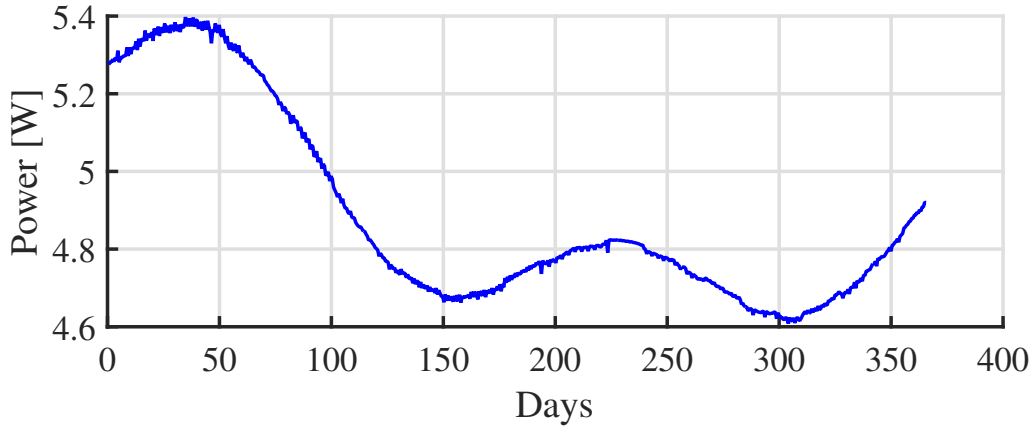


FIGURE 6.24: *Power generated over a year, SSO 400[km], 10h30 LTDN without attitude control*

This curve looks like the one of Figure 6.21 but the power generated is lower. Indeed, this result could have been predicted. A lower orbit experiences longer eclipses with respect to its own period. Hence, the power generated is lower. In this case, the minimum and maximum power generated are respectively 4.6[W] and 5.4[W]. It is approximately 1[W] lower than for the 800[km] SSO.

6.3.3 Summary of the results

The following tables summarize the previous results for each orbit studied.

ISS	+y face	-z face
Min [W]	3.6	4.0
Max [W]	8.8	8.8

TABLE 6.6: *Power generated for ISS orbit*

Best case	no A.C	A.C
Min [W]	7.4	7.8
Max [W]	9.1	10.5

TABLE 6.7: *Power generated for 800[km] SSO, 18h LTDN (Best case)*

Worst case	no A.C	A.C
Min [W]	4.24	6.85
Max [W]	4.7	6.85

TABLE 6.8: *Power generated for a 800[km] SSO, 12h LTDN (Worst case)*

Mean case	no A.C	A.C	no A.C 400[km]
Min [W]	5.5	6.9	4.6
Max [W]	6.2	7.07	5.4

TABLE 6.9: Power generated for 10h30 LTDN SSO (Mean case)

6.4 Power budget

The available electrical power is not unlimited. It was indeed computed in the previous section. Therefore, one has to pay attention to the power consumption of the CubeSat. A power budget must be performed to assess if the power generated is sufficient or not. Since the power generated depends on the orbit, several power budgets are required. Eventually, the capacity of the batteries can be evaluated thanks to these power budgets.

6.4.1 ISS orbit

Table 6.10 presents a high consumption power budget for the ISS orbit. The power consumption of each subsystem is evaluated thanks to data coming from real system datasheets. For instance, the payload consumption comes from datasheet of the FLIR detector and the ADCS was arbitrarily chosen from MAI. It is assumed that there is always a communication from the satellite to the ground station (COMM Rx). Telemetry (COMM Tx) as well as payload data (S-band Tx) are downlinked during all the maximum visibility duration. The beacon (BCN) is used half of the time. OBC and ADCS are used continuously while the sensor (payload) is cooled during 10[min] per orbit before taking images. Eventually, the thermal subsystem is active half of the time while OUFTI-Next is in eclipse.

	Peak [mW]	Peak time [min]	Peak time [%]	Average [mW]
COMM Rx	250	91.60	100.0	250
COMM Tx	3000	6.17	6.7	202
BCN	500	45.80	50.0	250
S-band Tx	6000	6.17	6.7	404
OBC	400	91.60	100.0	400
THER	3500	16.21	17.	619
ADCS	1300	91.60	100.0	500
Payload	8000	10.00	10.9	873
Total allocated				4299

TABLE 6.10: High consumption power budget for ISS orbit

When looking back to Figures 6.12 and 6.13, one can remark that the minimum power generated is inferior to 4.3[W]. Therefore, it should not be sufficient to supply all subsystems in this high consumption case.

Nevertheless, a check should be performed to assess whether batteries can provide enough power when all subsystems are used in eclipse. To be more precise, COMM Rx, OBC, ADCS and BCN are used all the time while COMM Tx, S-band Tx, THER and Payload are used in eclipse. Here, it is assumed that BCN is used all the time but at 250[mW]. If there is no eclipse during a period, it is assumed that all subsystems are still active. This is considered as the

worst case: high power consumption with all subsystems active in eclipse and once per orbit at least.

Figure 6.25 displays the charge/discharge cycles of batteries for one year for the worst case. Batteries capacity is set to 20[Wh] and half-charged at the beginning of the simulation. OUFTI-Next points its long face to the NADIR direction (disadvantageous situation). A short code has been developed to perform these simulations.

Battery capacity is not set to 20[Wh] by chance. The following calculation was performed to assess the minimum capacity required:

$$\begin{aligned}
 \text{Battery} &= (\text{CommRx} \times T_{\text{eclipse}}) + (\text{CommTx} \times T_{\text{vis}}) + (\text{BCN} \times T_{\text{eclipse}}/2) + (\text{Sband} \times T_{\text{vis}}) \\
 &+ (\text{OBC} \times T_{\text{eclipse}}) + (\text{THER} \times T_{\text{eclipse}}/2) + (\text{ADCS} \times T_{\text{eclipse}}) + (\text{Payload} \times 10.00) \\
 &= 320275.00[\text{mW}] \\
 &= 5.34[\text{Wh}]
 \end{aligned}
 \tag{6.1}$$

The depth of discharge of a battery is an important parameter concerning its lifetime and long-term performance. A maximum depth of discharge around 25% is recommended for limiting the loss of performance. 20 and 40[Wh] batteries are common for CubeSats. Therefore, batteries of 20[mW] should be used.

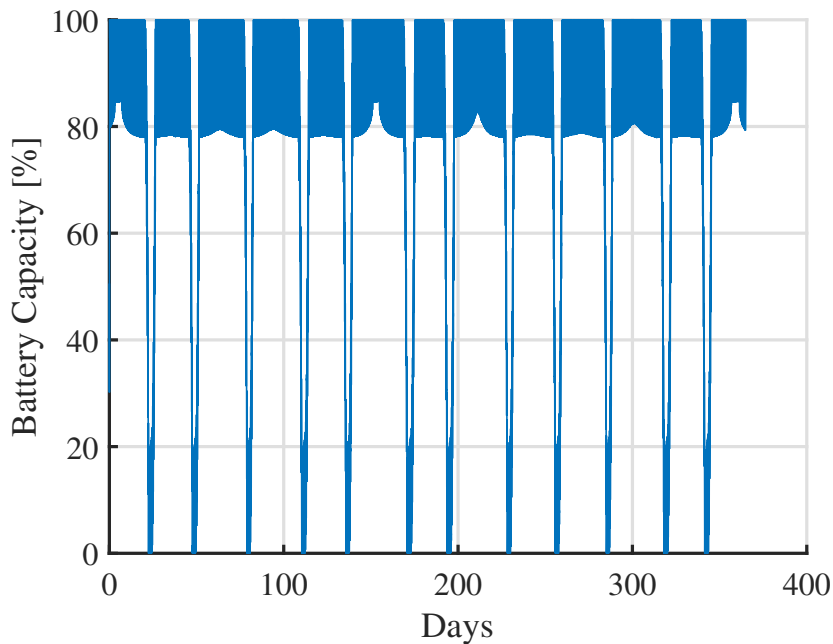


FIGURE 6.25: Batteries cycles over a year, ISS orbit

The charges and discharges of the batteries are not visible on this graph because cycles are too short compared to one year. The envelope of these cycles is what is observed. At the beginning, batteries are half-charged and OUFTI-Next is in eclipse. Therefore, batteries discharge below 50%. Then, it quickly charges. For most of the time, batteries depth of discharge is just above 20% as expected. When there is no eclipse and that the power generated is maximum (day 5, 153 and 359), the depth of discharge is even below 20%. Nevertheless when the power generated is minimum, which happens 12 times in a year, batteries are not able to provide enough power

and completely discharge. These periods when the power generated is not sufficient have a 5.05 days duration. Since there are 12 periods, this worst case scenario is not possible during 60.6 days. An alternative solution to avoid this problem would be to orientate the satellite optimally towards the Sun in such a way that it can receive more power. This solution would affect neither communications nor the payload utilization because both are only active in eclipse. Further simulations must be performed to confirm this solution.

If the satellite orbits with its short face pointed to the NADIR direction, the minimum power generated is 4[W] (Fig. 6.13). This is not enough neither to provide power to all subsystems. This case is less critical but a solution to orientate the satellite optimally towards the Sun while in sunlight must also be implemented.

To be able to observe the batteries cycles, the simulation duration should be shortened. Figure 6.26 displays the batteries cycles during the first day for the disadvantageous situation (long face pointed to the NADIR direction).

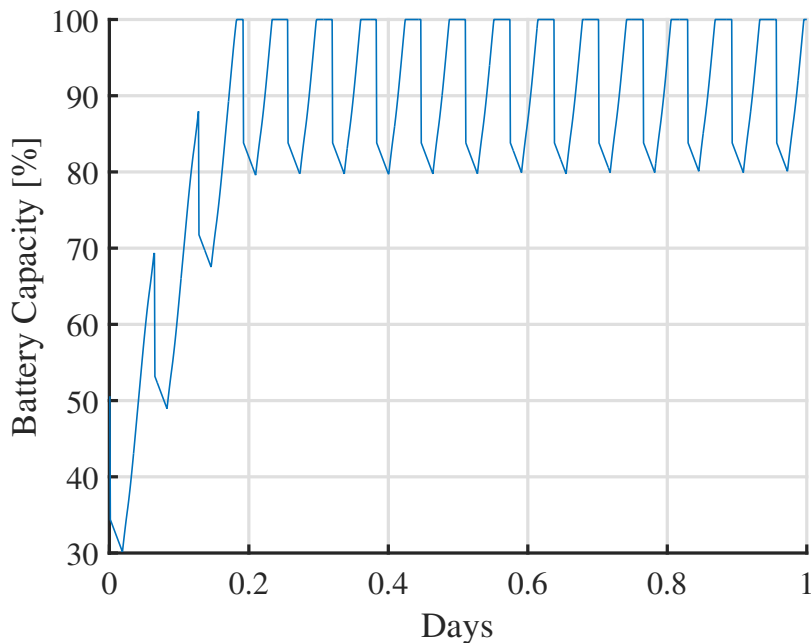


FIGURE 6.26: *Batteries cycles during the first day, ISS orbit*

Now, charges and discharges are well visible. In the beginning, batteries are discharged to 30.0% because of the eclipse. Nevertheless, they can recharge completely within only 3 orbits.

6.4.2 SSO 400[km]

Table 6.11 presents a high consumption power budget for a 400[km] SSO with 10h30 LTDN. All values were computed in the same way as for the ISS orbit.

	Peak [mW]	Peak time [min]	Peak time [%]	Average [mW]
COMM Rx	250	92.55	100.0	250
COMM Tx	3000	6.3	6.8	204
BCN	500	46.28	50.0	250
S-band Tx	6000	6.30	6.8	408
OBC	400	92.55	100.0	400
THER	3500	17.47	18.9	661
ADCS	1300	92.55	100.0	1300
Payload	8000	10.00	10.8	864
Total allocated				4338

TABLE 6.11: High consumption power budget for 400[km] SSO, LTDN 10h30

When looking back at Figure 6.24 where the short face is pointed to the NADIR direction, the minimum power available is 4.6[W] which is superior to the power needed 4.3[W]. Nevertheless, one should check if the batteries are able to provide enough power in eclipse with the worst case. Thanks to equation 6.1, one can compute the minimum capacity of the batteries. This time, it is equal to 5.6[Wh]. So, 20[Wh] batteries should be sufficient to limit the depth of discharge. Figure 6.27 shows the cycles of the batteries for one year.

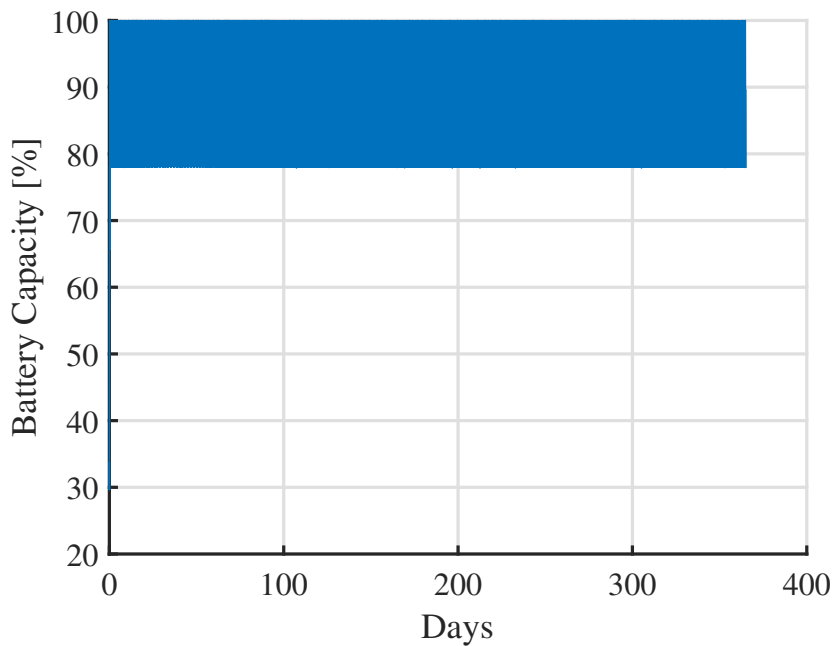


FIGURE 6.27: Batteries cycles over a year in 400[km] SSO, LTDN 10h30

The envelope of the cycles is relatively homogeneous. This is due to the relative constant period of eclipse and sunlight for such orbit. As expected, the depth of discharge is slightly above 20% except at the beginning where it goes to 70% since the batteries are half-charged and OUFTE-Next is in eclipse. Contrary to the ISS case, batteries are never completely discharged. This is due to the fact that the power generated is higher than the power consumed.

The charge/discharge cycles over the first day are shown on Figure 6.28.

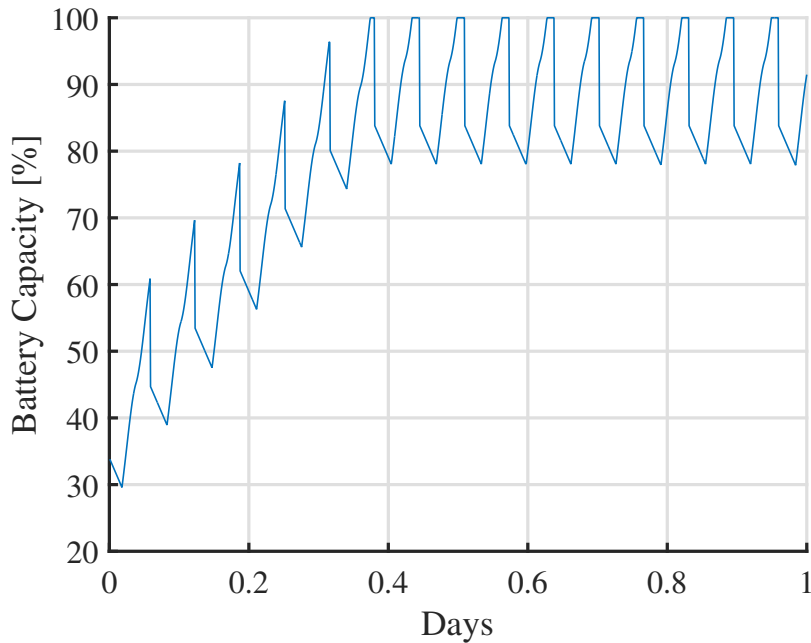


FIGURE 6.28: Batteries cycles during the first day, 400[km] SSO

The maximum depth of discharge is reached after the first eclipse, then batteries are totally charged after 6 orbits.

6.4.3 SSO 800[km]

Eventually, Table 6.12 presents a high consumption power budget for a 800[km] SSO with 12h00 LTDN. This LTDN is the worst case concerning the power generated for a SSO. Values in the table were computed as previously.

	Peak [mW]	Peak time [min]	Peak time [%]	Average [mW]
COMM Rx	250	100.87	100.0	250
COMM Tx	3000	10.62	10.5	316
BCN	500	50.43	50.0	250
S-band Tx	6000	10.62	10.5	632
OBC	400	100.87	100.0	400
THER	3500	17.39	17.2	603
ADCS	1300	100.87	100.0	1300
Payload	8000	10.00	9.9	793
Total allocated				4544

TABLE 6.12: High consumption power budget for 800[km] SSO, LTDN 12h00

Figure 6.16 showed that when the short face of OUFTE-Next points to the NADIR direction without attitude control to orientate itself optimally towards the Sun, the minimum power generated is close to 4.23[W]. This minimum value is lower than the power needed 4.54[W]. Hence, the power generated should not be sufficient to supply the satellite in this worst case. With equation 6.1, one can compute the minimum capacity of the batteries. It is equal to

6.2[Wh]. So, 20[Wh] batteries should be sufficient to limit the depth of discharge. Figure 6.29 presents the charge/discharge cycles of the batteries for one year.

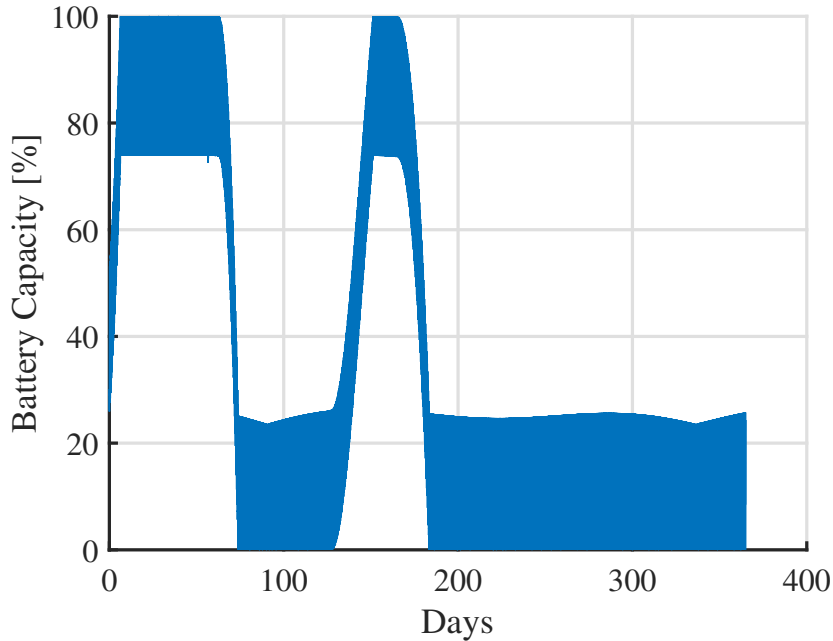


FIGURE 6.29: Batteries cycles over a year in 800[km] SSO, LTDN 12h00

The power generated is not sufficient for 261 days over a year. During this period, batteries completely discharged at each orbit and cannot provide enough power to all subsystems in this worst-case scenario. One solution to produce more power while keeping activities in eclipse is to orientate the satellite optimally towards the Sun while it is in sunlight. Figure 6.17 presented the power over a year for such a configuration. The power produced is more or less constant and equal to 6.85[W]. It is clearly superior to the power consumption. In this way, batteries never discharge below 75%.

All other cases presented in Section 6.3.2 for 800[km] SSO have a minimum power consumption superior to 4.54[W]. Hence, they can provide enough power to all subsystems in this worst-case scenario and batteries never discharge below 75%.

It is also interesting to assess how much time is required to charge the batteries completely after the launch. Figure 6.30 presents the batteries cycles during the first ten days.

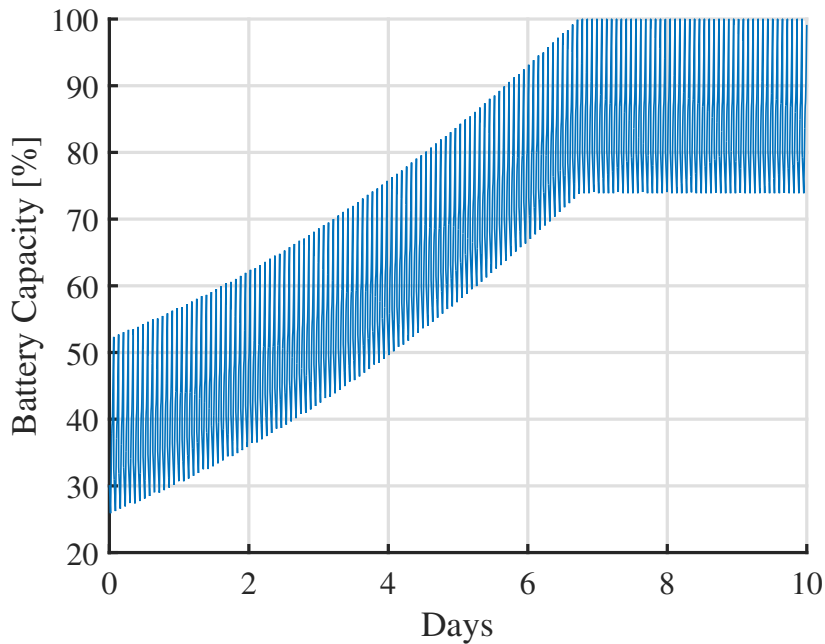


FIGURE 6.30: *Batteries cycles during the first two days, 800[km] SSO*

Just after the launch, the satellite is in eclipse and therefore, the power available decreases to 26.5%. Then, 6.47 days and 101 orbits are necessary to charge the batteries completely for the first time.

6.4.4 Conclusion

Three power budgets have been performed for three different orbits: an ISS orbit, a 400[km] SSO 10h30 and an 800[km] SSO 12h00. These power budgets are said to be high consumption because the subsystems have been used during the maximum of their useful time. For example, the S-Band Tx subsystem is considered active during all the maximum visibility over the ground station.

A worst-case scenario has also been created. All subsystems must be active at least once per orbit and COMM TX, S-band Tx, THER and Payload are used in eclipse. In this way, one can design the batteries and simulate their charge/discharge cycles over a year. This worst-case scenario combined with the high consumption power budgets led to different results. OUFTI-Next is able to provide enough power when it is on the 400[km] SSO. Nevertheless, it is not the case for the ISS orbit. It is not the case neither when the CubeSat is placed on a 12h LTDN 800[km] SSO with its short face pointing to the Earth. Indeed, the power generated is sometimes lower than the power consumed. Hence, batteries completely discharge after a while. There are several ways to avoid that. One way is to increase the capacity of the batteries but is not convenient. One can also play with the attitude of the satellite to orientate its solar panels optimally towards the Sun while no other attitude control is required.

It is important to highlight that these power budgets are first approximations. Indeed, the power consumption of several subsystems have been chosen arbitrarily out of existing datasheets. Nevertheless, it is not yet decided which subsystems will be used. For example, power budgets would be completely different if the Kinglet detector is used instead of the FLIR detector. Thus, these power budgets should be performed again once all subsystems are fixed.

Finally, batteries performance decreases with the number of cycles. It is also linked to the depth of discharge. The larger is the depth of discharge, the faster batteries will decrease in performance. These phenomena were not modelled in this code. Incorporating these parameters in the code should be done in the future for more accurate results.

6.5 Mass budget and space occupation

6.5.1 Mass budget

The maximum mass authorized for a 3U CubeSat is 4[kg]. Table 6.13 shows the mass of the different components as well as the total mass. Some values come from real datasheets of COTS components whereas others were estimated.

Components	Estimated mass [g]
Structure	400
Solar panel -x	150
Solar panel +x	150
Solar panel -y	150
Solar panel +y	150
Solar panel +z	50
Patch antenna support S-band	70
Patch antenna S-band	50
Antennas VHF & UHF + support	100
Payload	
FLIR Neutrino	450
TMA telescope	150
Visible camera	100
Payload interface plateforme	200
ADCS	800
Electronics	
COMM VHF & UHF	85
COMM S-band	62
EPS	86
OBC	70
Batteries	350
Total	3623

TABLE 6.13: *Mass budget*

The total mass estimated is equal to 3623[g]. The current mass margin is about 9.4%. Nevertheless, small and light components which are not possible to account for the moment such as spacers and threaded rods are lacking. Furthermore, some components have been roughly estimated such as the visible camera and the payload interface platform. Also, the TMA telescope will certainly evolve in the future and the MWIR detector is not yet fixed. For all these reasons, this mass budget is subject to changes and must be actualized in the future. Eventually, a 10% margin is not a lot and it is hardly possible to play on these parameters. Therefore, the mass budget should be carefully watched out.

6.5.2 Space occupation

Every component must then be placed inside the 3U structure. The electronics which includes a COMM UHF/VHF PCB, COMM S-band PCB, an EPS PCB, an OBC PCB and batteries must be stacked one above the other with a certain spacing between each of them. Therefore, the electronics can be grouped together in 1U. The ADCS size is minimum 0.5U. Eventually, there is 1.5U left for the payload.

If the FLIR detector (Fig 3.2) and the TMA telescope (Fig 3.7) are used in their original configuration, the payload cannot fit in 1.5U. FLIR detector is 12.7[cm] long and the distance between the TMA focal plane and mirror M3 is 4[cm]. As the focal plane must be at the same location as the detector photosensitive part (in purple in Figure 3.1), the total length of the payload is 16.7[cm] which is bigger than 1.5U. In this configuration, it is impossible to fit all subsystems in a 3U structure. If the FLIR detector can be folded, i.e placing the cooling part of the detector next to the photosensitive part instead of behind, it could maybe fit in 1.5U depending on its new configuration. This question must still be asked to the people from FLIR. In any case, the slit in front of the telescope must be placed on a small face of OUFTI-Next. In this case, the satellite rotates around the Earth like in Figure 6.11.

Another solution would be to change a little bit the design of the TMA telescope. If the focal plane can be placed perpendicularly to the original one, the available space could be optimized. Indeed, the slit of the telescope would be on a long face and the detector also along this long face. Some space could then be spared on the previous 4[cm] distance between mirror M3 and the focal plane. Once again, it has to be discussed with people from AMOS to see what is feasible.

Kinglet detector is more compact than the FLIR and is available in two configurations (Fig. 3.4). The configuration on the left hand is the most compact. With this configuration and the standard TMA, the payload can fit in 1.5U if the slit of the telescope is placed on a small face. Kinglet detector is 8[cm] long. If one adds the 4[cm] needed for the TMA, the payload is thus 12[cm] long.

If the TMA configuration can be changed like detailed above, one can place the slit of the telescope on a long face. The Kinglet detector can then be placed along the long face as with the FLIR.

6.5.3 Conclusion

The total mass estimated is 3623[g] and the margin is 9.4%. Certain components have been roughly estimated and subsystems are not yet fixed. Therefore, one should keep an attentive eye on the mass budget. The space occupation is even more critical. If the FLIR detector and the TMA are not modified, all subsystems cannot fit in a 3U CubeSat. Contrariwise, the Kinglet detector and the original TMA fit in the available space. Nevertheless, FLIR detector might be folded and the TMA design could perhaps be changed. If these modifications are possible, solutions may exist to fit the FLIR detector and TMA inside OUFTI-Next.

6.6 Summary

To sum up, OUFTI-Next design depends on the mission analysis and several budgets were performed to assess the feasibility of the mission. These budgets were based on real COTS components (antennas, communication systems, solar panels, ADCS, structure...).

Six different COTS ADCS for 3U CubeSats were investigated. Three of them size 0.5U or less. They are XACT, MAI-400 and iADCS-100. Among these ones, XACT and MAI-400 are the most efficient and can perform every attitude control needed with the required accuracy. Nevertheless, the cryocooler used to cooldown the MWIR detector produces vibrations which cannot be damped by these ADCS. These vibrations can blur the images obtained. A solution could be to cooldown the detector to the required temperature just before taking images. The cryocooler is then stopped while taking images. Further analyses must be carried out to determine if this solution is adequate.

Link budget confirmed that S-band can be used to downlink payload data. Depending on the orbit, high-quality images with lengths varying between 500[km] and 1500[km] can be downlinked per day. Link budget also showed that uplink communications should be in UHF while the downlink of telemetry data should be in VHF whatever the orbit. Antenna system, S-band patch antenna, UHF/VHF transceiver and S-band kit ground station are COTS components.

The orbit and orientation of the satellite have a major impact on the power generated over a year. This power generation influences the power budget. With a high power consumption in a worst-case scenario, only a satellite in a 400[km] SSO can generate enough power. For 800[km] SSO and ISS orbit, batteries discharge completely when the power generated is inferior to the power consumed. For both orbits, attitude controls should be performed to orientate optimally solar panels towards the Sun and generate more power. These attitude controls have no influence on the communication and payload activities in this worst-case scenario.

Eventually, a preliminary mass budget was performed. The total mass estimated is equal to 3623[g] which leads to a 9.4 % mass margin. The space occupation is even more critical. FLIR detector with TMA in their classical configurations cannot fit in the space left by other subsystems. Kinglet detector is more compact and can fit with the TMA in the 3U structure. Other solutions are possible if the FLIR and/or TMA can be arranged in other configurations.

To conclude, some points are concerning and must be carefully watched out. One of the most critical is space occupation. If the Neutrino is the only available detector and if it cannot be folded, then TMA in the current configuration and this detector cannot fit in a 3U CubeSat and the project is unfeasible under the working hypothesis. Moreover, the mass budget is concerning because the margin is less than 10% and flexibility is poor. Power budget should also be carefully analyzed because the power generated is not always sufficient. Finally, vibrations due to the cryocooler are an issue for the mission and solutions should be investigated. This problem cannot be solved by increasing OUFTI-Next size.

Figures 6.31 and 6.32 present a CAD model of OUFTI-Next. It is a model where the Neutrino MWIR detector is on a small face and no TMA is modelled. For this reason, there is some space left between the detector and the ADCS. A deployable S-band patch antenna is required because it must point to the NADIR direction.

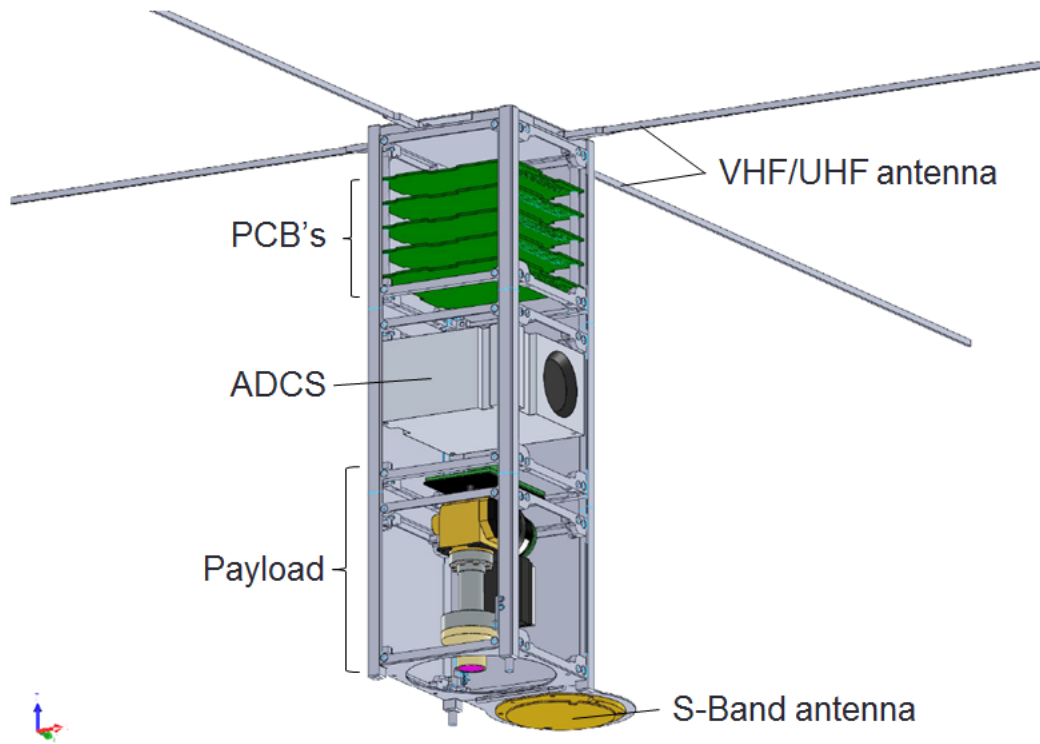


FIGURE 6.31: *OUFTI-Next CAD model*

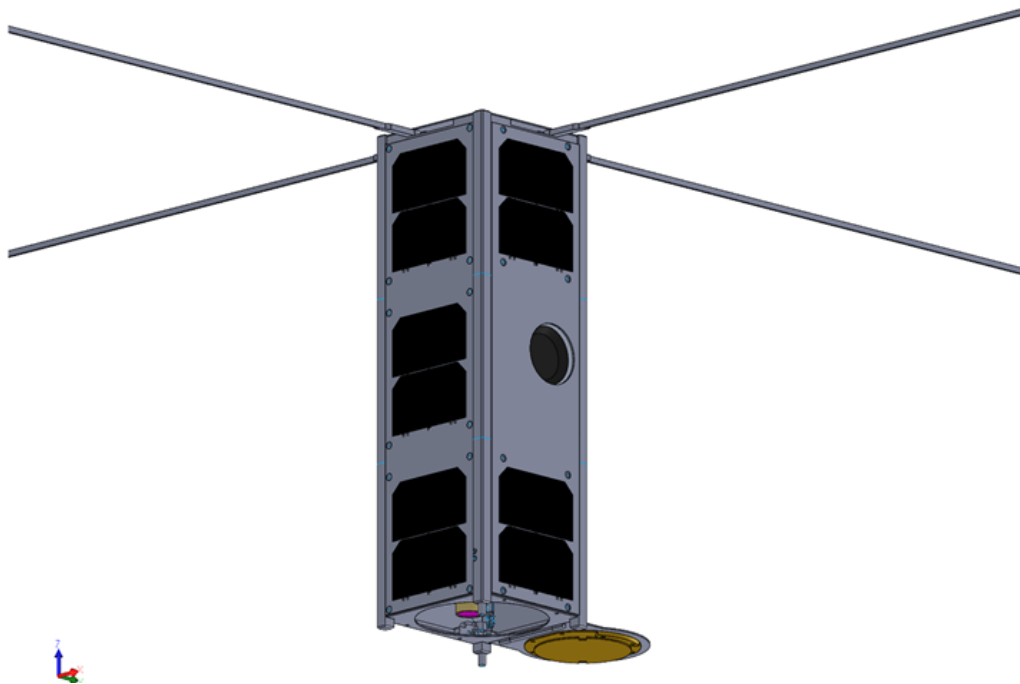


FIGURE 6.32: *OUFTI-Next CAD model with body mounted solar panels*

Chapter 7

Conclusion

The objective of this thesis was to assess the feasibility and legitimacy of the OUFTI-Next project. To this end, a technology demonstrator must be first realized. Requirements for this 3U CubeSat have been a bit relaxed compared to the constellation mission. If the OUFTI-Next mission is not realizable with a 3U CubeSat, a 6U form-factor CubeSat should be then considered.

The first part of this work was dedicated to the presentation of the objectives and requirements of the constellation mission. The legitimacy and usefulness of the mission have been assessed by analyzing the MWIR band and highlighting the importance of hydric stress detection in agricultural fields. Then, lifetime predictions have been performed and finally a constellation has been modelled to obtain a daily coverage.

Chapter 3 presented OUFTI-Next mission. The objectives and requirements have been detailed. The payload consisting of a MWIR detector, a TMA telescope and classical camera has been described.

Chapter 4 was dedicated to the state of the art. The first section consisted in an analysis of five large MWIR missions. The aim was to present the large spectrum of applications of MWIR measurements and to show the improvements over the years in this domain. A table referencing CubeSats observing the Earth in the infrared has been presented. This table contains the main characteristics of these missions such as the size, mass, status, power, ADCS, orbit... The reasons of success or failure were also discussed.

Chapter 5 focused on the mission analysis. The different relevant orbits and their characteristics (period, eclipse, visibility...) have been presented. The revisit time over a particular region for three different orbits has been detailed. Patterns could be deduced. The lifetime of OUFTI-Next has been also evaluated thanks to the STK tool *lifetime*. To this end, parameters influencing the orbital decay have been studied and a comparison between STK results and two real missions has been led to validate OUFTI-Next lifetime predictions.

In chapter 6, a preliminary design of OUFTI-Next was developed. First, a list of COTS ADCS for 3U CubeSats has been created with their relative characteristics. Then, a data budget has been performed for each orbit to evaluate the amount of data that can be downlinked per day in function of the communication band used. Link budgets based on real COTS components have been computed. It turned out that only two bands (VHF and S-band) were appropriate to downlink data. Different simulations of power generation over a year for various orbits and attitude controls have been carried out. Two models of OUFTI-Next have been created to

simulate the power generation with STK. These results were then exploited to perform power budgets and design batteries. Eventually, OUFTI-Next mass has been evaluated and the space occupation issue has been highlighted.

This thesis permitted to point out that some aspects of OUFTI-Next mission must be carefully watched out. Solutions to these sensible points exist and must be deeper examined. Furthermore, thorough analyses must be performed in the future. They concern various domains such as antennas and S-band patch deployment, electrical power system, thermal and structural analyses, on-board computer... This feasibility study should also be continued when additional information about the possible configurations of the TMA and detectors will be available. At that moment only, a clear affirmative or negative answer on the feasibility of this mission may be given.

Personally, I have been very pleased and honoured to contribute to this wonderful and ambitious project. It gave me the opportunity to learn many things about satellite engineering and space domain in general. I could also handle new tools such as STK. I learned new concepts in various engineering fields such as telecommunication or imaging techniques. Moreover, this work helped me to understand how the numerous interactions between satellite subsystems impact each other.

I had the chance to meet many valuable professors from different faculties and exchange very interesting ideas with them during the ideation session. Meetings with OUFTI-Next team were also the occasion to discuss with highly experienced people in the space domain and gain new knowledge. In addition, I had the opportunity to converse by mail with numerous engineers and space companies from all around the world. Finally, I enjoyed the team work where each individual feels concerned about the project and tries to make it a success!

Appendices

Appendix A

SSO database

Name	Altitude [km]	Inclination [°]	LTAN	LTDN
AIM	600	97.78	12h	/
AIS Sat-1	635	97.71	/	9h30
AIS Sat-2	635	97.71	/	9h30
ASNARO	504	97.4	/	11h30
Alsat-2	670	98.23	/	21h30
Aprizesat 3-4	686	98.13	10h30	/
Aqua	705	98.2	13h30	/
Asnaro	504	97.4	/	11h
Brite Austria	775	98.63	6h	/
Brite Canada	630	98	10h30	/
Brite Poland	600x900	97.8	/	9h30
Calipso	705	98.04	13h30	/
CEBERS 4	778	98.5	/	10h30
ChubuSat 1	504	97.4	/	11h
Sentinel 1	693		18h	/
Sentinel 2	786		/	10h30
Sentinel 3	814.5		/	10h
Deimos-1	661	98	10h39	/
Deimos-2	630	98	10h30	/
Delfi-C3	635	97.94	/	9h30
DMC-3	650		10h30	/
DMSP 5D (F14)			17h22	/
DMSP 5D (F15)			19h35	/
DMSP 5D (F16)			20h03	/
DMSP 5D (F17)			17h32	/
Dubaisat-1	686	97.7	10h30	/
Dubaisat-2	600	97.1	0h	/
Eros A	480	97.3	/	10h
Eros B	500	97.4	/	14h
Formosat-2	888	97.7	/	10h
Gaofen 1	645	98	/	10h30
Gaofen 2	631	97.9	/	10h30
GHGSat-D	512	97.5	/	9h30
HJ-1C	502	97.3	/	6h
Hodoyoshi-1	504	97.4	/	11h

Hodoyoshi-3-4	630	97.97	10h30	/
Horyu-2	680	98.19	13h30	/
HumSatD	600	97.8	10h30	/
Kazeosat-1	750	98.54	/	10h30
Kazeosat-2	630	98	10h30	/
Kompsat-2	685	98.13	10h50	/
Kompsat-3	685.1	98.13	13h30	/
Kompsat-3a	528	97.5	13h30	/
Kompsat-5	550	97.6	6h	/
Landsat-7	705	98.2	/	10h
Landsat-8	705	98.2	/	10h
Lapan A3	515	97.5	/	9h30
M3Msat	515	97.5	/	9h30
Meteor M2	825	98.8	9h30	/
Metop			21h30	/
MTI	575x609	97.52	13h	/
Nanosat-1	661	98.2	13h	/
Nanosat-1B	578x706	98.1	10h30	/
Neosat	786	98.55	6h	/
NigeriaSat-2	700x733	98.24	10h15	/
OceanSat-2	720	98.28	12h	/
OCO 2	705	98.2	13h30	/
Odin	600	97.77	18h	/
Optos	600	97.8	/	10h30
Pleiades-1B	694	98.2	/	10h30
Popsat-.ip1	630	98	10h30	/
PRISM	660	98	13h	/
Proba-1	542x657	97.9	/	10h30
Proba-2	725	98.44	6h	/
Proba-V	820	98.8	/	10h30
Radarsat-2	798	98.6	18h	/
RapidEye	630	98	/	11h30
Rasat	700	98.25	10h30	/
Resourcesat-2	817	98.78	/	10h30
Resurs-P	475	97.3	/	10h30
SDS-4	677	98.19	13h30	/
Seeds-2	635	97.94	/	9h30
Shijian-9	623x650	98	/	10h30
Skysat	600	97.8	/	10h30
SMAP	685	98	18h	/
SMOS	755	98.44	6h	/
SPOT-5	832	98.7	/	10h30
SPOT-7	694	98.2	22h	/
SSOT	620	97.9	10h30	/
Strand-1	786	98.55	6h	/
Stsat-3	600	97.8	/	10h30
TET-1	510	97.8	11h27	/
Tisat-1	635	97.8	/	9h30
Tsubame	504	97.4	/	11h
UK-DMC-2	686	98.13	10h30	/

VnredSat-1	820	98.8	/	10h30
Vrss-1	626x662	98	/	10h30
Wnisat-1	600	97.8	/	10h30
WorldView-1	496	97.2	/	10h30
WorldView-2	767	97.8	/	10h30
WorldView-3	617	98	/	13h30
YouthSat	822	97.78	/	10h30
Zacube 1	600	97.8	/	10h30

TABLE A.1: SSO database with corresponding LTDN/LTAN

Appendix B

Large MWIR missions

Instrument Name Short	Instrument Agencies	Instrument Type	Waveband Categories
AATSR	UKSA	Imaging multi-spectral radiometers (vis/IR) and multiple direction/polarisation radiometers	VIS, NIR, SWIR, MWIR, TIR
AMSR	JAXA	Imaging multi-spectral radiometers (passive microwave)	MWIR
ATSR/M	CNES	Imaging multi-spectral radiometers (passive microwave)	SWIR, MWIR
ATSR-2	UKSA (CSIRO)	Imaging multi-spectral radiometers (vis/IR) and multiple direction/polarisation radiometers	VIS, NIR, SWIR, MWIR, TIR, MW
AVHRR/2	NOAA	Imaging multi-spectral radiometers (vis/IR)	VIS, NIR, MWIR, TIR
AVHRR/3	EUMETSAT, NOAA	Imaging multi-spectral radiometers (vis/IR)	VIS, NIR, SWIR, MWIR, TIR, FIR
AWFI	INPE	Imaging multi-spectral radiometers (vis/IR)	VIS, NIR, MWIR, TIR
ERBE	NASA	Earth radiation budget radiometers	UV, VIS, NIR, SWIR, MWIR, TIR, FIR
GLI	JAXA	Imaging multi-spectral radiometers (vis/IR)	VIS, NIR, SWIR, MWIR, TIR
HIRS/2	NOAA	Atmospheric temperature and humidity sounders	VIS, NIR, SWIR, MWIR, TIR
HIRS/3	NOAA	Atmospheric temperature and humidity sounders	VIS, NIR, SWIR, MWIR, TIR, FIR
HSRS	DLR	Imaging multi-spectral radiometers (vis/IR)	MWIR, TIR
ILAS-II	MOE (Japan) (JAXA)	Atmospheric chemistry	NIR, MWIR, TIR
IMAGER	JMA	Imaging multi-spectral radiometers (vis/IR)	VIS, MWIR, TIR
IVISSR (FY-2)	NRSCC (NSMC-CMA, CNSA, CAST)	Imaging multi-spectral radiometers (vis/IR)	VIS, MWIR, TIR
MIPAS	ESA	Atmospheric temperature and humidity sounders and atmospheric chemistry	NIR, MWIR, TIR
MSU-MR	ROSKOSMOS (ROSHYDROMET)	Imaging multi-spectral radiometers (vis/IR)	VIS, NIR, SWIR, MWIR, TIR
MVISR (10 channels)	NRSCC (NSMC-CMA, CAST)	Imaging multi-spectral radiometers (vis/IR)	VIS, NIR, SWIR, MWIR, TIR
SeaWinds	NASA	Scatterometers	MWIR, MW
Sounder	NOAA	Atmospheric temperature and humidity sounders	VIS, NIR, SWIR, MWIR, TIR

FIGURE B.1: *Past large MWIR missions*

Instrument	Instrument Agencies	Instrument Type	Waveband Categories
ACE-FTS	CSA	Atmospheric chemistry	SWIR, MWIR, TIR
AIRS	NASA	Atmospheric temperature and humidity sounders	VIS, NIR, MWIR, TIR
AVHRR/3	EUMETSAT, NOAA	Imaging multi-spectral radiometers (vis/IR)	VIS, NIR, SWIR, MWIR, TIR, FIR
CERES	NASA	Earth radiation budget radiometers	UV, VIS, NIR, SWIR, MWIR, TIR, FIR
CrIS	NOAA	Atmospheric temperature and humidity sounders	NIR, MWIR, TIR
ERM	NRSCC	Earth radiation budget radiometers	UV, VIS, NIR, SWIR, MWIR, TIR, FIR
GERB	EUMETSAT (RAL, ESA)	Earth radiation budget radiometers	UV, VIS, NIR, SWIR, MWIR, TIR, FIR
HIRS/3	NOAA	Atmospheric temperature and humidity sounders	VIS, NIR, SWIR, MWIR, TIR, FIR
HIRS/4	EUMETSAT, NOAA	Atmospheric temperature and humidity sounders	VIS, NIR, SWIR, MWIR, TIR
IASI	EUMETSAT (CNES)	Atmospheric temperature and humidity sounders and atmospheric chemistry	MWIR, TIR
IMAGER	JMA	Imaging multi-spectral radiometers (vis/IR)	VIS, MWIR, TIR
Imager (INSAT)	ISRO	Imaging multi-spectral radiometers (vis/IR)	VIS, SWIR, MWIR, TIR
IR (HJ-1B)	CAST	Imaging multi-spectral radiometers (vis/IR)	NIR, SWIR, MWIR, TIR
IRAS	NRSCC	Atmospheric temperature and humidity sounders	VIS, NIR, SWIR, MWIR, TIR
IVISSR (FY-2)	NRSCC	Imaging multi-spectral radiometers (vis/IR)	VIS, MWIR, TIR
MI	KARI (KMA, ITT)	Imaging multi-spectral radiometers (vis/IR)	VIS, SWIR, MWIR, TIR
MODIS	NASA	Imaging multi-spectral radiometers (vis/IR) and ocean colour instruments	VIS, NIR, SWIR, MWIR, TIR
MOPITT	CSA (NASA)	Atmospheric chemistry	NIR, MWIR
MSU-GS	ROSKOSMOS	Imaging multi-spectral radiometers (vis/IR)	VIS, NIR, SWIR, MWIR, TIR
MSU-MR	ROSKOSMOS	Imaging multi-spectral radiometers (vis/IR)	VIS, NIR, SWIR, MWIR, TIR
MWIR (GF-4)	CRESDA	Imaging multi-spectral radiometers (vis/IR)	MWIR
OMPS	NOAA	Atmospheric chemistry	UV, VIS, NIR, SWIR, MWIR, TIR
SeaWinds	NASA	Scatterometers	MWIR, MW
SEVIRI	EUMETSAT (ESA)	Imaging multi-spectral radiometers (vis/IR)	VIS, NIR, SWIR, MWIR, TIR
Sounder	NOAA	Atmospheric temperature and humidity sounders	VIS, NIR, SWIR, MWIR, TIR
Sounder (INSAT)	ISRO	Atmospheric temperature and humidity sounders	VIS, MWIR, TIR
TANSO-FTS	JAXA, NIES	Atmospheric chemistry	NIR, SWIR, MWIR, TIR
TES	NASA	Atmospheric chemistry	MWIR, TIR
VIIRS	NOAA (NASA)	Imaging multi-spectral radiometers (vis/IR) and ocean colour instruments	VIS, NIR, SWIR, MWIR, TIR
VIRR	NRSCC	Imaging multi-spectral radiometers (vis/IR)	VIS, SWIR, MWIR, TIR

FIGURE B.2: *Operational large MWIR mission*

Instrument Name Short	Instrument Agencies	Instrument Status	Instrument Type	Waveband Categories
ABI	NOAA	Being developed 2016 - 2038	Imaging multi-spectral radiometers (vis/IR)	VIS, NIR, SWIR, MWIR, TIR
Advanced IKFS-2	ROSHYDROMET	Proposed 2023 - 2030	Atmospheric temperature and humidity sounders	MWIR, TIR
Advanced MI	KARI (KMA, ITT)	Proposed 2018-2028	Imaging multi-spectral radiometers (vis/IR)	VIS, NIR, SWIR, MWIR, TIR
Advanced MSU-MR	ROSHYDROMET	Proposed 2023 - 2030	Imaging multi-spectral radiometers (vis/IR)	VIS, NIR, SWIR, MWIR, TIR
BBR (EarthCARE)	ESA	Approved 2018 - 2021	Earth radiation budget radiometers	UV, VIS, NIR, SWIR, MWIR, TIR, FIR
BIK-SD 1	ROSKOSMOS	Proposed 2020 - 2031	Imaging multi-spectral radiometers (vis/IR)	MWIR, TIR
FCI	EUMETSAT (ESA)	Being developed 2020 - 2041	Imaging multi-spectral radiometers (vis/IR)	VIS, NIR, SWIR, MWIR, TIR
IASI-NG	EUMETSAT (CNES)	Being developed 2021 - 2042	Atmospheric temperature and humidity sounders	MWIR, TIR
IK-radiometer (1)	ROSKOSMOS	Proposed 2023 - 2032	Imaging multi-spectral radiometers (vis/IR)	MWIR, TIR
IR Correlation Radiometer (GeoCape)	NASA	Proposed 2023 - 2026	Imaging multi-spectral radiometers (vis/IR)	SWIR, MWIR
IRS	EUMETSAT (ESA)	Being developed 2022 - 2039	Atmospheric temperature and humidity sounders	MWIR, TIR
MCSI	NRSCC (NSMC-CMA, CNSA, CAST)	Approved 2016 - 2040	Imaging multi-spectral radiometers (vis/IR)	VIS, NIR, SWIR, MWIR, TIR
METimage	EUMETSAT (DLR)	Being developed 2021 - 2042	Imaging multi-spectral radiometers (vis/IR)	UV, VIS, NIR, SWIR, MWIR, TIR
MSU-GS/VE	ROSKOSMOS	Approved 2017 - 2024	Imaging multi-spectral radiometers (vis/IR)	VIS, NIR, SWIR, MWIR, TIR
MSU-IK-SR	ROSKOSMOS (ROSHYDROMET)	Approved 2017 - 2022	Imaging multi-spectral radiometers (vis/IR)	MWIR, TIR
Multi-spectral thermal infrared imager (HyspIRI)	NASA	Proposed 2023 - 2026	Imaging multi-spectral radiometers (vis/IR)	MWIR, TIR
MVIRS	NRSCC (CNSA, CAST)	Approved 2019 - 2028	Imaging multi-spectral radiometers (vis/IR)	VIS, SWIR, MWIR, TIR
OMPS-L	NASA (NOAA)	Being developed 2021 - 2038	Atmospheric chemistry	UV, VIS, NIR, SWIR, MWIR, TIR
PCW PHEOS - Atmospheric	CSA (EnvCan)	Proposed 2021 - 2036	Atmospheric chemistry	NIR, SWIR, MWIR, TIR
PCWMP	CSA (EnvCan)	Proposed 2021 - 2036	Imaging multi-spectral radiometers (vis/IR)	VIS, NIR, SWIR, MWIR, TIR
RBI	NASA	Being developed 2021 - 2038	Earth radiation budget radiometers	UV, VIS, NIR, SWIR, MWIR, TIR, FIR
TANSO-FTS-2	JAXA (MOE (Japan), NIES (Japan))	Being developed 2018 - 2023	Atmospheric chemistry	NIR, SWIR, MWIR, TIR

FIGURE B.3: *Future large MWIR missions*

Bibliography

- [1] URL: <http://www.flir.com/uploadedFiles/OEM/Products/MWIR-Cameras/Neutrino/FLIR-Neutrino-Datasheet.pdf>.
- [2] URL: https://www.scdusa-ir.com/kinglet-4/?doing_wp_cron=1495440013.8476729393005371093750.
- [3] URL: <http://database.eohandbook.com/database/instrumenttable.aspx>.
- [4] URL: https://en.wikipedia.org/wiki/Normalized_Difference_Vegetation_Index.
- [5] URL: <http://digitalcommons.unl.edu/cgi/viewcontent.cgi?article=1523&context=usdeptcommercepub>.
- [6] URL: https://icdc.cen.uni-hamburg.de/fileadmin/user_upload/icdc_Dokumente/MODIS/kilpatricketal_AdecadeofSeaSurfaceTemperaturefromMODIS_RSE_165_27-41_2015.pdf.
- [7] URL: <https://amsat-uk.org/satellites/non-operational/techedsat-f-1-fitsat-1-we-wish/>.
- [8] URL: <https://amsat-uk.org/tag/we-wish/>.
- [9] URL: <https://directory.eoportal.org/web/eoportal/satellite-missions/s/srmsat#foot5%29>.
- [10] URL: <http://www.newindianexpress.com/education/edex/2014/dec/08/It\%\%80\%99s-Indeed-Rocket-Science-691728.html>.
- [11] URL: <https://eoportal.org/web/eoportal/satellite-missions/c-missions/copper>.
- [12] URL: <http://www.airspacemag.com/daily-planet/cubesats-are-great-even-if-they-die-you-180952745/>.
- [13] URL: <http://weebau.com/satellite/L/lemur1.htm>.
- [14] URL: http://space.skyrocket.de/doc_sdat/lemur-1.htm.
- [15] URL: http://www.amsat.org/?page_id=3316.
- [16] URL: <http://spaceflight101.com/spacecraft/antelsat/>.
- [17] URL: http://iie.fing.edu.uy/investigacion/grupos/lai/files/ANTELSAT_brochure_2012W01.pdf.
- [18] URL: <http://www.antel.com.uy/antel/institucional/sala-de-prensa/eventos/2015/exitosa-culminacion-del-proyecto-antelsat>.
- [19] URL: <http://iie.fing.edu.uy/investigacion/grupos/lai/status.html>.
- [20] URL: http://www.amsat.org/wordpress/wp-content/uploads/2014/01/LilacSat2_info-20151007.pdf.
- [21] URL: http://space.skyrocket.de/doc_sdat/lilacsat-2.htm.

- [22] URL: http://space.skyrocket.de/doc_sdat/stacem.htm.
- [23] URL: http://space.skyrocket.de/doc_sdat/sathyabamasat.htm.
- [24] URL: http://www.amsatuk.me.uk/iaru/finished_detail.php?serialnum=189.
- [25] URL: <http://spaceflight101.com/pslv-c34/sathyabamasat/>.
- [26] URL: http://space.skyrocket.de/doc_sdat/kausat-5.htm.
- [27] URL: http://www.amsatuk.me.uk/iaru/finished_detail.php?serialnum=443.
- [28] URL: <https://directory.eoportal.org/web/eoportal/satellite-missions/q/qbito>.
- [29] URL: http://space.skyrocket.de/doc_sdat/lilacsat-1.htm.
- [30] URL: http://www.amsatuk.me.uk/iaru/finished_detail.php?serialnum=343.
- [31] URL: http://space.skyrocket.de/doc_sdat/corvus-bc.htm.
- [32] URL: <https://astrodigital.com/downloads/brochure-astro.pdf>.
- [33] URL: http://space.skyrocket.de/doc_sdat/corvus-hd.htm.
- [34] URL: http://space.skyrocket.de/doc_sdat/parikshit.htm.
- [35] URL: http://www.amsatuk.me.uk/iaru/finished_detail.php?serialnum=442.
- [36] URL: <https://www.carthage.edu/live/files/2874-canopcodrv11.pdf>.
- [37] URL: <https://directory.eoportal.org/web/eoportal/satellite-missions/c-missions/ciras>.
- [38] URL: <https://www.trisat.um.si/en/mission/>.
- [39] URL: http://space.skyrocket.de/doc_sdat/ciris.htm.
- [40] URL: <http://www.coloradospacenews.com/ball-aerospace-to-implement-earth-science-cubesat-mission-for-nasa/>.
- [41] URL: <http://spie.org/Publications/Proceedings/Volume/9978>.
- [42] URL: http://www.amsatuk.me.uk/iaru/finished_detail.php?serialnum=500.
- [43] URL: http://space.skyrocket.de/doc_sdat/golden-eagle-1.htm.
- [44] URL: <https://marquettewire.org/3856853/tribune/tribune-news/student-satellite-almost-ready-for-launch/>.
- [45] URL: https://en.wikipedia.org/wiki/Sun-synchronous_orbit.
- [46] URL: <https://en.wikipedia.org/wiki/Outgassing>.
- [47] URL: <https://srag.jsc.nasa.gov/spaceradiation/What/What.cfm>.
- [48] URL: https://www.nasa.gov/mission_pages/station/news/orbital_debris.html.
- [49] URL: <http://help.agi.com/stk/index.htm#stk/tools-11.htm>.
- [50] URL: <http://adsabs.harvard.edu/full/1966SAOSR.207.....J>.
- [51] URL: http://www.hamamatsu.com/us/en/community/optical_sensors/articles/tdi_imaging_for_aoi_axi_ndt/index.html.
- [52] URL: <http://www.antdevco.com/ADC-1501230948\%20R1\%20-%20X-band\%20Patch\%20Array\%20data\%20sheet.pdf>.
- [53] Kyle Leveque Daniel L. Oltrogge. In: (). URL: <http://digitalcommons.usu.edu/cgi/viewcontent.cgi?article=1144&context=smallsat>.

- [54] Enrico Ghidoli. “MWIR Observation Feasibility Study”. In: (2017).
- [55] Hannah R. Goldberg. “Asteroids to agriculture: carving a niche in earth observation using asteroids prospecting instruments on a earth-orbiting cubesat constellation, publisher = Planetary Resources”. In: ().
- [56] Ji Hyun Park In-Seuck Jeung. URL: http://www.unisec-global.org/pdf/uniglo2/UNIGLO2_Day1/POC/1_1650_Korea.pdf.
- [57] Gaëtan Kerschen. “Astrodynamics, chapter 5”. In: (2016).
- [58] Bryan Klofas. URL: http://klofas.com/papers/ESG-P-14-165-cubesat_comm_update.pdf.
- [59] Jet Propulsion Laboratory. “HyspIRI Comprehensive Development Report”. In: (2015).
- [60] S. Grabarnik C. De Clercq-F. Michel G. Taglioni W. Moelans M. Taccola D. De Wilde. “MINIATURIZED HYPERSPECTRAL IMAGERS FOR CUBESATS”. In: (2010).
- [61] Peter Marquez. URL: https://swfound.org/media/205527/marquez_secure-world_-5-6-16.pdf.
- [62] Peter Marquez. URL: https://swfound.org/media/205527/marquez_secure-world_-5-6-16.pdf.
- [63] Steve Massey. URL: http://mst1.atl.calpoly.edu/~bklofas/Presentations/SummerWorkshop2011/Massey_COPPER.pdf.
- [64] Brian Cooper Michael Bertino. URL: http://mst1.atl.calpoly.edu/~bklofas/Presentations/DevelopersWorkshop2015/Bertino_Perseus-M_Corvus-BC.pdf.
- [65] Brian Cooper Michael Bertino. URL: <http://parikshit.org/subsystems/>.
- [66] Connor D. Noyes. URL: https://www.nasa.gov/mission_pages/station/news/orbital_debris.html.
- [67] Austin Richards. URL: <https://www.photonics.com/EDU/Handbook.aspx?AID=25132>.
- [68] Aidan Roche John Mergenthaler Robert Chatfield John Kumer. “Robust IR Remote Sensing for Formaldehyde, Carbon Monoxide, Methane, and Ozone Profiles”. In: ().
- [69] Scanex. “UniScan: X-band satellite ground receiving station”. In: (2015). URL: <http://www.scanex.ru/en/station/uniskan/>.
- [70] A. Spiteri. “Remote Sensing ’96: Integrated Applications for Risk Assessment and Disaster Prevention for the Mediterranean”. In: (1996).
- [71] B. Tychon. “OUFTI-Next presentation”. In: (2017).
- [72] P. Ciais G. Broquet A. Fortems-Cheiney I. Pison Y. Yin F. Chevallier and M. Saunois. URL: <http://www.atmos-chem-phys.net/15/13433/2015>.